

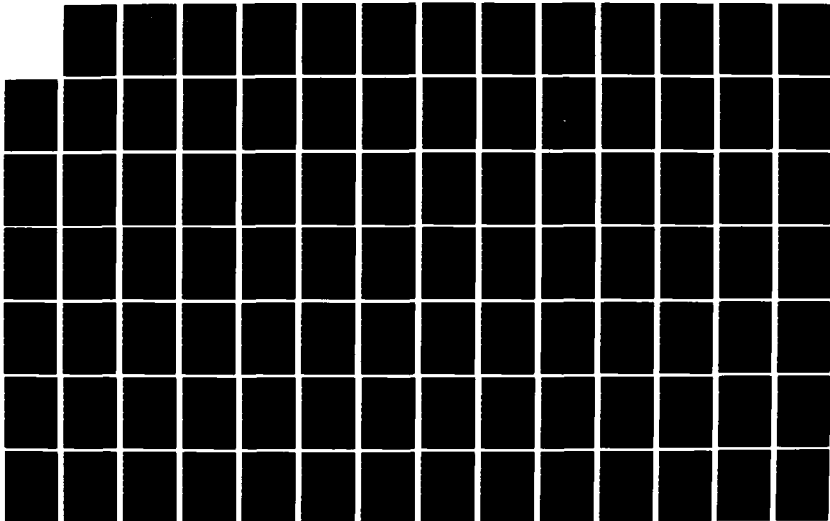
AD-A124 683

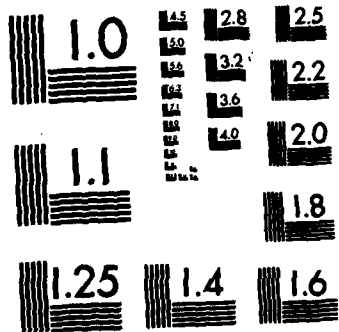
SCATTERING OF CYLINDRICAL ELECTRIC FIELD WAVES FROM AN
ELLIPTICAL DIELECT. (U) AIR FORCE INST OF TECH
WRIGHT-PATTERSON AFB OH SCHOOL OF ENGI... E A URBANIK
DEC 82 AFIT/GE/EE/82D-67 F/G 28/14

1/2

UNCLASSIFIED

NL





MICROCOPY RESOLUTION TEST CHART
NATIONAL BUREAU OF STANDARDS-1963-A

100
①



ADA 124683

SCATTERING OF CYLINDRICAL ELECTRIC
 FIELD WAVES FROM AN ELLIPTICAL
 DIELECTRIC CYLINDRICAL SHELL

THESIS

AFIT/GE/EE/82D-67 Edward A. Urbanik
 Captain USAF

This document has been approved
 for public release and sale; its
 distribution is unlimited.

DTIC
 UNCLASSIFIED
 D

DTIC FILE COPY

DEPARTMENT OF THE AIR FORCE
 AIR UNIVERSITY (ATC)
AIR FORCE INSTITUTE OF TECHNOLOGY

Wright-Patterson Air Force Base, Ohio

83 02 022 1371

Approved for public release; distribution unlimited

A
DTIC ELECTE
FEB 22 1983

AFIT/GE/EE/82D-67 Edward A. Urbanik
Captain USAF

THESIS

SCATTERING OF CYLINDRICAL ELECTRIC
FIELD WAVES FROM AN ELLIPTICAL
DIELECTRIC CYLINDRICAL SHELL

AFIT/GE/EE/82D-67



DTIC	<input checked="" type="checkbox"/>
COPY	<input type="checkbox"/>
INSPECTED	<input type="checkbox"/>
2	<input type="checkbox"/>
Distribution/	
Availability Codes	
Special Handling	
Special	

SCATTERING OF CYLINDRICAL ELECTRIC
FIELD WAVES FROM AN ELLIPTICAL
DIELECTRIC CYLINDRICAL SHELL

THESIS

Presented to the Faculty of the School of Engineering
of the Air Force Institute of Technology
Air University
in Partial Fulfillment of the
Requirements for the Degree of
Master of Science

by

Edward A. Urbanik, B.S.E.E.
Capt USAF

Graduate Electrical Engineering

December 1982

Approved for public release; distribution unlimited

Preface

The ALR-69 radar warning receiver on the F-16 has been hampered by the presence of secondary lobes which cause errors in the direction finding routine. This study examined this problem in terms of cylindrical wave scattering from a large dielectric shell. The shell was modeled as an ellipse since this was a conic shape that was close to the actual shape of the radome. The intent of this study was to examine the problem and see if the side lobes are caused by scattering.

The solution method was to use a Galerkin application of the method of moments. The electric field expansion function was the piecewise sinusoidal basis function. The integral equation developed was Richmond's Integral Equation which is valid for any dielectric cylindrical shell. The shape of the object resulted in the use of elliptic coordinates which is not one of the standard orthogonal coordinate systems. The combination of elliptic coordinates and Hankel functions made the integration nonexistent in closed form. The resultant numerical integration took a great deal of computational time. This time problem was further compounded by the presence of a line singularity involving the Hankel function. Considerable

discussion is given the subject from both the mathematical aspect and the programming aspect.

This thesis did not generate any far field plots of the electric field since the program used to calculate the reaction matrix elements produced erroneous data. The exact reason is unknown. The theory employed by this work is not new, it is only a different application. The simple fact that it took over 1300 CPU seconds to fill a 33x33 matrix and a 33 element vector on a machine as fast as the CDC Cyber 175 indicates an impractability of the method used.

A special note of thanks to my sponsors, Mr. William Kent and First Lieutenant Robert Schneider, ASD/ENAMA. The amount of help given by providing me with an ASD/EN problem number and account for the cyber is immeasurable. Thanks are due to my advisor, Captain Thomas W. Johnson, who was personally excited and motivated by the research. Finally, a special note of gratitude to Mary Browning, Linda Stoddart, and Veleta Kendall, AFIT/LDE. These people found information from the most unusual sources possible, and were a real help in getting this project anywhere.

Dedication

This thesis is dedicated to: first the lovely lady, Karen Urbanik, who stuck by me throughout the eighteen months. Not being close to a brilliant student, she single-handedly brought up our fatherless child as she took care of the house; doing what I should have done. Her true love has been manifested and my devotion to her deepened, by this experience. Secondly (and most importantly) to Jesus Christ who allowed this to happen so that I might finally get in step with Him and realize that He is in control. Maranatha!

Contents

	Page
Preface	ii
Dedication	iv
List of Figures	vii
List of Tables	ix
Abstract	x
I. Introduction	1
Background	1
Rationale	3
Literature Review	5
Previous Work	9
Experimental	9
Theoretical	9
Proposed Solution	11
Assumptions	13
Scope	13
II. Development of a One-dimensional Fredholm Integral Equation of the Second Kind	14
Model	14
Richmond Integral Equation	16
Elliptic Coordinates	17
The Singular Kernel	19
Principal Value Integral	22
Determination of the Correction Term	23
Reduction of the Double Integral to One	30
III. Solution of the Richmond Integral Equation by the Method of Moments	36
Method of Moments	36
General Application	38
Basis Functions	42
Testing Functions and Solution Methods	48
Solution Methods	48

	Page
IV. Programming the Moment Method Solution	51
Machine	52
Program Overview	53
Library Subroutines	57
Functions	57
Integrators	58
Matrix Equation Solvers	60
Input Program	61
Wave Number	61
Matrix Generation and Algebra Solver	66
Algorithm	67
Endpoints	68
Singularity	73
Test Runs	76
Unresolved Problems	77
Radiation Calculation	78
V. Lessons Learned	80
VI. Conclusions	82
Bibliography	84
Appendix A: The Elliptic Coordinate System	89
Appendix B: FUNPACK Release 2	95
Appendix C: Input and Segmentation Program	100
Appendix D: Matrix Program and Linear Algebra Solver.	106
Vita	124

List of Figures

Figure	Page
1. Comparison Between Ideal and Actual Antenna Patterns	2
2. ALR-69 Antenna Location	2
3. ALR-46 Antenna Patterns on B-52	4
4. ALR-46 Location	5
5. GD Proposed Solution	10
6. Dielectric Scatterer	12
7. Elliptic Coordinate System	18
8. Coordinate Systems	20
9. Contour Integration About B	22
10. Notation Associated with a Principal Volume V_{ϵ} Used to Define the Dyadic $\underline{\underline{L}}$	25
11. Notation Associated with a Principle Area A_{ϵ} Used to Define the 2-D Dyadic $\underline{\underline{\ell}}$	26
12. Various Shapes of ΔV for the Calculation of Principle-Volume Integration	32
13. E-plane Radiation Pattern Through a Spherical Radome	34
14. Integration Around the Source Region	34
15. Basis and Testing Functions	46
16. Job Stream on CYBER 175	55
17. Dielectric Slab Waveguide	62
18. Segment (Cell) Length Determination	65
19. Cell Endpoint Determination	66

Figure		Page
20.	Integration Over Cells	69
21.	Current Contribution from Beyond the Line of Symmetry	70
22.	Image Cells	72
23.	Singularity Classes	74
A-1.	Elliptic-Hyperbolic Cylinder Coordinate System	90
A-2.	Angular Coordinates	91

List of Tables

Table		Page
1.	Tabulation of Source Dyadic $\bar{\bar{L}}$, and Correspondence to Previous Authors	27
2.	Tabulation of 2-D Source Dyadic $\bar{\bar{L}}$	28
3.	Discrepancies in $E_c (-j\omega\epsilon_0)$ in the Literature .	31
4.	Moment Method Functional Pairs	49
5.	Program Singularities	73

Abstract

↘ This thesis examines the scattering of cylindrical waves by large dielectric scatterers of elliptic cross section. The solution method was the method of moments using a Galerkin approach. Sinusoidal basis and testing functions were used resulting in a higher convergence rate. The higher rate of convergence made it possible for the program to run on the Aeronautical Systems Division's CYBER computers without any special storage methods.

The program thus developed required very large run times. This makes the program impractical for scatterers of size greater than one wavelength. ↘ This report includes discussion on moment methods, solution of integral equations, and the relationship between the electric field and the source region or self cell singularity. Since the program produced unacceptable run times, no results are contained herein. The importance of this work is the evaluation of the practicality of moment methods using standard techniques. The long run times for a mid-sized scatterer demonstrate the impracticality of moment methods for dielectrics using standard techniques. ↗

SCATTERING OF CYLINDRICAL ELECTRIC
FIELD WAVES FROM AN ELLIPTICAL
DIELECTRIC CYLINDRICAL SHELL

I. Introduction

Background

The radar warning receiver (RWR) on the F-16 is the AN/ALR-69 built by Dalmo Victor Corporation. Its function is to provide warning to the pilot of enemy radar activity. It informs the pilot what the threat is, where it is, and the current threat status (i.e. search, track, missile launch, etc.). The performance of the ALR-69's direction finding (DF) routine is degraded by a side or secondary lobe (SL) located 30° off the forward position opposite to the main or desired lobe [1]. This is associated with the two forward antennas only. Figure 1a is a sketch of the desired pattern. Compare this to Figure 1b which is a sketch of the actual pattern. Figure 2 shows the location of the antennas on the aircraft. The SL causes the DF routine of the RWR's processor to give erroneous indications. As the aircraft approaches the threat emitter, the RWR compares the received relative signal strength from each of the antennas. The threat is displayed on the side of the aircraft that received the

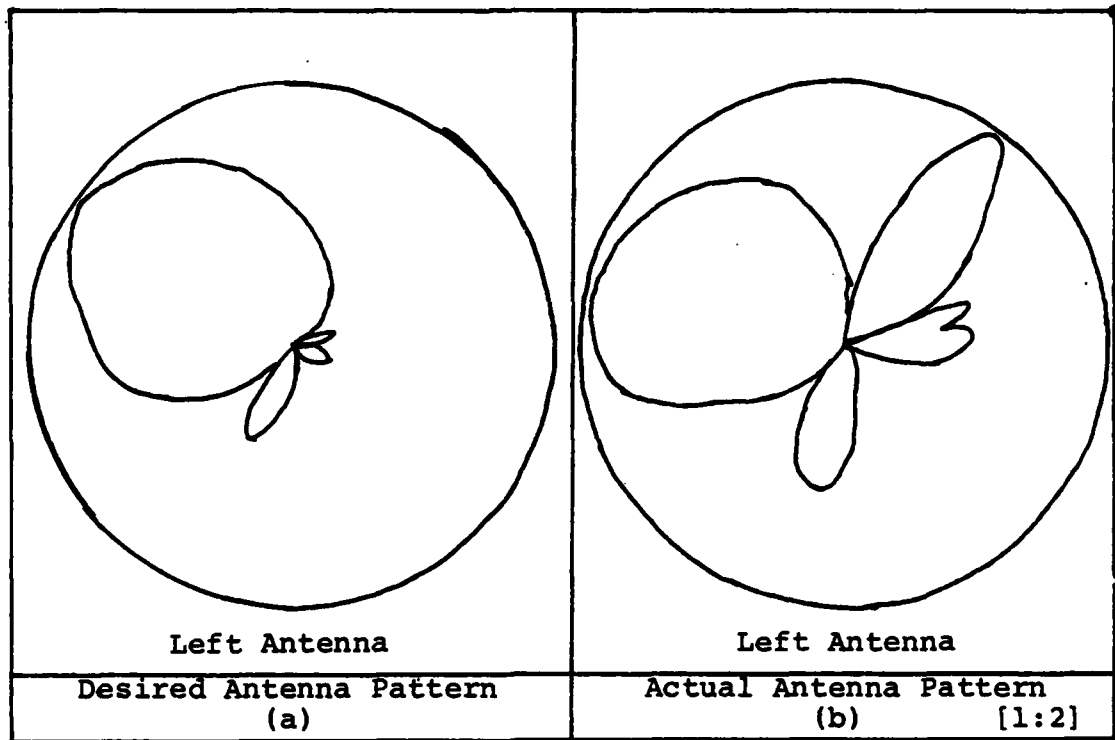


Figure 1. Comparison Between Ideal and Actual Antenna Patterns

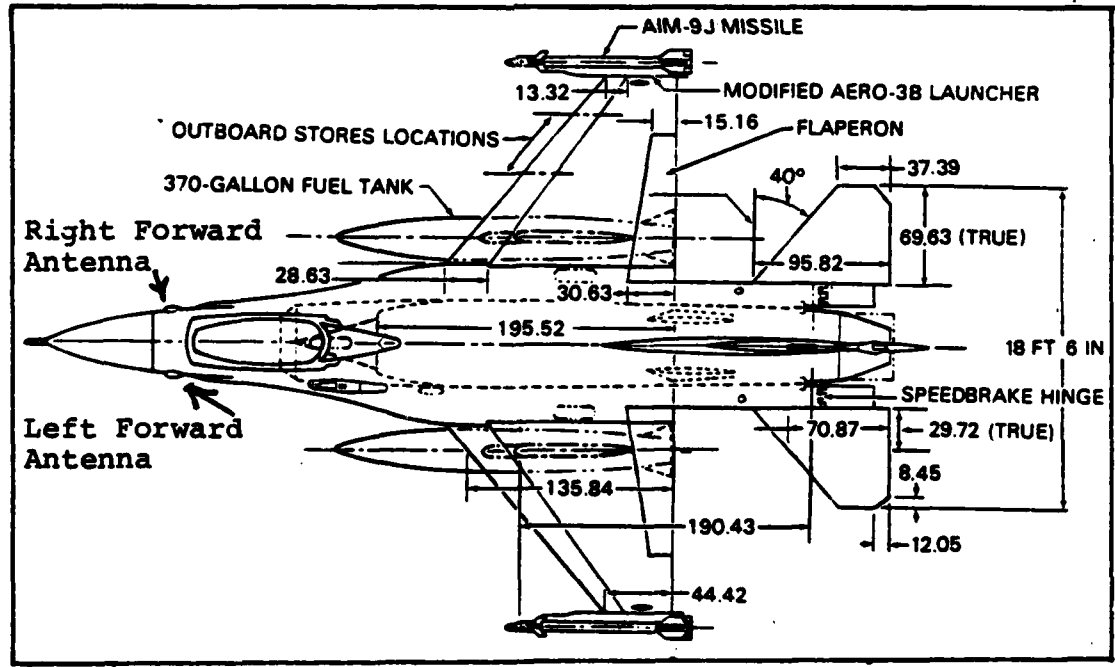


Figure 2. ALR-69 Antenna Location [41:2-2]

stronger signal. However, due to the secondary lobe several events may occur:

1. Both antennas receive the signal equally well; put the threat in front of the aircraft.

2. Both antennas receive the signal equally well; the RWR can't decide where to put the threat and the result is:

a. Displays the threat location correctly,
b. Displays the threat on the wrong side, or
c. Displays "flip-flops" around to both sides of the aircraft.

3. One antenna receives the signal better; displays the threat on that side of the aircraft which may or may not be the correct side.

Flight tests run by the Tactical Air Warfare Center at Eglin Air Force Base have verified condition 3 in that the threat was displayed on the wrong side, the display "wandered" around on the screen, and then jumped to the correct side as the aircraft passed by the target [2].

Rationale

This situation must be corrected since it affects the ability of the F-16 to perform its mission. All threats identified forward of the aircraft are suspect as far as their location since it is impossible to tell if the signal is being picked up by the main or secondary lobe. The pilot is not able to determine where the threat

is, and he has no idea what maneuver to take when approached by a threat. With the speed of the F-16 and the speed of an approaching aircraft or surface-to-air missile, indecision could result in lost aircraft and lives. It should be noted that this condition has been found with other aircraft RWR systems as well. Figure 3 is a sketch of the antenna pattern for the forward RWR antennas of the B-52 AN/ALR-46 [3]. Figure 4 shows their position on the aircraft. The ALR-46 uses the same antennas as the ALR-69.

It is also well to note that the ALR-69 is used on the A-10 aircraft. In this case there is no side lobe.

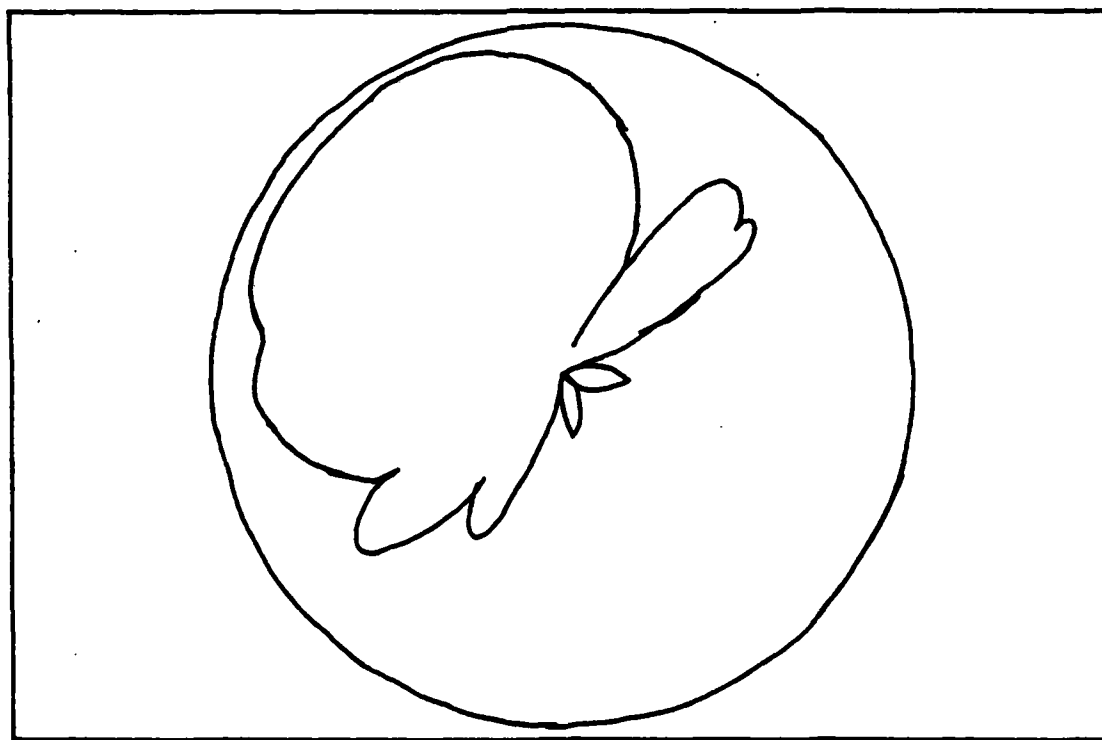


Figure 3. ALR-46 Antenna Patterns on B-52 [3]

The A-10 has a metallic nose cone. If the mechanism of the side lobe can be understood, changes could be made to correct this problem on the F-16, B-52, and on future weapon systems.

Literature Review

The majority of literature on scattering by dielectric objects concerns the scattering of plane waves with either ice crystals and water droplets (meteorological

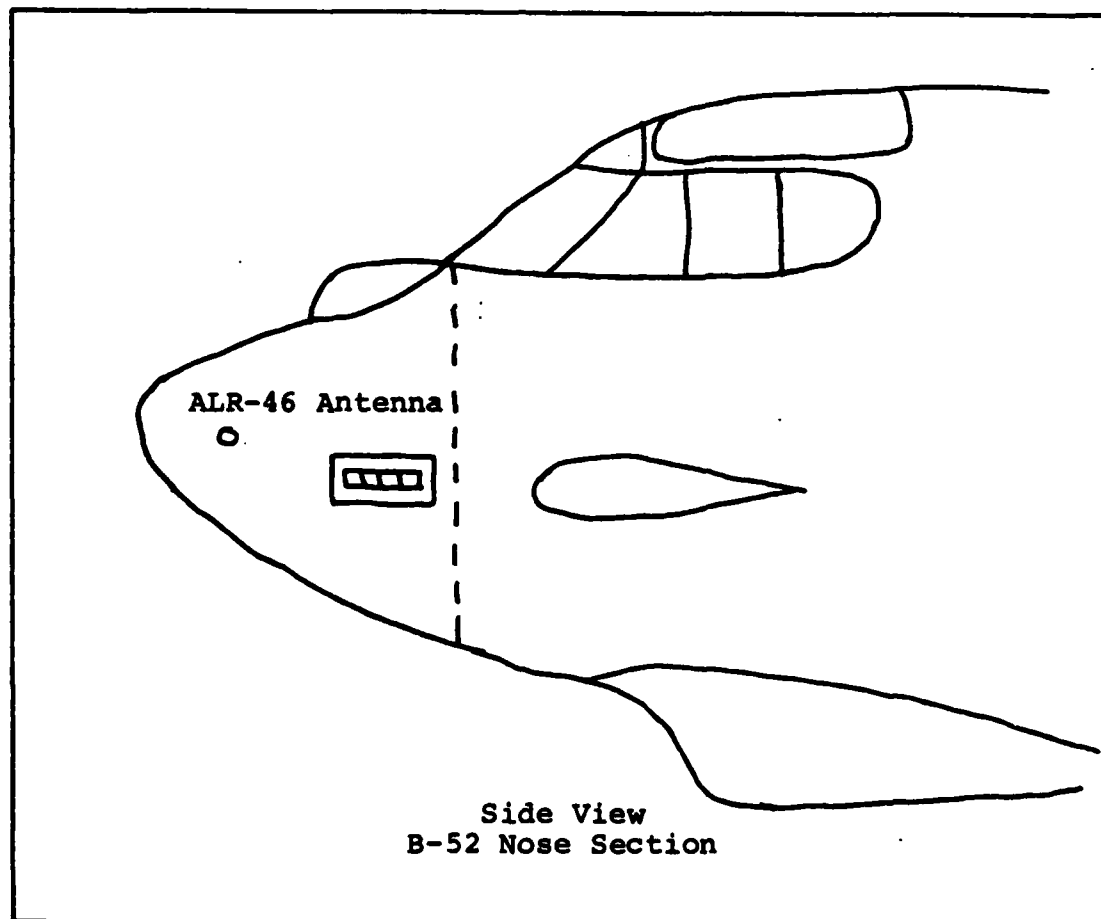


Figure 4. ALR-46 Antenna Location

interference with radar or data links) [6] or biological tissue (affects of microwaves on humans) [7]. Holt, Uzunoglu, and Evans were concerned with the meteorological scattering. They developed an integral equation of the Fredholm type directly from Maxwell's equation without reference to the scatterer [6]. The equation developed was a general second kind integral equation with a singular kernel. The singularity was removed by the use of a transform function. The result is a pair of coupled integral equations that were solved by numerical quadrature, which produced a numerically stable linear algebra equation, assuring convergence.

The disadvantage of this procedure is that now there are two equations to solve. The storage requirements and the computational time increase rapidly as the size of the scatterer becomes large.

Another method discussed was a finite element method known as the "Unimoment Method" [8; 9]. The unimoment method offers the ability to apply the radiation condition without the use of complicated programming procedures as required in the past use of finite element methods. Chang and Mei's procedure also reduces the storage requirements, when compared to past finite element programs [9:761].

Chang and Mei essentially solved the problem using the T-matrix procedure. After creating the artificial boundary outside the scatterer, the interior problem is

solved using the finite element method. The field between the artificial and the actual boundary is approximated by linear combinations of functions which satisfy the Helmholtz wave equation. Chang and Mei used the Fourier series [8:36]. The exterior fields were expanded in terms of Hankel functions.

While this procedure does offer advantages by separating the interior and exterior problems, for large scatterers a significant algebraic equation still must be solved. Thus this method will only handle up to moderately sized scatterers without taking considerable time and storage resources.

The standard method used in the past has been the method of moments. Richmond [10] used this technique in solving the problem of scattering from infinitely long dielectric shells. The integral equation is generated by examining the polarization current that results when the scatterer is illuminated by the incident field. The unknown electric field is expanded in terms of pulse functions.

Since Richmond subdivided the shell into cells that were approximately square, integration over each cell, including the self cell, could be accomplished analytically. The cells were approximated by circles with a radius of half the length of the cell.

The ability to analytically solve the integration over circular cells forces the shell wall to be thin. If

the wall is thicker, assumptions will have to be made concerning the electric field in the shell. Using Richmond's procedure, the electric field is assumed to be constant over a cell. For anything very large, this would require large amounts of storage and computational time.

It is possible to solve this scattering problem in terms of orthogonal functions such as Bessel functions for circular cylinders or Legendre polynomials for spherical objects. In the elliptic cylinder, the resultant functions are Mathieu functions. There is not, however, a closed form solution to the problem. Dr. Cavour W. H. Yeh has done considerable work with scattering and traveling wave problems in connection with elliptic shapes. In each case. Dr. Yeh presented a solution in terms of Mathieu functions.

In a study of sound waves scattering from penetrable objects, plane waves were incident on to an ellipse at different aspect angles [11]. The resultant patterns contained side lobes that would move as the angle of incidence changed.

The primary difficulty with this type of approach is the Mathieu functions. Currently a library does not exist on the base cyber computer facility for generating Mathieu functions.

Previous Work

Experimental [1; 2]. General Dynamics, the manufacturer of the F-16, attempted to remove the side lobe through trial and error. They moved the antennas, the radome, added material to the radome, the airframe, etc. It was through this work that some important information was obtained.

1. The SL is due to the presence of the radome. When the radome was removed, the side lobe disappeared [1:6].

2. The SL is not due to the metal/dielectric boundary between the airframe and the radome. The radome was moved away from the airframe by a small amount. This introduced a new boundary layer (metal airframe, air, radome material) and the lobe became larger [2].

3. The SL is not being diffracted or scattered by the dielectric/metal boundary. The RWR antennas were moved up to the radome, removing the break between the radome and the airframe. The results did not change [2]. General Dynamics was able to reduce the magnitude of the SL by adding radar absorbing material (RAM) to the airframe. Figure 5 shows the amount of reduction [1:5] and the location of the RAM.

Theoretical. Schneider [4] modeled the radius of curvature of the radome. He used a circular cylinder large enough so that the curvature of the cylinder would come

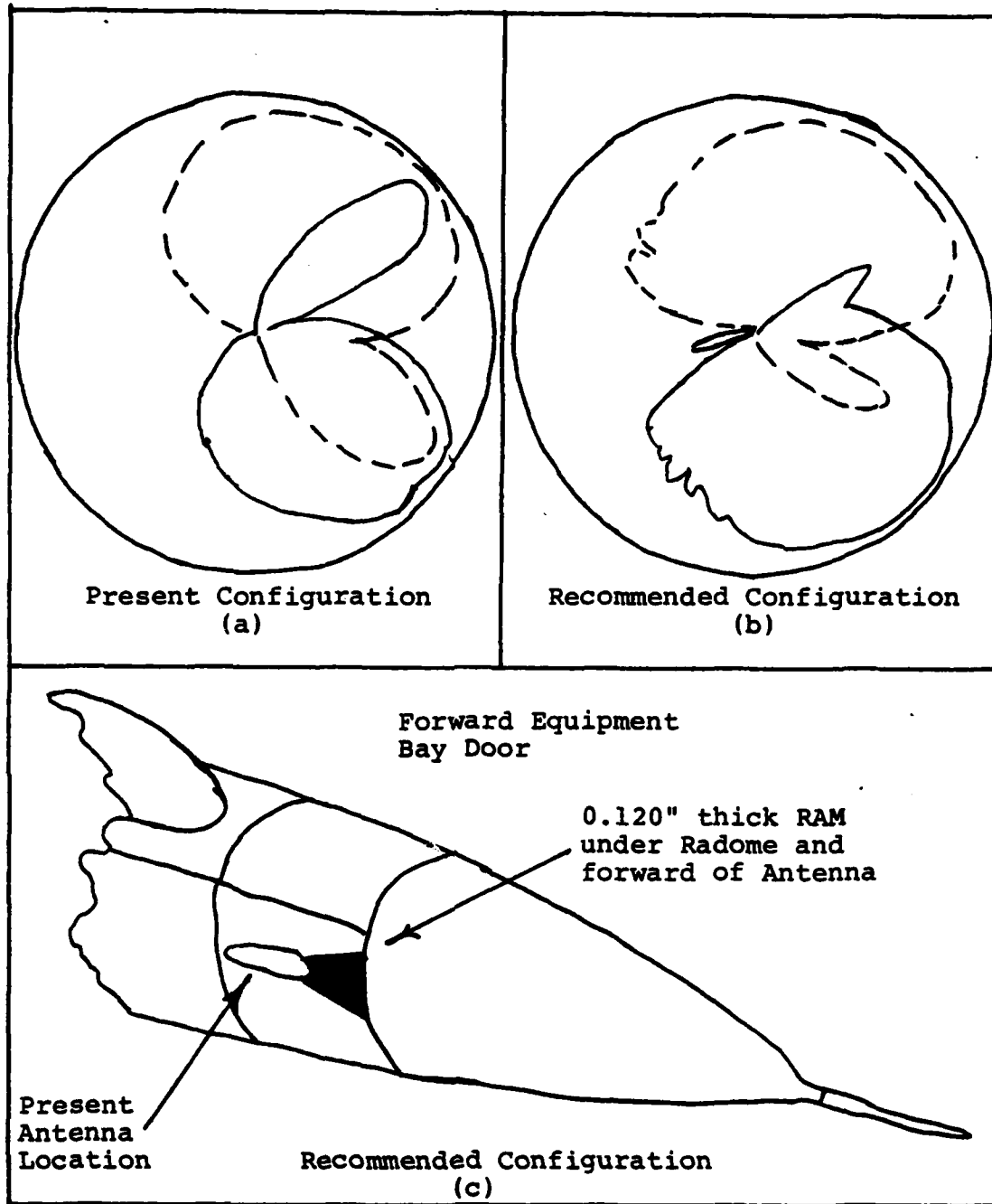


Figure 5. GD Proposed Solution [1:6]

close to the curvature of the F-16 radome [4:5,35,37] [5].¹ This model results in a large radius (60 wavelengths) [4:2,35,37]. Schneider used two methods, a series solution and a numerical approximation, to solve the boundary value problem.

In either method, Schneider was unable to reproduce the SL. He was hampered by a small computer solving the large matrix (3700 x 3700 elements) that resulted from applying point matching with the moment method. Therefore, he presented results good only for the cylinder with radii of 0.6 and 6.0 wavelengths [4:31,32; Appendix E]. The series solution for the 60 wavelength scatterer was calculated, but the validity of the results is questionable since deep nulls down to zero appear in the plots, and the normalized maximums never go up to one [4:29,30]. Schneider admits that there is an error in the series solution where the coefficient of one term is half of the correct value [3:ii,iii]. This error will effect the 60 wavelength plot and may account for the deep nulls and low peak values.

Proposed Solution

This paper will present a discussion on the scattering of cylindrical waves from a large dielectric

¹Note that this differs from the model used in this thesis. In this work, the radome is being modeled as an elliptic cylinder. Schneider modeled the curvature of the radome.

scatterer. The scatterer will be an infinitely long, cylindrical shell with an elliptic cross section (see Figure 6). This is an improvement over Schneider's model in that: (1) the ellipse represents a closer approximation to the F-16 radome, and (2) the ellipse has a much higher

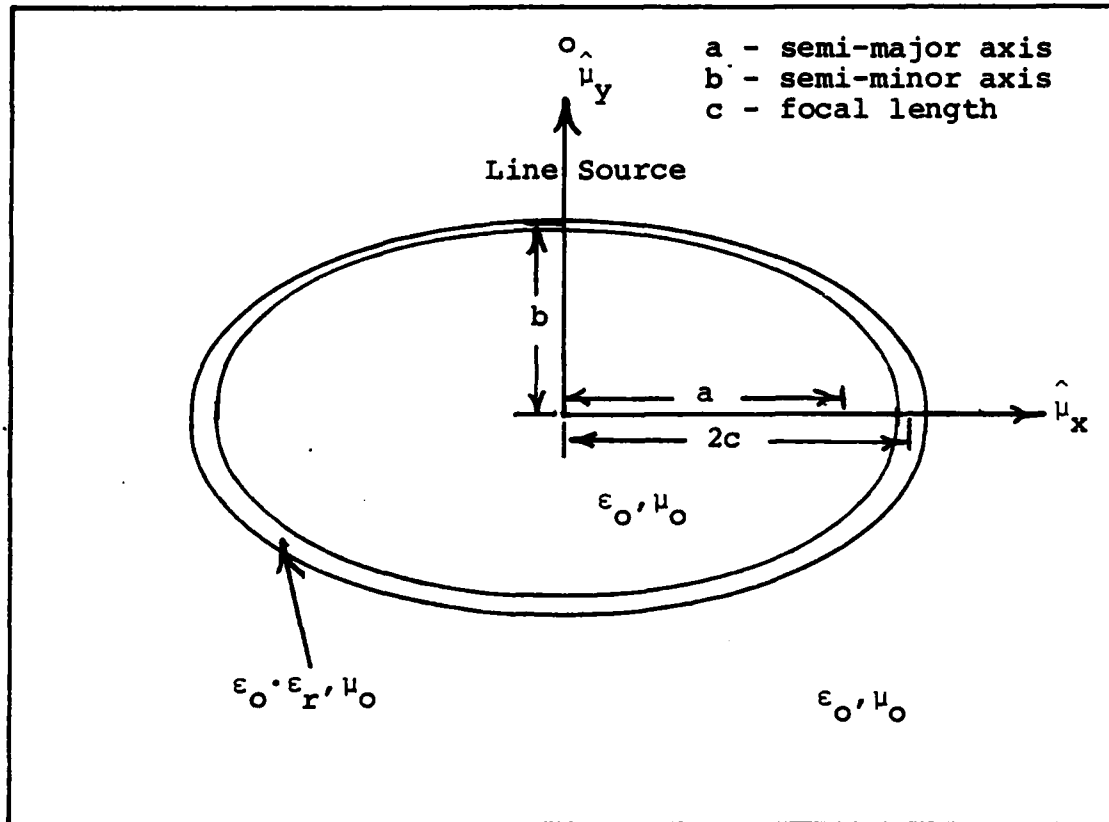


Figure 6. Dielectric Scatterer

rate of curvature toward the tip of the surface. The increased curvature around the tip of the ellipse will cause the scattered wave to be "thrown" in a particular direction. This hypothesis was suggested by the work done by Chang and Mei [8:41] and by Poggio and Miller [12:210].

To solve the integral equation, the method of moments will be used. Harrington [13], and Stutzman and Thiele [14:306-372], provide discussion for application of the procedure.

Assumptions

In doing this work it was assumed that the radome could be modeled apart from the metal airframe. This assumption was suggested by the General Dynamics study [1]. It was assumed that the thickness of the dielectric shell is thin when compared to wavelength. This will simplify the numerical analysis and is consistent with Schneider's work [4:28].

Scope

This study is a theoretical study which is almost entirely removed from the actual problem except for the dimensional data and the basis for the models. The problem will be limited to the two-dimensional case only. This will not affect the results since the actual antennas are coplanar. There will be no attempt made to solve the lobe problem. The goal is to obtain polar plots of the total electric field to see if the side lobe is caused by scattering. The real need is to understand what is taking place as the electromagnetic fields cross the boundary of free space and the dielectric shell.

II. Development of a One-dimensional Fredholm Integral Equation of the Second Kind

Solving the problem using moment methods requires the derivation of an integral equation. The equation used herein was developed by Richmond [10:335-336], extended to elliptic cylinder coordinates. Considerable difficulty was encountered with the reduction from an area integral to a line integral. This was further compounded by the singularity of the kernel. This discussion will include a description of the model, the Richmond integral equation (IE) in elliptic coordinates, the handling of the singularity, and the reduction of the IE to a line integral. Appendix A provides further insight into the coordinate system.

Model

Figure 6 is a diagram of the elliptic scatterer. The shell of the ellipse is 0.05 wavelengths thick. This value was chosen to insure applicability of the thin shell approximation and to be consistent with Schneider's work [4:28]. In elliptic coordinates the thickness must be defined as a dimensionless quantity to be consistent with the elliptical coordinate μ . Let the thickness of the shell be defined as τ . If μ_0 defined the mid-radii, then the outer wall of the cylinder is $\mu_0 + \tau/2$ and the inner

is $\mu_0 - \tau/2$. From Appendix A, when $\nu = 90^\circ$, $b = c \sinh \mu$. This means that for the inner and outer walls,

$$b - T/2 = c \sinh (\mu_0 - \tau/2) \quad (2.1a)$$

$$b + T/2 = c \sinh (\mu_0 + \tau/2) \quad (2.1b)$$

Solving for the arguments of the hyperbolic sines and subtracting (a) from (b), the result is

$$\tau = \sinh^{-1} \left(\frac{b + T/2}{c} \right) - \sinh^{-1} \left(\frac{b - T/2}{c} \right) \quad (2.2)$$

Expanding the arguments of (2.2) in a Taylor series about T and taking the small argument approximation of the inverse hyperbolic sine,

$$\tau \approx \frac{T/c}{\sqrt{1 + (b/c)^2}} \quad (2.3)$$

or

$$\tau \approx T/a$$

since $c^2 = a^2 - b^2$ and a , b , and c are large when compared to T , τ , and λ . This development was due to Johnson [15].

When making reference to a dimension (i.e., a or b), it will be done with reference to an ellipse drawn through the center of the shell. It is assumed that the thickness is constant for all 360° and that the focal length is the same for the inner, middle and outer radii. The error

introduced by this assumption is small since the shell is thin.

To insure a two-dimensional case, the shell and current sources are infinitely long in both the +/-z directions. The relative permeability is constant for all positions in the shell. The value for ϵ_r is four. This will not be altered in the ensuing programming. The dielectric is perfect and no losses will be accounted for. The line source is infinitesimally thin and has no losses.

Richmond Integral Equation

The equation developed by Richmond is applicable since the scatterer is a dielectric cylindrical shell. The equation, used by Schneider for moderately sized scatterers [4:14,20], is

$$\bar{E}^i(x,y) = \bar{E}(x,y) + \frac{jk^2}{4} \iint_{s'} (\epsilon_r - 1) \bar{E}(x',y') \cdot H_0^{(2)}(k\rho) dx' dy' \quad (2.4)$$

[10:336]

where

$$\bar{E}(x,y) = \bar{E}^i + \bar{E}^s$$

$$\bar{E}^i(x,y) = \frac{-k_0^2 I}{4\omega\epsilon} H_0^{(2)}(k\rho) \bar{u}_z \quad [16:224]$$

The superscript i and s signify the incident and scattered field, respectively. The primed terms are the source terms on the shell. Due to the shape of the scatterer, the use of the more widely understood polar cylindrical

coordinate system could not be used. It was too cumbersome to describe the angle-dependent radii that is present in an ellipse. Therefore, the Richmond IE was converted to the elliptical cylindrical coordinate system.

Elliptic Coordinates. The elliptic cylindrical coordinate system describes one of two conic sections, depending on which of the two coplanar parameters is held constant. As Figure 7 indicates, if the angular coordinate, ν , is constant, the surface is a hyperbolic cylinder. If μ is constant, an elliptic cylinder results. The angle ν describes the angle of the asymptote of the hyperbola that intersects the point in question. It can easily be shown that the relation between the polar and elliptical angles is

$$\phi = \tan^{-1} [(b/a) \tan \nu] \quad (2.5)$$

The range of ν is from 0 to 360° and the range of μ is from 0 to ∞ . The definition of μ ,

$$\mu = \tanh^{-1}(b/a) = \cosh^{-1}(a/c) = \sinh^{-1}(b/c) \quad (2.6)$$

blows up when the ratio of a to b is one (or c is 0). See Appendix A for a more detailed description of the coordinate system.

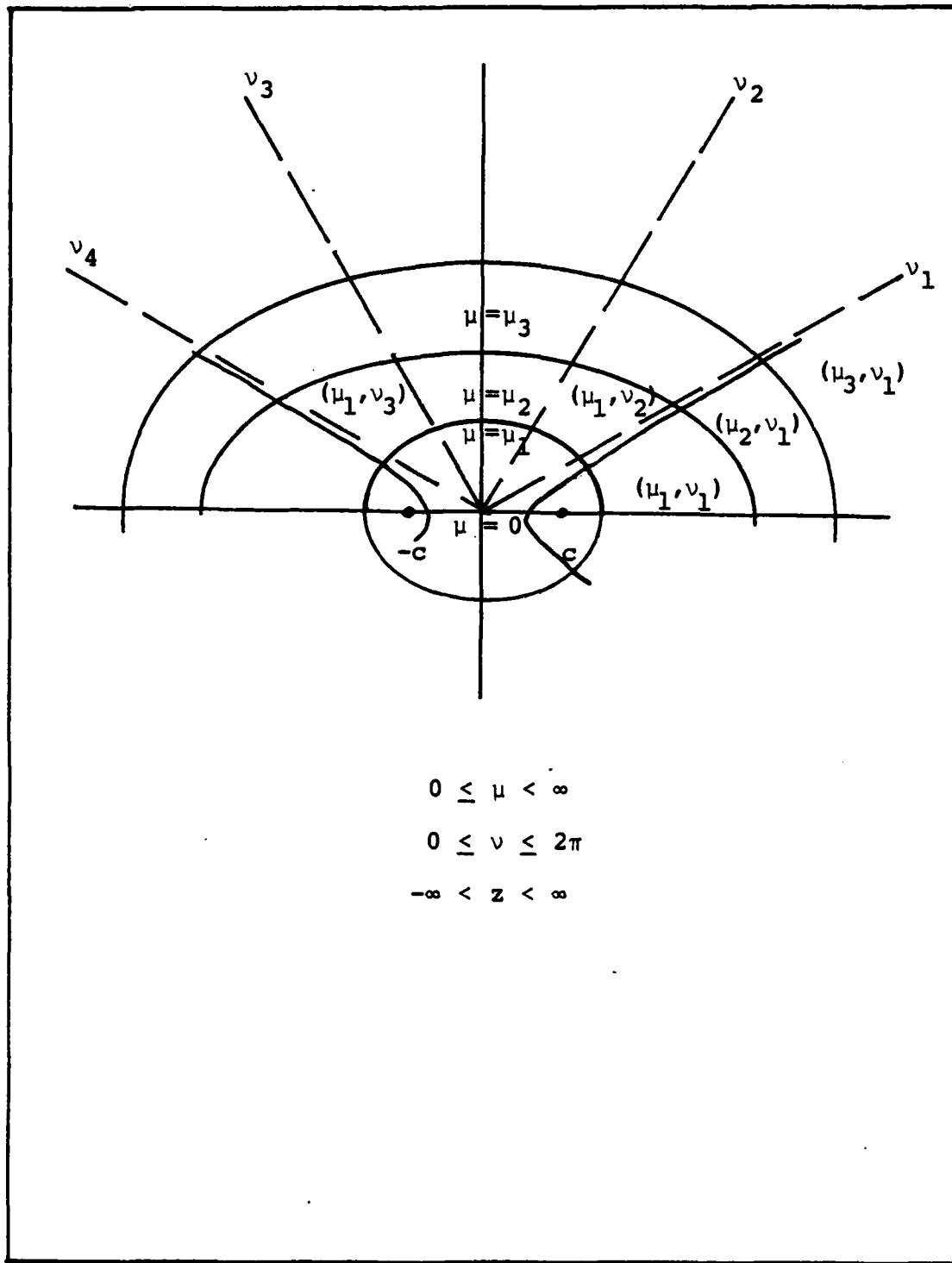


Figure 7. Elliptic Coordinate System

The differential area functions for elliptic coordinates are

$$dA = c^2 \cdot \left\{ \begin{array}{l} \cosh^2 \mu - \cos^2 \nu \\ \sinh^2 \mu + \sin^2 \nu \end{array} \right\} d\mu d\nu \quad (2.7)$$

Both of these expressions are equivalent. Using (2.7) with (2.4), the Richmond IE in elliptic coordinates becomes

$$\begin{aligned} \bar{E}^i(\mu, \nu) = \bar{E}(\mu, \nu) + \frac{j3k^2 c^2}{4} \iint_{S'} \bar{E}(\mu', \nu') H_0^{(2)}(k\rho) \\ \cdot (\cosh^2 \mu' - \cos^2 \nu') d\mu' d\nu' \end{aligned} \quad (2.8)$$

Note that the c^2 term from the differential area function has been pulled out of the integral as well as the $\epsilon_r - 1$ term.

The Singular Kernel

Since the unknown electric field is both part of the kernel and the separate function, the equation is a Fredholm Integral Equation of the second kind (FIE II). The equation accounts for the interaction between the line source and a point on the shell, and it accounts for the interaction between that point and the rest of the points on the shell. There are essentially two coordinate systems within the framework of the problem. Figure 8a shows the coordinate system for which the line source is considered the source point and the shell is considered the observation point. In Figure 8b the point indicated in Figure 8a

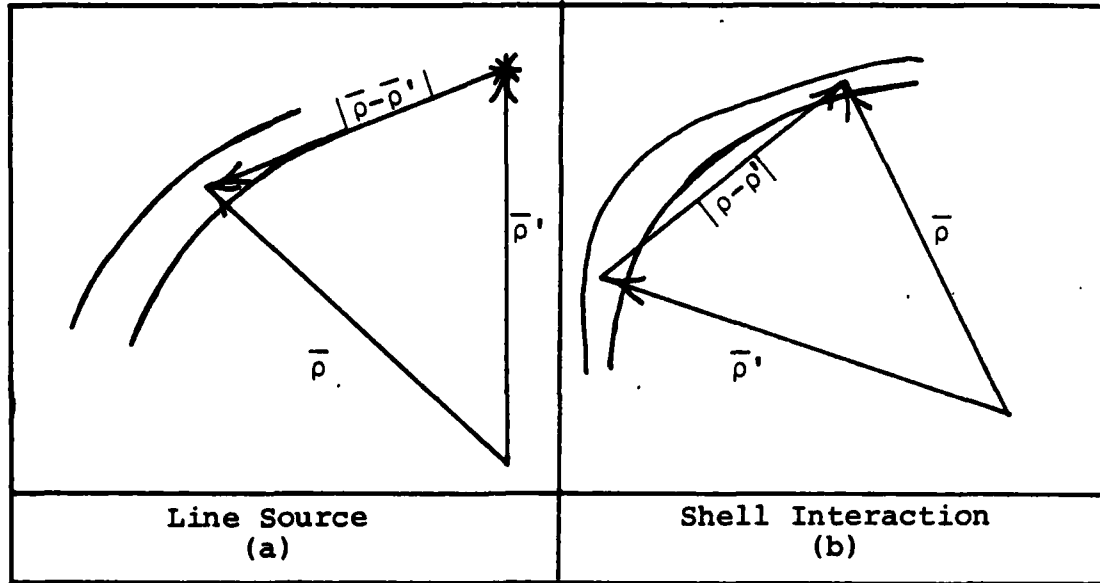


Figure 8. Coordinate Systems

is now the source point and the observation point is any point on the shell including the source point itself. As the electric field from the line sources contacts the scatterer, a polarization current is induced. This current reradiates the incident field as the scattered field which in turn reacts with the other points on the ellipse. Each point on the scatterer is affected by two electric fields; the incident field from the line sources and the scattered field from the rest of the shell.

The problem in the mathematical analysis of (2.8) is the consideration of the interaction between a point on the shell with itself. This point on the shell, known as the source region or the self cell, causes the Hankel function of (2.8) to blow up as kp goes to zero. The source region interaction with itself must be considered for

this may make a non-neglectable contribution to the total field.

The contribution of the self cell is done by the determination of a correction term. This correction term accounts for the electric field generated at the source region. Chen discussed the source region in terms of the tensor Green's function [17:1201-1204]. In a volume the electric field is determined at an arbitrary point outside the source region by

$$\bar{E}(r_1) = \iiint_{V'} \bar{G}(r_1, r) \cdot \bar{J}(r) dv \quad (2.9)$$

where

$$\bar{G}(r_1, r) = j\omega\mu \left[\bar{I} + \frac{\nabla\nabla}{k_0^2} \right] \phi(r_1, r)$$

$$\phi(r_1, r) = \frac{1}{4\pi|\bar{r}_1 - \bar{r}|} e^{-jk_0|\bar{r}_1 - \bar{r}|}$$

\bar{G} is the tensor Green's function,

\bar{I} is the unit dyadic, and

ϕ is the free space scalar Green's function.

Accounting for the source region (2.9) becomes

$$\bar{E}(r_0) = PV \int_V \bar{G}(r_0, r) \cdot \bar{J}(r) dv + \bar{E}_c(r_0) \quad (2.10)$$

where the "PV" denotes the principal value (PV) integral and $E_c(r_0)$ is the correction term for the source region.

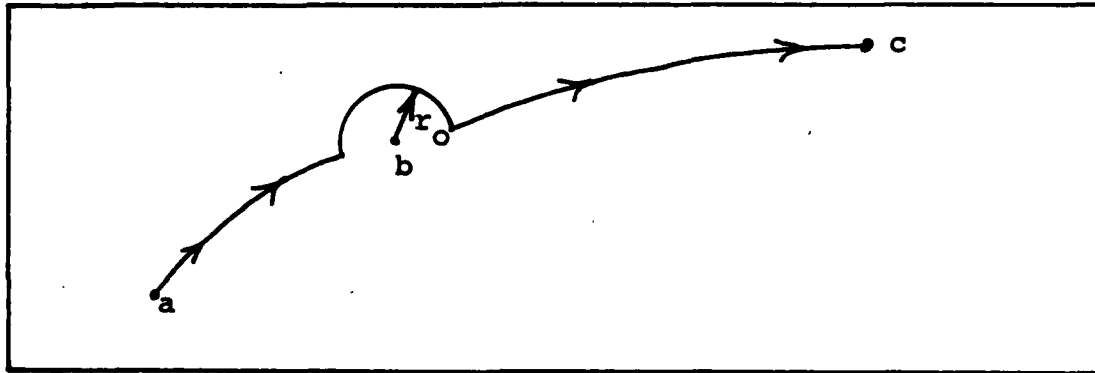


Figure 9. Contour Integration About B

Principal Value Integral. Before discussing the determination of the electric field correction term, it would be prudent to define the principal value (or the Cauchy principal value) integral. The principal value (PV) integral of $f(x)$ over $[a,c]$ when $f(x)$ is singular at $x = b$ is defined as

$$PV \int_a^c f(x) dx = \lim_{r \rightarrow 0} \left[\int_a^{b-r} f(x) dx + \int_{b+r}^c f(x) dx \right] \quad (2.11)$$

provided the limit exists [18:195]. Essentially, the PV integral is an integral taken across the interval excluding the point of singularity. At that point a contour (or area or sphere) is taken around the singularity. The radius of that contour, r , is then allowed to approach zero (see Figure 9). The correction term is the field from across the excluded contour. The two-dimensional case involves a circular area and the three-dimensional case a spherical volume around the point.

The requirement that the limit exist is met in the case of the Hankel function. According to A. N. Tychonov, the improper integral

$$\iiint \frac{c}{r^\alpha} dv \quad (2.12a)$$

does converge as long as $\alpha < 3$ [19:294]. In the two-dimensional case, the integral converges for $\alpha < 2$. The Hankel function is singular as $\ln |r|$. However, $1/r$ is more singular than $\ln |r|$. Therefore, the area integral of the Hankel function exists.

Determination of the Correction Term. The value of $E_c(r_0)$ is a function of the shape of the volume excluded in the integral evaluation. In calculating E_c , Chen determined the surface charge density using conservation of charge. The electric field can then be determined by the gradient of the potential due to the surface charge.

$$\bar{E}_c(r_0) = -\nabla\phi \quad (2.12b)$$

Yaghjian presented a complete discussion of the determination of the Green's function in NBS Technical Note 1000, A Direct Approach to the Derivation of Electric Dyadic Green's Functions [20]. This approach does not utilize delta-function techniques, but determined a generalized electric dyadic Green's function which is valid in the source region. Yaghjian provided a table of the

correction terms for various principal value geometries.

He determined the correction factor in terms of

$$\bar{L} = \frac{1}{4\pi} \int_{S_\epsilon} \frac{\hat{n}' \hat{e}_{R'}}{R'^2} ds' \quad [20:56] \quad (2.13a)$$

(See Figure 10.)

In the two-dimensional case the correction term becomes

$$\bar{\ell} = \frac{1}{2\pi} \int_{C_\epsilon} \frac{\hat{n}' \hat{e}_{T'}}{T} dc' \quad [20:59] \quad (2.13b)$$

(See Figure 11.)

There the electric field is now determined by equation

(2.14).

$$\bar{E}(\bar{r}) = j\omega\mu_0 \lim_{V_\epsilon \rightarrow 0} \int_{V_J - V_\epsilon} \bar{G} \cdot \bar{J} dv' + \frac{\bar{L} \cdot \bar{J}}{j\omega\epsilon_0} \quad [20:12] \quad (2.14)$$

Or, in the two-dimensional case

$$\bar{E}(\bar{r}) = j\omega\mu_0 \lim_{A_\epsilon \rightarrow 0} \int_{A_J - A_\epsilon} \bar{G} \cdot \bar{J} dA' + \frac{\bar{\ell} \cdot \bar{J}}{j\omega\epsilon_0} \quad [20:40] \quad (2.15)$$

In (2.14) and (2.15), the $V_J - V_\epsilon$ and $A_J - A_\epsilon$ represent the integral excluding the source region, i.e. the principal value integral.

Tables 1 and 2 present correction terms for various principal geometries. The reader is encouraged to read NBS Technical Note 1000 for further insight into this problem.

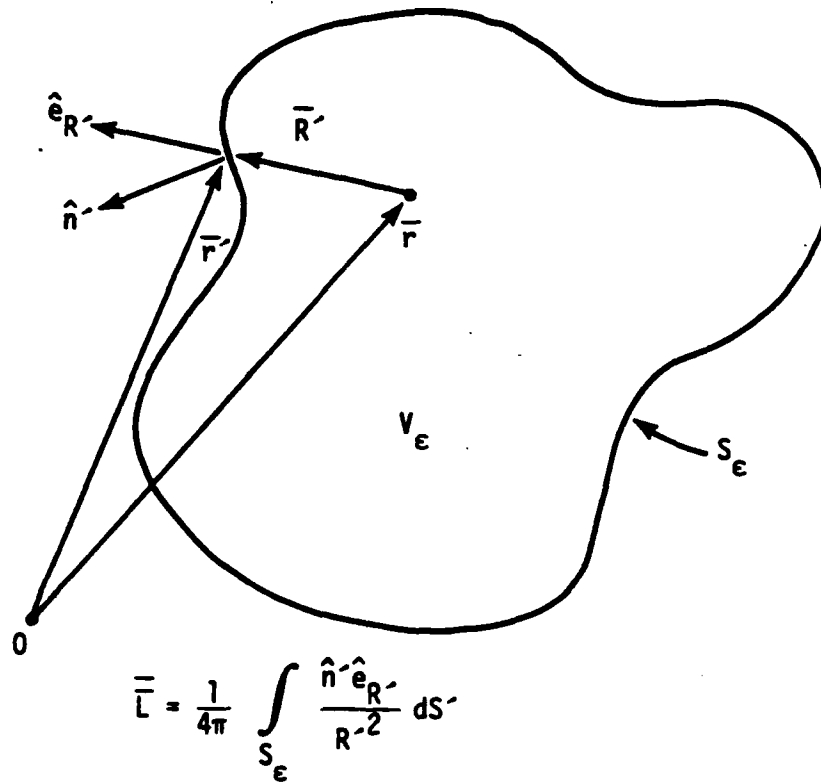
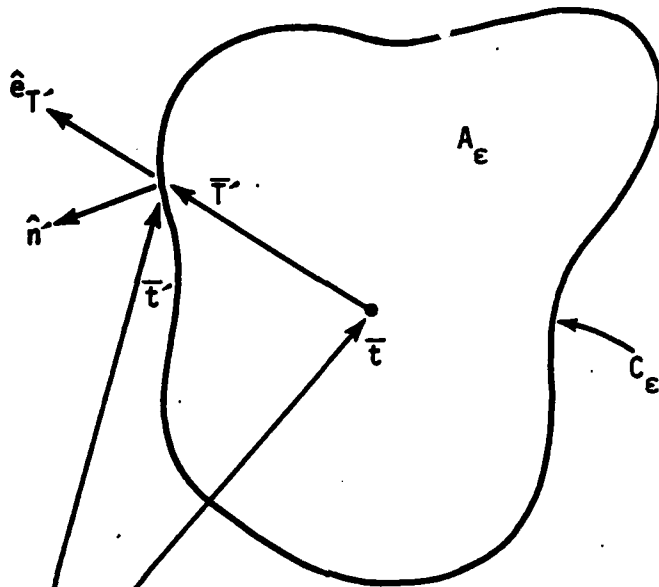


Figure 10. Notation Associated with a Principal Volume V_ϵ Used to Define the Dyadic \bar{L} [20:56]



$$\bar{\bar{\lambda}} = \frac{1}{2\pi} \int_{C_\epsilon} \frac{\hat{n} \hat{e}_T}{r} dc$$

Figure 11. Notation Associated with a Principle Area A_ϵ Used to Define the 2-D Dyadic $\bar{\bar{\lambda}}$ [20:59]

Table 1. Tabulation of Source Dyadic $\bar{\bar{L}}$, and Correspondence to Previous Authors [20:60]

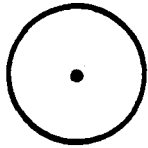
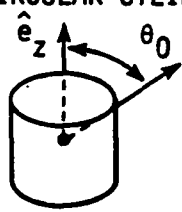
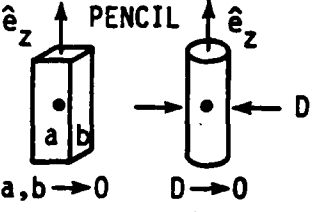
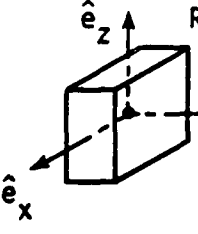
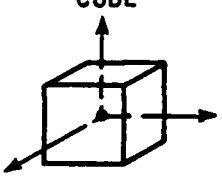
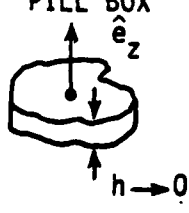
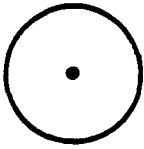
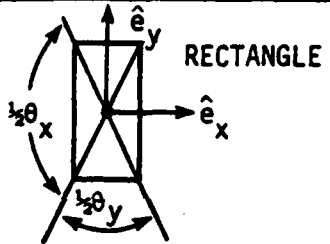
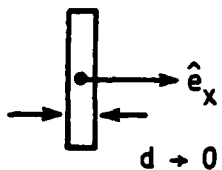
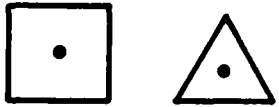
PRINCIPLE VOLUME (\bar{r} AT CENTER)	$\bar{\bar{L}}$	PROBLEM & AUTHOR(S)
<p>SPHERE</p> 	$\frac{\bar{\bar{I}}}{3}$	<p><u>FREE-SPACE</u></p> <p>WILCOX (1957) VANBLADEL (1961)</p>
<p>RIGHT CIRCULAR CYLINDER</p> 	$(1 - \cos \theta_0) \hat{e}_z \hat{e}_z + \frac{1}{2} \cos \theta_0 \bar{\bar{I}}_t$	
<p>CIRCULAR OR SQUARE PENCIL</p> 	$\frac{\bar{\bar{I}}_t}{2}$	
<p>RECTANGULAR BOX</p> 	$\frac{1}{4\pi} (\Omega_x \hat{e}_x \hat{e}_x + \Omega_y \hat{e}_y \hat{e}_y + \Omega_z \hat{e}_z \hat{e}_z) \quad (\Omega_x + \Omega_y + \Omega_z = 4\pi)$ <p>$\Omega_x, \Omega_y,$ AND Ω_z ARE TWICE THE SOLID ANGLE SUBTENDED BY A SIDE \perp TO THE x, y, and z, DIRECTION RESPECTIVELY.</p>	
<p>CUBE</p> 	$\frac{\bar{\bar{I}}}{3}$	<p><u>RECTANGULAR CAVITY</u></p> <p>RAHMAT-SAMII (1975)</p>
<p>PILL BOX</p> 	$\hat{e}_z \hat{e}_z$	<p><u>RECTANGULAR WAVEGUIDE AND CAVITY</u></p> <p>TAI (1973, 1976)</p> <p><u>WAVEGUIDE ONLY</u></p> <p>COLLIN (1973) RAHMAT-SAMII (1975)</p>

Table 2. Tabulation of 2-D Source Dyadic $\overline{\overline{\ell}}$ [20:61]

PRINCIPAL AREA ($\overline{\overline{\ell}}$ AT CENTER)	$\overline{\overline{\ell}}$
<p style="text-align: center;">CIRCLE</p> 	$\frac{\overline{\overline{I}}_t}{2}$
<p style="text-align: center;">RECTANGLE</p> 	$\frac{1}{2\pi}(\theta_x \hat{e}_x \hat{e}_x + \theta_y \hat{e}_y \hat{e}_y)$ $(\theta_x + \theta_y = 2\pi)$
<p style="text-align: center;">SLIT</p> 	$\hat{e}_x \hat{e}_x$
<p style="text-align: center;">SQUARE AND EQUILATERAL TRIANGLE</p> 	$\frac{\overline{\overline{I}}_t}{2}$

In the two-dimensional case, if the electric field is aligned with the vector of infinite length (i.e. the z axis in this case), then the electric field is determined by

$$E_{(z)}(\mathbf{r}) = \frac{-\omega\mu_0}{4} \int_{A_J - A_\delta} H_0^{(2)}(|\bar{\mathbf{r}} - \bar{\mathbf{r}}'|) J_z(\bar{\mathbf{r}}) dA' \quad [21:261] \quad (2.16)$$

and the correction term is zero. This is easily seen via Chen's approach since the surface current distribution is zero in this configuration since the normal is orthogonal to $\bar{\mathbf{J}}$. For example, for the finite cylinder, the current distribution is only across the top and bottom caps of the cylinder [17:1203]. In the two-dimensional case, the top and bottom of the cylinder are at $\pm\infty$, and make no contribution to the field. Looking at the integral that Richmond evaluated in closed form for the self cell [10:336]; for the case where $n = m$, Richmond determined that the self cell integral of the Hanlel function was

$$\int_{\text{cell}}^{2\pi} \int_n^a H_0^{(2)}(ka) \sin\phi' d\phi' = j/2(\pi ka H_1^2(ka) - 2j) \quad (2.17)$$

Richmond had approximated the square cells with circular cells of radius a . If a is allowed to go to zero, then the value of the integral goes to zero. This was verified with Bessel tables and a hand calculator. In Richmond's formulation, there was no PV integral;

therefore, a has a finite value and the source region ($m = n$ cell) had to be calculated.

It would be well to note that not all of the literature agree in the calculation of the correction term. J. J. H. Wang compiled a list of discrepancies [30:3-1]. Table 3 and Figure 12 list his results. Since there is no correction term involved in the two-dimensional case, this does not impact in this work.

Reduction of the Double Integral to One

According to what has just been discussed, the principal value integral can be taken over the shell without any major difficulty. It would simplify the solving of the integral equation if it could be reduced to a single integral.

The integral in (2.8) is repeated in expression (2.18).

$$\lambda_F \text{ PV} \int_0^{2\pi} \int_{\mu_0^{-\tau/2}}^{\mu_0^{+\tau/2}} \bar{E}(\mu', \nu') H_0^{(2)}(k\rho) \cdot (\cosh^2 \mu' - \cos^2 \nu') d\mu' d\nu' \quad (2.18)$$

where

$$\lambda_F = \frac{jk^2 c^2}{4}$$

ρ = distance function between two points in elliptic coordinates

Table 3. Discrepancies in E_c ($-j\omega\epsilon_0$) in the Literature [30:10]

Boundary	Principal Volume ΔV^*	Yaghjian	Chen	Tai	Rahmat-Samii	Collin
Free Space	Sphere	$\underline{J}/3$	$\underline{J}/3$			
	Circular Cylinder	$(1-\cos\theta) \underline{J} \hat{z} + 1/2 \cos\theta \underline{J}$	$(1-\cos\theta_0) \underline{J}$			
Rectangular Cavity	Cube	$\underline{J}/3$	$\underline{J}/3$			
	Cube	$\underline{J}/3$		$\underline{J} \hat{z}$	\underline{J}	
	Pill Box	$\underline{J} \hat{z}$				
Rectangular Waveguide	Cube	$\underline{J}/3$		$\underline{J} \hat{z}$		$\underline{J} \hat{z}$
	Pill Box	$\underline{J} \hat{z}$				$\underline{J} \hat{z}$

*See Figure 12.

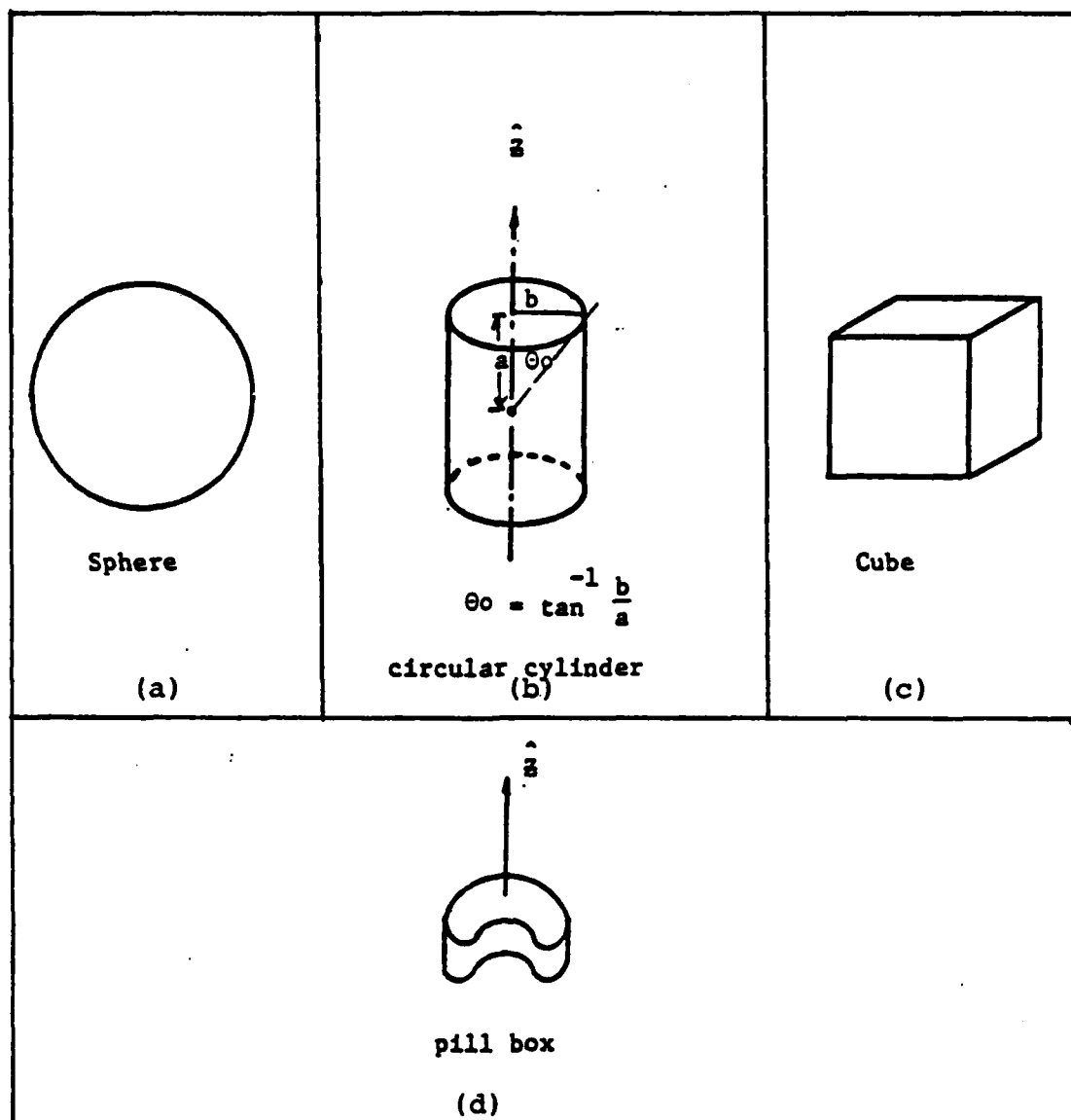


Figure 12. Various Shapes of ΔV for the Calculation of Principal-Volume Integration [30:11]

$$= c[(\cosh \mu \cos \nu - \cosh \mu' \cos \nu')^2 + (\sinh \mu \sin \nu - \sinh \mu' \sin \nu')^2]^{\frac{1}{2}}$$

Note that the constant "c" is the focal length of the ellipse, not the speed of light. The "c" was chosen since this is standard notation for the focal length.

Since the thickness of the shell wall is small (0.05 wavelengths) it was assumed that the electric field was constant through the shell thickness. This assumption is backed up by the work done by Lee, Sheshadri, Jamnejad, and Mittra [22]. They showed that through dielectric shells, with a thickness of 0.5 wavelengths, that the electric field, pattern, was only slightly altered from the no dielectric case (see Figure 13) [22:377]. Therefore with T being $\lambda/20$, the effect of the shell on the field would be minimal. The electric field could then be pulled out of the first integral.

Figure 14 is a diagram of the integral around the self cell. The source region has an area A_{SR} , which goes to zero as μ_e and ν_δ go to zero. Since the integral exists, the limits about ν_δ and μ_e may be taken independently of each other. If ν_δ goes to zero first, the areas indicated by a "1" become very small and their total contribution may be neglected. Therefore, the singularity becomes a line singularity and the principal value is taken over ν only.

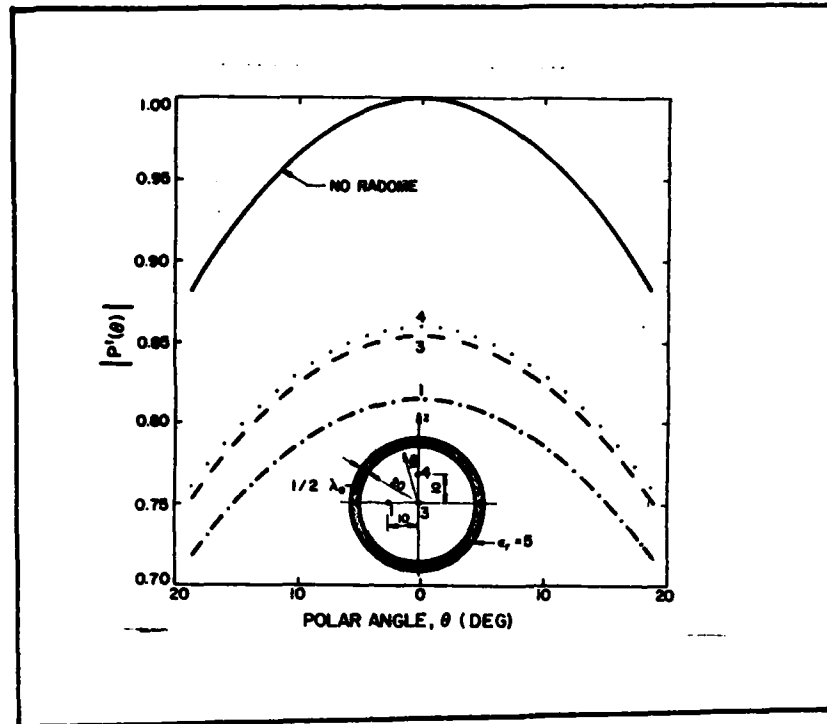


Figure 13. E-plane Radiation Pattern Through a Spherical Radome [22:277]

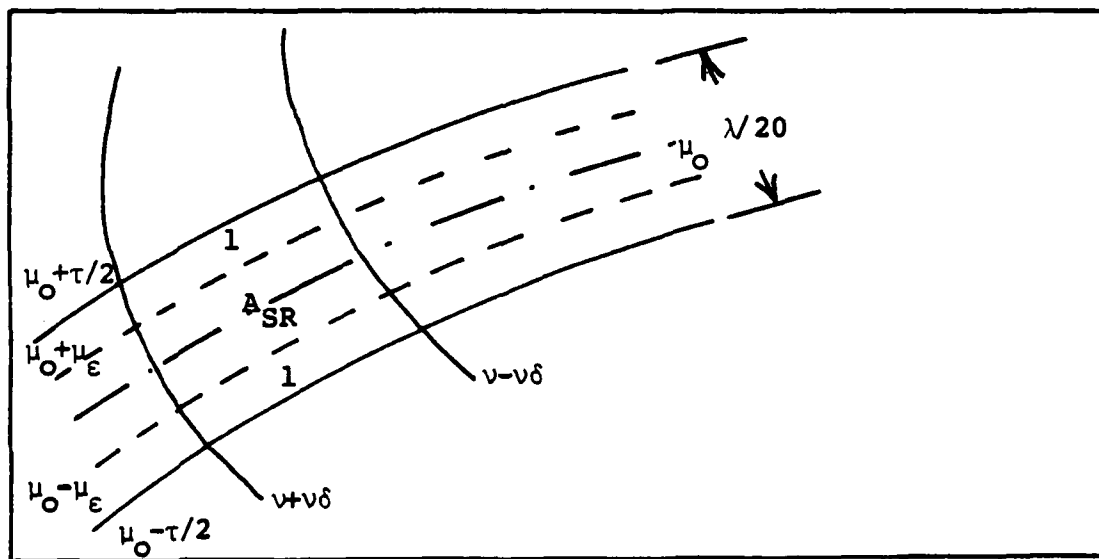


Figure 14. Integration Around the Source Region

Since the electric field is assumed to be constant across the thickness of the shell, the μ coordinate is a constant and may be integrated directly. This procedure is the same used by Stutzman and Thiele in the derivation of Pocklington's integral equation for wire scatterers [14:307-310]. Therefore, the resultant integrand is

$$\lambda_F \tau PV \int_0^{2\pi} E_z(\mu_0, \nu') H_0(kc\rho_0) \cosh^2 \mu_0 - \cos^2 \nu' \, d\nu' \quad (2.19)$$

The Richmond integral equation reduced to one variable is:

$$\begin{aligned} \bar{E}^i(\mu, \nu) = \bar{E}(\mu, \nu) + \lambda_F \tau PV \int_0^{2\pi} \bar{E}(\mu_0, \nu') \\ \cdot H_0^{(2)}(kc\rho_0) (\cosh^2 \mu_0 - \cos^2 \nu') \, d\nu' \quad (12.20) \end{aligned}$$

where (from 2.4)

$$\bar{E}^i(\mu, \nu) = \frac{-k_0^2 I}{4\omega\epsilon_0} H_0^{(2)}(k\rho) \bar{\mu}_z$$

$$\lambda_F = j3k^2 c^2 / 4$$

$$\rho_0 = \sqrt{(\cosh \mu \cos \nu - \cosh \mu_0 \cos \nu')^2 + (\sinh \mu \sin \nu - \sinh \mu_0 \sin \nu')^2}$$

In doing this integration, it was assumed that the focal length, c , is constant for the entire shell. This is justified by the thin shell approximation. Therefore, c may be pulled out of ρ_0 .

III. Solution of the Richmond Integral Equation by the Method of Moments

Method of Moments

General discussion on moment methods and application to wire antenna problems may be found in any of the newer antenna texts. Stutzman and Thiele [14:Chapter 7] provide an excellent tutorial for the new student. Unfortunately, discussion on the use of moment methods for non-metallic scatterers is severely limited. Mittra's book, Computer Techniques for Electromagnetics, has a discussion of such problems in a very general sense [28]. Harrington [13] discusses the dielectric problem; however, the discussion is based exclusively on Richmond's results [10].

Moment Methods are a general procedure converting problems posed as integral equations into linear equations, which then can be solved numerically. The method of moments is a projection method in which the unknown is approximated or projected. The approximated equation is then solved exactly [23:3]. Consider the relation

$$L(f) = g \tag{3.1}$$

where L is a linear operator operating on f , and g is a known result. The unknown to be determined is f . Expand

f by a series of functions in the domain of L such that

$$f \approx \sum_n^N \alpha_n f_n \quad (3.2)$$

These functions are known as basis or expansion functions.

Letting L operate on f, (3.1) becomes

$$\sum_n^N \alpha_n L(f_n) = g \quad (3.3)$$

An inner product is then taken with a weighting or testing function and $L(f_n)$ and g , respectively. This function is in the range of L. Therefore 3.3 becomes

$$\sum_n^N \alpha_n \langle w_m, L(f_n) \rangle = \langle w_m, g \rangle \quad m = 1, 2, 3, \dots \quad (3.4)$$

In matrix form, this is

$$(l_{mn})(\alpha_n) = (g_m)$$

where

$$(l_{mn}) = \begin{bmatrix} \langle w_1, L(f_1) \rangle & \langle w_1, L(f_2) \rangle & \langle w_1, L(f_3) \rangle & \dots \\ \langle w_2, L(f_1) \rangle & \langle w_2, L(f_2) \rangle & \langle w_2, L(f_3) \rangle & \dots \\ \langle w_3, L(f_1) \rangle & \langle w_3, L(f_2) \rangle & \langle w_3, L(f_3) \rangle & \dots \\ \vdots & \vdots & \vdots & \vdots \\ & & & \langle w_n, L(f_n) \rangle \end{bmatrix} \quad (3.5a)$$

$$\begin{pmatrix} \alpha_1 \\ \alpha_2 \\ \alpha_3 \\ \vdots \\ \alpha_n \end{pmatrix} = (g_m) = \begin{pmatrix} \langle w_1, g \rangle \\ \langle w_2, g \rangle \\ \langle w_3, g \rangle \\ \vdots \\ \langle w_n, g \rangle \end{pmatrix} \quad g_m = \langle w_m, g \rangle \quad (3.5b)$$

Solving for α_n with a nonsingular matrix, the unknown f can be determined. The selection of f_n and w_m is as much art as science and has been widely discussed in the literature. A thorough treatment will be given later in this chapter. This discussion on the general theory of moment methods is from Harrington [13:3-7].

With this brief introduction, the intent of this chapter is to apply the method of moments to solve a Fredholm Integral Equation of the second kind; specifically (2.20). This chapter will include the theory of moment methods and the application to the elliptic scattering problem.

General Application

Starting with equation (2.20),

$$\begin{aligned}
 \bar{E}^i(\mu, \nu) = \bar{E}(\mu, \nu) + \lambda_F \tau \int_0^{2\pi} \bar{E}(\mu_0, \nu') \\
 \cdot H_0^{(2)}(kcp) (\cosh^2 \mu_0 - \cos^2 \nu') d\nu' \quad (3.6)
 \end{aligned}$$

expand the unknown electric field on the dielectric shell ($\mu=\mu_0$) in terms of the general basis function

$$E_z \approx \sum C_n P(\nu_n - \nu) \quad (3.7)$$

(Note that in (3.6) the "cut integral" symbol \int , is used instead of "PV". This signifies that the singularity is not included or has been "cut out"). This makes (3.6) become

$$E_z^i(\mu, \nu) = \sum C_n P(\nu_n - \nu) + \lambda_F \tau \int_0^{2\pi} \sum C_n P(\nu_n - \nu') \cdot H_0^2(kc\rho) (\cosh^2 \mu_0 - \cos^2 \nu') d\nu' \quad (3.8)$$

Now apply the testing function to (3.6) and (3.8). Moving the summation sign outside of the integrals and taking the inner product (as shown in (3.4), we obtain

$$\begin{aligned} & c^2 \int_{\nu_{m-1}}^{\nu_{m+1}} \int_{\mu_0 - \tau/2}^{\mu_0 + \tau/2} E^i(\mu, \nu, \mu_s, \nu_s) W(\nu_m - \nu) (\cosh^2 \mu - \cos^2 \nu) d\mu d\nu \\ &= c^2 \sum C_n \int_{\nu_{m-1}}^{\nu_{m+1}} \int_{\mu_0 - \tau/2}^{\mu_0 + \tau/2} W(\nu_m - \nu) P(\nu_n - \nu) (\cosh^2 \mu - \cos^2 \nu) d\mu d\nu \quad (3.9) \\ &+ \lambda_F \tau c^2 \sum C_n \int_{\nu_{m-1}}^{\nu_{m+1}} \int_{\mu_0 - \tau/2}^{\mu_0 + \tau/2} \int_0^{2\pi} W(\nu_m - \nu) P(\nu_n - \nu') \\ &\cdot H_0^{(2)}(kc\rho) (\cosh^2 \mu - \cos^2 \nu) \cdot (\cosh^2 \mu_0 - \cos^2 \nu') d\nu' d\mu d\nu \\ &\quad m=1, 2, 3, \dots \end{aligned}$$

The order of integration may be interchanged except that the integration over v' must be done before the integration over v . This is due to the fact that v' is over the entire shell and is part of the IE to be solved, whereas the integration in v is done only over the domain of the weighting function. This is not the most general since it is assumed that $P(v_n)$ and $W(v_m)$ are sub-domain functions. Therefore the functions are zero for v not within the domain of $P(v)$. The use of entire-domain functions, which are valid across the entire range of v (the entire scatterer) is not considered here.

In this discussion, it should be noted that a two-dimensional application of the method of moments is possible. Essentially, in assuming that the μ coordinate was a constant and could be integrated out, μ was expanded by a pulse basis function valid across the entire domain of μ . The integration over μ was done in the same manner for the voltage term (the term containing E_z^i). The "middle" integrals (i.e., they are physically located in the middle of (3.9)) were done directly since these integrals, involving only the differential area function, exist in closed form. After the integration over μ , (3.9) becomes

$$\begin{aligned}
& c^2 \tau \int_{v_{m-1}}^{v_{m+1}} \bar{E}^i(\mu_o, \nu, \mu_s, \nu_s) W(v_m - \nu) (\cosh^2 \mu_o - \cos^2 \nu) d\nu \\
&= \frac{c^2}{2} [\cosh(2\mu_o) \sinh(\tau) + \tau] \Sigma c_n \int_{v_{m-1}}^{v_{m+1}} W(v_m - \nu) P(v_n - \nu) d\nu \\
&- c^2 \tau \Sigma c_n \int_{v_{m-1}}^{v_{m+1}} W(v_m - \nu) P(v_n - \nu) \cos^2 \nu d\nu \quad (3.10) \\
&+ \lambda_F \tau^2 c^2 \Sigma c_n \int_{v_{m-1}}^{v_{m+1}} \int_{v_{n-1}}^{v_{n+1}} W(v_m - \nu) P(v_m - \nu') \\
&\cdot H_o^{(2)}(k\rho) (\cosh^2 \mu_o - \cos^2 \nu') (\cosh^2 \mu_o - \cos^2 \nu) d\nu' d\nu
\end{aligned}$$

where

$$\bar{E}^i(\mu_o, \nu, \mu_s, \nu_s) = \frac{-k_o^2 I}{4\omega \epsilon_o} H_o^{(2)}(k\rho_s) \bar{\mu}_z$$

$$\lambda_F = j3k^2 c^2 / 4$$

$$\rho_s = [\cosh^2 \mu_o (c \cos \nu - c_s \cos \nu_s)^2 + \sinh^2 \mu_o (c \sin \nu - c_s \sin \nu_s)^2]^{\frac{1}{2}}$$

μ_s, ν_s ~ line source coordinates

μ_o, ν, ν' ~ scatterer coordinates (primed denotes source region)

Equation (3.10) can be written as

$$\bar{V}_m = \bar{C}_n [Z_m + Z'_{mn}] = C_n Z_{mn} \quad (3.11)$$

where the vector in the brackets Z_m , is the single integral from the total electric field and Z'_{mn} is the double integral over v and v' involving the Hankel function.

Together these make up the reaction matrix, Z_{mn} .

Solving (3.11) for C_n and using (3.7), the electric field and the induced current can be calculated. The radiation pattern can then be determined in the far field using

$$A_z(\rho) = \sum_{m=1}^N \frac{e^{-jk_0 \rho}}{\sqrt{8j\pi k_0 \rho}} \iint_{\text{cell } m} J_z(\rho') e^{jk_0 \rho' \cos(\phi - \phi')} ds' \quad (3.12a)^2$$

[16:229]

$$E_z = -j\omega\mu_0 A_z \quad [14:25] \quad (3.12b)$$

where $J_z(\rho')$ is based on the integration over the cell of the basis functions and the Hankel function. Equation (3.12c) is derived with $\bar{H} = \nabla \times \bar{A}$ consistent with Harrington [16:77].

Basis Functions

The rest of this discussion will center on the basis and weight functions, how they are applied in moment

²The summation over n from 1 to N shows that the contribution from each cell must be summed together to obtain the total vector potential at a point.

methods, and the set of functions used in this problem. Harrington states that one of the main tasks in using this problem solving technique is the choice of $P(v_n)$ and $W(v_m)$ ($P(v_n)$ and $W(v_m)$ are the basis and testing functions, respectively). $P(v_n)$ needs to be as close an approximation to f as possible and linearly independent. $W(v_m)$ should also be linearly independent and chosen so that the inner products with g depend on the properties of g (the solution of $L(f)$). Additional factors are the solution accuracy, relative ease in the evaluation of the matrix elements, the number of segments required for convergence, and the stability of the resultant matrix equation [13:7].

Below is a list of the standard basis and weight functions commonly used. These are sub-domain functions since they are defined to be zero outside the domain of the function.

Piecewise Uniform (Pulse Function):

$$J_j(z) = \begin{array}{ll} I_j & z_j \leq z \leq z_{j+1} \\ 0 & \text{elsewhere} \end{array} \quad (3.13a)$$

Triangle Function (Piecewise Linear):

$$J_j(z) = \begin{cases} \frac{I_j(z - z_{j-1})}{z_j - z_{j-1}} & z_{j-1} \leq z \leq z_j \\ \frac{I_j(z_{j+1} - z)}{z_{j+1} - z_j} & z_j \leq z \leq z_{j+1} \\ 0 & \text{elsewhere} \end{cases} \quad (3.13b)$$

Piecewise Sinusoidal:

$$J_j(z) = \begin{cases} \frac{I_j \sin [k(z - z_{j-1})]}{\sin [k(z_j - z_{j-1})]} & z_{j-1} \leq z \leq z_j \\ \frac{I_j \sin [k(z_{j+1} - z)]}{\sin [k(z_{j+1} - z_j)]} & z_j \leq z \leq z_{j+1} \\ 0 & \text{elsewhere} \end{cases} \quad (3.13c)$$

Quadratic Interpolation:

$$J_j(z) = \begin{cases} A_j + B_j(z - z_j) + C_j(z - z_j)^2 & z_j \leq z \leq z_{j+1} \\ 0 & \text{elsewhere} \end{cases} \quad (3.13d)$$

Sinusoidal Interpolation:

$$J_j(z) = \begin{cases} A_j + B_j \sin [k(z - z_j)] \\ \quad + C_j \cos [k(z - z_j)] & z_j \leq z \leq z_{j+1} \\ 0 & \text{elsewhere} \end{cases} \quad (3.13e) \quad [47:23, 24]$$

Truncated Cosine:

$$J_j(z) = \begin{cases} \cos[k(z - \frac{z_j - z_{j-1}}{2})] & z_{j-1} \leq z \leq z_j \\ 0 & \text{elsewhere} \end{cases} \quad (3.13f) \quad [28:10]$$

Figure 15 illustrates three of these functions.

The use of the piecewise functions, forces the partitioning of the segments into two regions ranging from z_{j-1} to z_j and from z_j to z_{j+1} . The result of the integration is summed together to obtain the total contribution for each cell. This division is due to the derivative discontinuity at z_n [24:535]. Butler and Wilton discuss methods of modifying certain functions in order to increase the convergence rate. Specifically with (3.13e) in one procedure the constants B_j and C_j are adjusted to force the current and its derivative to be continuous at each of the cell's endpoints. This results in a basis set which causes the current and its derivative to be continuous across the cell. In another procedure, the current in the j th cell is required to satisfy Equation (3.14). This is known as extrapolated continuity [24:535].

$$J_j(z_{j-1}) = J_{j-1}(z_{j-1}) \quad (3.14)$$

$$J_j(z_{j+1}) = J_{j+1}(z_{j+1})$$

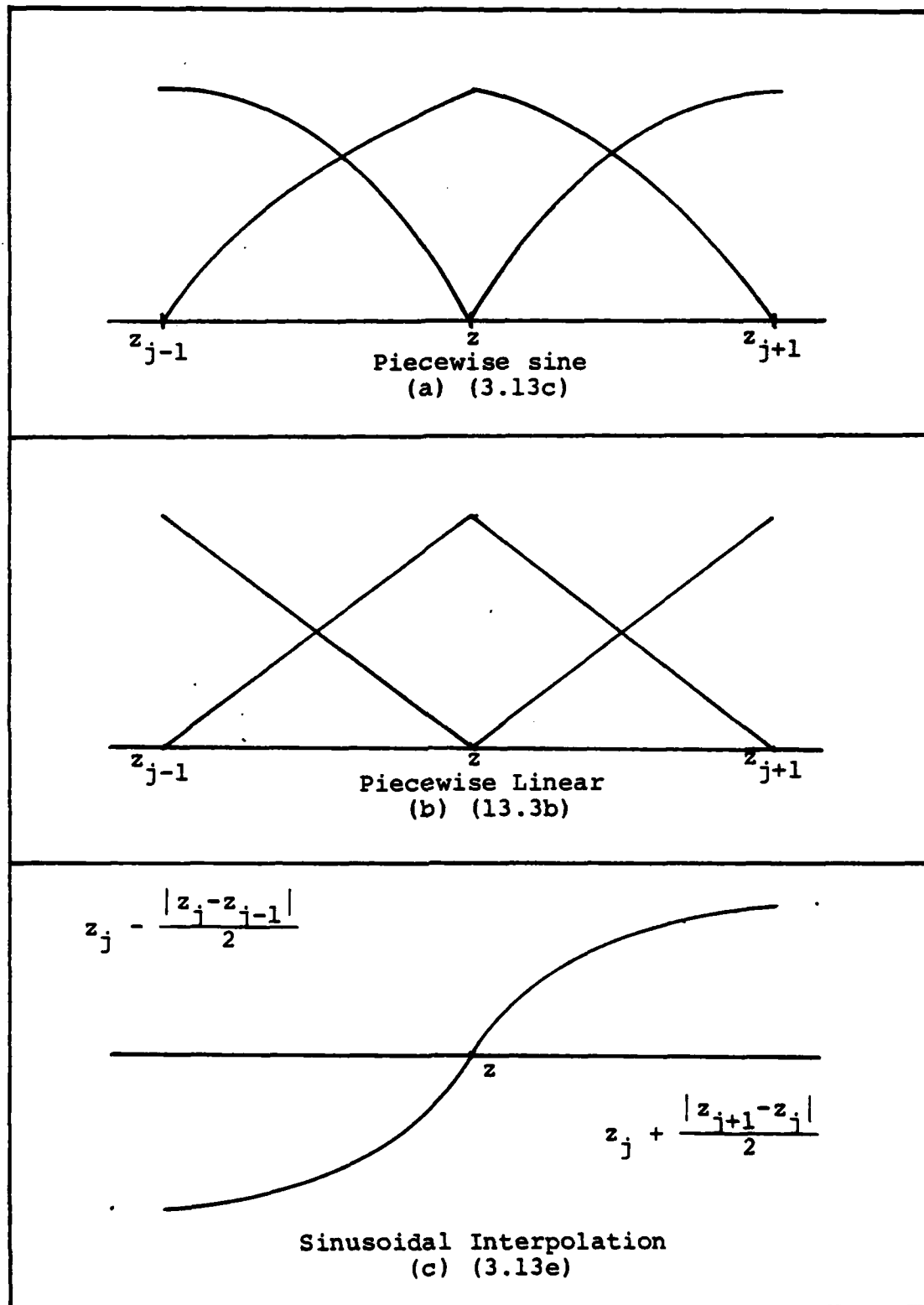


Figure 15. Basis and Testing Functions [24:535]

Richmond used square pulses in calculating the field in the dielectric shell [10:336]. Use of such functions assumes a constant field across the shell, which is a reasonable approximation if the shell is thin and the scatterer small (small compared to wavelength). Hagmann, et al. showed that larger cells may be used if variations are allowed for the field. In the plane-wave correction method, the field is represented by a superposition of plane waves (3.15).

$$E_z(r', \theta') = \sum_i B_i e^{-jk r' \cos(\theta' - \alpha_i)} \quad [25:744] \quad (3.15)$$

In the cylindrical-cell correction method, the square cells are replaced by circular cells as Richmond did [10:336,337]. The circular cylinder with TM excitation will have fields with the cell determined by

$$E_z = \sum_{n=0}^{\infty} b_n J_n(kr) \cos(n\theta + C_n) \quad (3.16)$$

where b_n and C_n are determined by the incident wave [25:746].

In another example of methods for improved convergence, Blue used different basis functions depending on the geometry of the problem and the location of the segment in relation to that geometry. Blue showed that a conducting strip, 60λ wide, could be done with only 17 basis functions [26:1894]. Analyzing the problem before

hand, Blue used three basis functions, each determined by the domain of the function [26:1902]. As an example with the problem being discussed in this paper; for the more pointed end of the ellipse (as y goes to zero), Hankel functions could have been used. This is based on the function which describes the electric field distribution in a curved optical waveguide [27:2125,2126]. A sinusoidal function could have been used in the smooth part of the ellipse (as x goes to zero) since the structure approaches a dielectric slab waveguide. This would mean, however, a tradeoff is being made for accuracy and convergence rate versus simplicity of implementation.

Testing Functions and Solution Methods

Testing Solutions. The choice of testing functions is the same as for the basis functions. As discussed earlier, the ideal testing functions would result in easy implementation, high speed computation, and a fast convergence rate to produce a highly accurate solution. However, it is not possible to have all four criteria and be able to solve all of the problems encountered.

Solution Methods. Table 4 provides five solution methods or function pairs commonly used. Each of the methods of Table 4 has advantages and disadvantages. Point Matching provides a highly accurate solution, but the number of cells required makes this functional pair impractical for scatterers of any significant size. The

Table 4. Moment Method Functional Pairs

Method	nth Term of A (basis)	Testing Function
Galerkin	$a_n b_n(x)$	$b_m(x)$
Least Square	$a_n b_n(x)$	$Q(x) \frac{\partial \epsilon(x)^1}{\partial a_m}$
Point Matching	$a_n \delta(x-x_n)$	$\delta(x-x_m)$
Point Collocation	$a_n b_n(x)$	$\delta(x-x_m)$
Subsectional Collocation	$V(x_n) \sum_{p=1}^P a_{np} b_p(x)$	$\delta(x-x_m)$

¹Q(x) is a positive definite function of position
² $\delta(x)$ is the delta function [12:188]

chief advantage of point matching is the easy implementation and quick calculation of matrix elements (low CPU time). Galerkin functional pairs converge faster than least square pairs, but a Galerkin pair will not always converge to a solution. Sarkar showed that the least squares method will always produce meaningful solutions, even when the solution, g , is not within the range of L (the linear operator from (3.1)) [23:2]. The results of this study showed that Galerkin's method also takes considerable CPU time to calculate matrix elements when the elements have to be integrated numerically. This statement would be true for any of the methods involving functions that could not be integrated analytically.

After careful consideration, the method used to solve the dielectric elliptical shell problem was Galerkin's method with the piecewise sinusoidal function set. This functional set, of the established ones, most closely resembled the electric field as it propagates in a dielectric slab. The use of Hankel functions, while suggested by Blue's article, would be too complicated to use even if a better match is obtained. Other reasons for choosing this set were: one of the most popular methods, well documented, and ease in understanding implementation. The biggest drawback is the need for numerical integration for each matrix element.

Therefore, the basis and testing functions are:

$$E(\mu_0 v') \approx C_n \left\{ \frac{\sin [k(v_{n+1} - v)]}{\sin [k(v_{n+1} - v_n)]} + \frac{\sin [k(v' - v_{n-1})]}{\sin [k(v_n - v_{n+1})]} \right\} \quad (3.17)$$

Please note that the $(v - v')$ of equation 3.17 is the distance between the angles at v and v' . The dimension is in meters. This is consistent with the fact that the dimension of the wavenumber, k , is rad/m.

A good reference for the implementation of the sinusoidal basis function is Richmond's report, Computer Analysis of Three-Dimensional Wire Antennas from The Ohio State University [29]. While dealing with metallic scatterers, the features such as segment division, integration, etc., are demonstrated better than in the textbook dipole implementation.

IV. Programming the Moment Method Solution

The final step in the procedure is the generation of code to implement the method of moments and solve the linear algebra equation, $(A)\bar{x} = \bar{b}$. The Fredholm integral equation of the second kind,

$$\begin{aligned} \bar{E}^i(\mu, \nu) = \bar{E}(\mu, \nu) + \lambda_F \tau \int_0^{2\pi} \bar{E}(\mu_0, \nu) H_0^{(2)}(k\rho) \\ \cdot (\cosh^2 \mu_0 - \cos^2 \nu') d\nu' \end{aligned} \quad (4.1)$$

has been reduced to a linear algebra problem. The matrix, A , consists of two elements, Z'_{MN} and Z_M where

$$\begin{aligned} Z'_{MN} = \lambda_F \tau^2 c^2 c_n \int_{\nu_{m-1}}^{\nu_{m+1}} \int_{\nu_{m-1}}^{\nu_{m+1}} P(\nu_n - \nu') W(\nu_m - \nu) \\ \cdot H_0^{(2)}(k\rho) (\cosh^2 \mu_0 - \cos^2 \nu') \\ \cdot (\cosh^2 \mu_0 - \cos^2 \nu) d\nu' d\nu \end{aligned} \quad (4.2a)$$

$$\begin{aligned} Z_M = c^2 \int_{\nu_{m-1}}^{\nu_{m+1}} \int_{\mu_0 - \tau/2}^{\mu_0 + \tau/2} P(\nu_n - \nu) W(\nu_m - \nu) \\ \cdot (\cosh^2 \mu - \cos^2 \nu) d\mu d\nu \end{aligned} \quad (4.2b)$$

and the voltage vector is

$$V_{MN} = \frac{-k_o^2 c^2}{4\omega\epsilon} \int_{v_{m-1}}^{v_{m+1}} P(v_m - v) H_o^{(2)}(k_o \rho_s) \cdot (\cosh^2 \mu_o - \cos^2 v) dv \quad (4.3)$$

where k is the wave number in the dielectric if integrating for Z_{MN} or $k_o (\omega^2 \sqrt{\mu_o \epsilon_o})$ for free space when calculating V_{MN} . $P(v_n - v')$ and $W(v_m - v)$ are the sinusoidal basis functions just discussed.

To calculate the matrix elements and solve this the linear algebra problem will require special function calculators, numeric integrators, and linear algebra solvers. The self cell (cell where $n = m$) will require special handling as will the cells at the $\pm 90^\circ$ points. This chapter will discuss the programs developed to solve the linear algebra equation. The discussion will include a description of the special functions and routines. The chapter will close with a discussion on the problems still unresolved with the program.

Machine

Due to the large core and time requirements, this program was processed on the Aeronautical Systems Division's CYBER computer system. The ASD system consists of two Control Data Corporation (CDC) mainframes, CYBER 74 and 750,

which operate in parallel. The 750 has 262,000 words of central memory. The CYBER 74 has 131,000 words. The CYBERs have 14 significant digits for real variables. The machines support a variety of languages and support packages. The system also includes interactive processing (INTERCOM), plotters (CALCOMP and DISSPLA), and special libraries (IMSL, FUNPACK, etc.) [31:3].

Program Overview

The language used in this program was FORTRAN V, with CDC extensions. Version 5 complies with the American National Standards Institute FORTRAN 77 [32:V]. The CDC extensions used were minor consisting of the use of sine, cosine, and tangent functions in degrees, hyperbolic arctangent, the CPU SECOND functions (returns current processing time elapsed since start), and CDC FORTRAN control statements. Due to the heavy use of the IF-THEN-ELSE statements and the use of zero index values, this program will not compile on a FORTRAN 4 compiler without major modifications. The programs were run with the optimizer set to 1 (OPT=1), where the compiler will optimize the code by the following steps:

1. Redundant instructions and expressions are removed.
2. PERT critical path scheduling is done to utilize the multiple functional units efficiently.

3. Subscript calculations are simplified and values of simple integer variables are stored in machine registers throughout loop execution for certain do loops [32:11-7,8].

Despite the reduction in the amount of cells required, the storage requirements for the program were large when the full sized scatterer (semi-major axis of 12λ , semi-minor axis of 6λ) was run. It was not possible to run all of the algorithms in one job. Therefore, it was necessary to break up the program into three programs which were completely separate. Figure 16 has a flow chart of the simple structure. The TRANSF control card was used to control the flow. Using the TRANSF card, the input program ran first, then the next job listed on the TRANSF card ran. Program 3 could not run until 2 was finished and 2 could not run until the first program was completed. This offered several advantages. Each module could be developed separately. Since the input program created a permanent file, once the geometry was set up and the file created, it did not have to be run again. It was possible to reduce core requirements which decreased turn-around time by running each program separately. This structure was much easier to understand and develop than using segmentation or overlays.

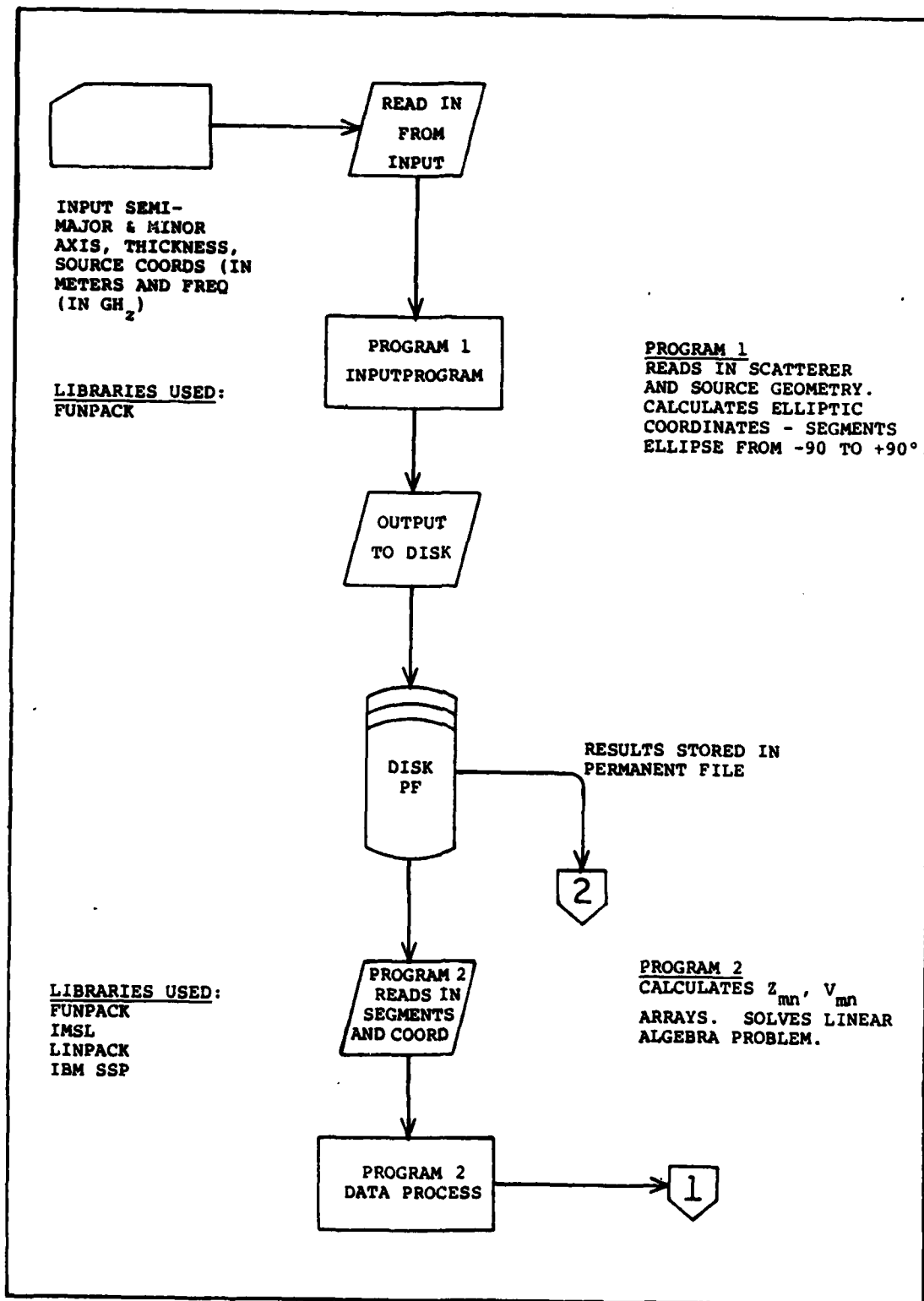


Figure 16. Job Stream on CYBER 175

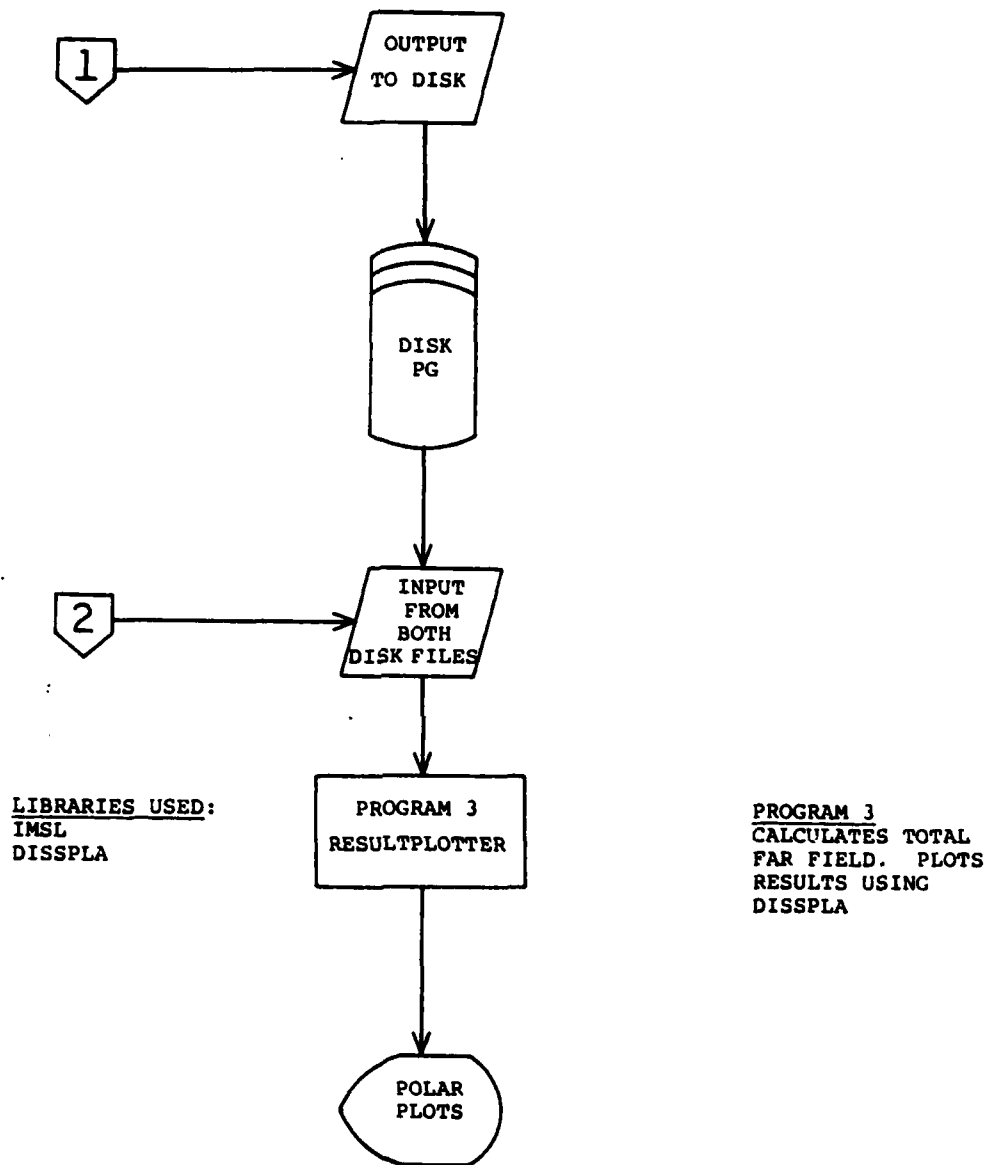


Figure 16--Continued

Library Subroutines

Due to the nature of the equation being solved, special functions and procedures were needed. These included elliptic integrals, Bessel functions, integrators (numeric quadrature), and linear algebra equation solvers. The ASD computer system has many functions and routines already built in through several different program packages. Rather than go through the procedure of developing and testing these programs, the "canned" programs were used. These offer the advantage that they are well known throughout the industry and tried and tested on many different machines.

Functions. The complete elliptic integral of the second kind was used to calculate the circumference of the ellipse. The Bessel, $J_0(x)$, and the Neumann, $N_0(x)$ (or $Y_0(x)$), functions were used to calculate the matrix elements. The library selected to calculate these functions was the FUNPACK library [33]. FUNPACK is a library of functions and subroutines that can return the results of Bessel functions of first and second kind, modified Bessel functions, elliptic, exponential, Dawson's integrals, and other functions. There are 13 programs in the current library which was released in 1976 as FUNPACK Release 2. FUNPACK was developed as part of the National Activity for Testing Software (NATS) project. Obtained from the Argonne Code Center, FUNPACK was specifically designed for the CDC 6000-7000 machines. The documentation that accompanied

the program [33], provides the description on how to use the code, the accuracies and limitations of the routines, and where they were tested. The results of the Bessel functions for J_0 and Y_0 were hand-checked against tables and found to be accurate. The only limitation to accuracy is the host's ability to accurately the values of the basic functions such as natural log, sine, cosine, etc. [33:11]. The nicest part of the FUNPACK library is that the package was developed for the CDC processors and take full advantage of the 14 working numbers of accuracy in standard precision. It was for this reason that the FUNPACK library was chosen over the better known International Mathematical and Statistical Library (IMSL). It should be noted that the FUNPACK libraries are still being supported by Argonne and will continue to receive support. Changes will be supplied automatically to users [33:11,22-23]. Another advantage of the library is that the function calls resemble the name of the function, making it much easier for the future user to read the program and understand what operation is being performed without a great number of comment statements.

Integrators. As can be seen from equations (4.1-3), the numerical integration is an important part of the program. The integrals of (4.2a) and (4.3) do not exist in closed form. While the single integral of (4.2b) can be done analytically, the integral over the angle, ν , was done numerically to reduce the chance of algebraic

error. The radiation routine used to calculate the far field also needs a single integrator. The IMSL has a single and double integrator. The documentation on IMSL is limited and the accuracy of the routines is not known except to rely on the reputation of the library. The AFIT Digital Computer Manual called the package ". . . the recommended routines" [34:55].

The single integration routine, DCADRE, uses a cautious Adaptive Romberg Extrapolation Algorithm. DCADRE is computed as the sum of estimates for the integral of a function, $F(x)$, over suitably chosen subintervals of the limits of integration. If the routine is unable to find an acceptable estimate on a given subinterval, the subinterval is divided and each of the new subintervals is handled separately [35:DCADRE-1,2]. It is because of this process of interval subdivision that DCADRE can take a great deal of time. The acceptability of an interval is determined by a relative error input in the function calling statement. If the routine can not get within the limits supplied, then the function writes out an error message and supplies the best answer. However, even if the error message is written, the best answer is still better than the standard integration routines. DCADRE may return wrong answers if the frequency of the integrand is very high, but this problem may be overcome by dividing the interval and calling the routine several times [35:DCADRE-2].

The double integrator is DBLIN, which uses DCADRE to do the single integration. However, use of the Romberg integration routine in two variables increased run times significantly. Therefore, the integral over v_m was done via a Simpson rule integrator [38:311] while DCADRE integrated over v_n .

Matrix Equation Solvers. The IMSL has two routines for the solving of complex linear algebra problems: LEQT1C and LEQ2C. There is also a library of linear algebra routines from the Argonne National Library known as LINPACK. LINPACK has come into being in the same manner that FUNPACK did and is well documented [36]. The referenced documentation includes a listing of all subroutines and tables of timing data on each routine for each of the test sites [36:B-1,D-11].

The best choice of these programs is not known. Since the second program never fully worked and produced correct answers, this question had not operationally been decided. The plan was to run several jobs through each of the programs and to see which came out best in terms of accuracy, speed, and ease of operation. The result of the test would decide which routine to use for the final runs. For the problem here, time is the biggest problem, not memory.

Input Program

The purpose of the input program was to:

1. Read in the geometrical data on the scatterer.
2. Calculate the elliptic coordinate system parameters.
3. Determine the endpoints of the segments.
4. Calculate constants used in subsequent programs.

The listing is given in Appendix C. The calculation of elliptic coordinates is done using the relationships given in Appendix A. In calculating the coordinates for the line source location, it was assumed that the sources have the same μ_0 value as the scatterer does. Therefore, only the source focal length, C_s , and angle coordinate, v_s , need to be determined.

Wave Number. As one of the constants, the wave number in the dielectric was determined. It has a value between, k_0 and k_d , the wave numbers in free space and for $\sqrt{4 k_0}$.

Assuming that the scatterer will locally act as a flat slab waveguide, the electric field within the scatterer is of the odd type. This is based on the assumption that the electric field is constant through the dielectric shell and, therefore, the electric field is symmetric about the middle of the slab. Since there is no variation in the electric field in the y direction, the modes excited are TM_z .

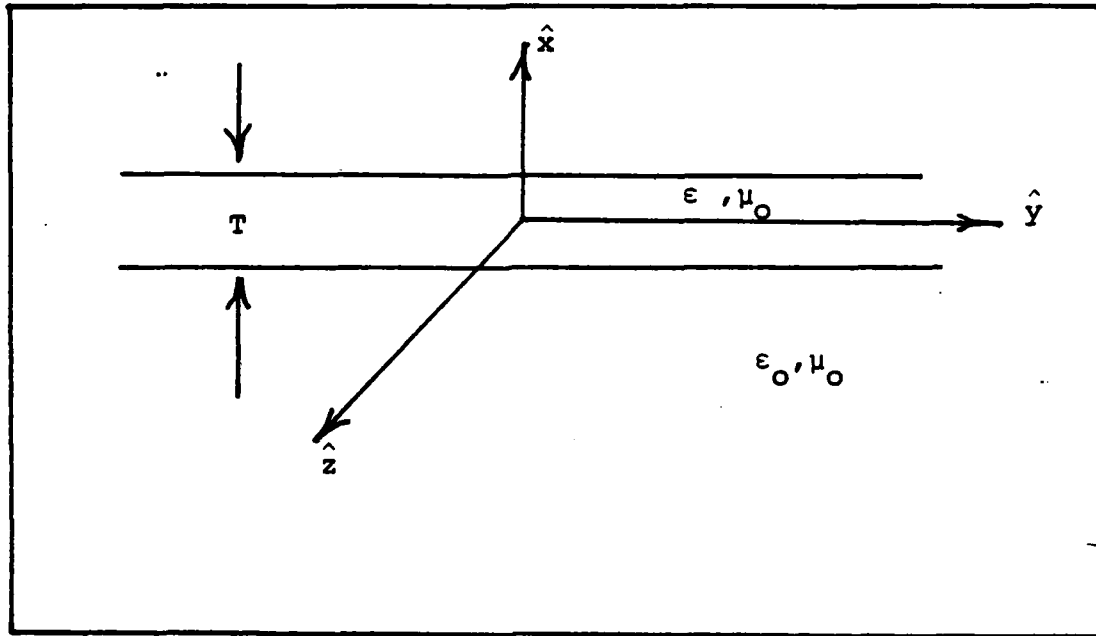


Figure 17. Dielectric Slab Waveguide

Figure 17 shows the coordinate system for this discussion. The electric and magnetic fields are

$$E_z = E_0 \frac{\cos k_{x1} x e^{-jk_y y}}{\cos\left(\frac{k_{x1} T}{2}\right)} \quad |x| < T/2$$

$$E_z = E_0 \frac{e^{-\Gamma_{x0} |x|}}{e^{-(\Gamma_{x0} T/2)}} e^{-jk_y y} \quad |x| > T/2 \quad (4.4)$$

$$H_y = \frac{1}{j\omega\mu} \frac{\partial E_z}{\partial x}$$

$$= -k_{x1} \frac{\sin k_{x1} x e^{-jk_y y}}{\cos\left(\frac{k_{x1} T}{2}\right)} \frac{E_0}{j\omega\mu} \quad |x| < T/2$$

$$= \frac{\Gamma_{x0}}{j\omega\mu} \operatorname{sgn}(x) E_0 \frac{e^{-\Gamma_{x0} |x|}}{e^{-(\Gamma_{x0} T/2)}} e^{-jk_y y} \quad |x| > T/2$$

where

$$k_{x1}^2 + k_y^2 = k_1^2 = \epsilon_r k_0^2$$

$$-\Gamma_{x0}^2 + k_y^2 = k_0^2$$

Forcing the tangential magnetic field to be continuous at $x = T/2$

$$\begin{aligned} -k_{x1} E_0 \frac{\sin(k_{x1} T/2) e^{-jk_y y}}{\cos\left(\frac{k_{x1} T}{2}\right)} \\ = -\Gamma_{x0} E_0 \frac{e^{-\Gamma_{x0} T/2}}{e^{-\Gamma_{x0} T/2}} e^{-jk_y y} \end{aligned} \quad (4.5)$$

or

$$\begin{aligned} \left(\frac{k_{x1} T}{2}\right) \tan\left(\frac{k_{x1} T}{2}\right) &= \left(\frac{\Gamma_{x0} T}{2}\right) \\ \left(\frac{k_{x1} T}{2}\right)^2 + \left(\frac{\Gamma_{x0} T}{2}\right)^2 &= (\epsilon_r - 1) \left(\frac{k_0 T}{2}\right)^2 \end{aligned} \quad (4.6)$$

Since T is $1/20$ wavelengths long, $k_{x1} T/2$ is much less than 1. Therefore

$$\left(\frac{k_{x1} T}{2}\right)^2 \cong \left(\frac{\Gamma_{x0} T}{2}\right)^2 \quad (4.7)$$

and from (4.6)

$$\left(\frac{k_{x1} T}{2}\right)^2 + \left(\frac{k_{x1} T}{2}\right)^4 = (\epsilon_r - 1) \left(\frac{k_0 T}{2}\right)^2 \quad (4.8)$$

This means that an approximate value for $k_{x1}T/2$ is

$$\left(\frac{k_{x1}T}{2}\right)^2 \approx -\frac{1}{2} + \frac{1}{2} \sqrt{1 + 4(\epsilon_r - 1) \left(\frac{k_o T}{2}\right)^2} \quad (4.9)$$

with $T = \lambda_o/20$ and $\epsilon_r = 4$

$$k_{x1}T = .5262$$

$$k_{x1}\lambda = 10.5246$$

$$(k_{y1}\lambda)^2 = \epsilon_r (k_o\lambda)^2 - (k_{x1}\lambda)^2 \quad (4.10)$$

or

$$k_{y1}\lambda = 6.87 \quad [37:12-13;15]$$

The determination of segment and points was a critical phase of the program. No segment was to have a length greater than $\lambda/4$ [29:5]. It was decided that for a radius of curvature of 2.5 or greater, that this segment length was adequate since a straight line $\lambda/4$ wavelength long would vary little from the arc of the ellipse. For the segments where the scatterer has a smaller radius of curvature, the segments were to be $\rho/10$ wavelengths long where ρ is the radius of curvature. This was based on a straight line extrapolation from the cutoff point of .25 for 2.5 (see Figure 18).

Based on this the cell end point (one was known) was determined by taking the arcsine of the cell length over the distance from the origin so that point as shown

in Figure 19. The cells ran from -90 to 90° , so the lower endpoint was always known. The angles were summed until the total reached $+90^\circ$. The ellipse was segmented from the -90 to 90° to take advantage of symmetry. For the large ellipse (12λ by 6λ) all segments were $.25\lambda$ long. For smaller ellipses, the number of cells increased near the end points and decreased to the ± 90 points, as was desired. Appendix C has a program listing of the input program. It was not determined if more or less segments were needed. In the last program step; the input data, elliptic coordinate information, and the array containing the cell endpoints were written on disk and stored in a permanent file.

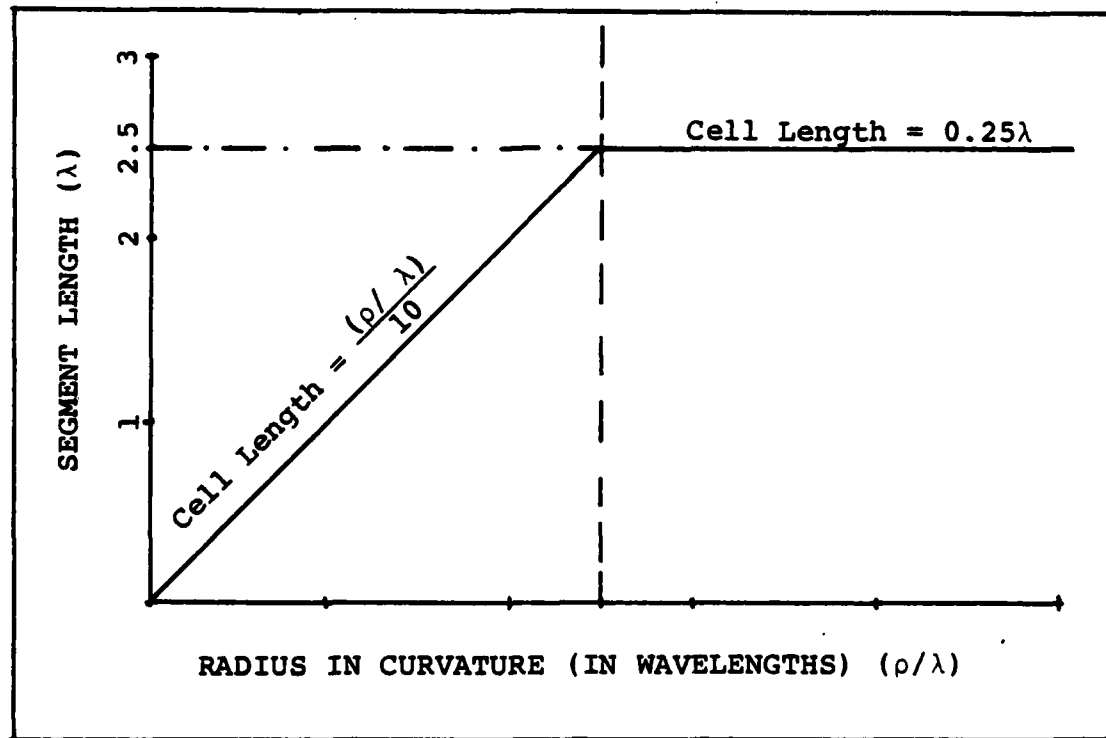


Figure 18. Segment (Cell) Length Determination

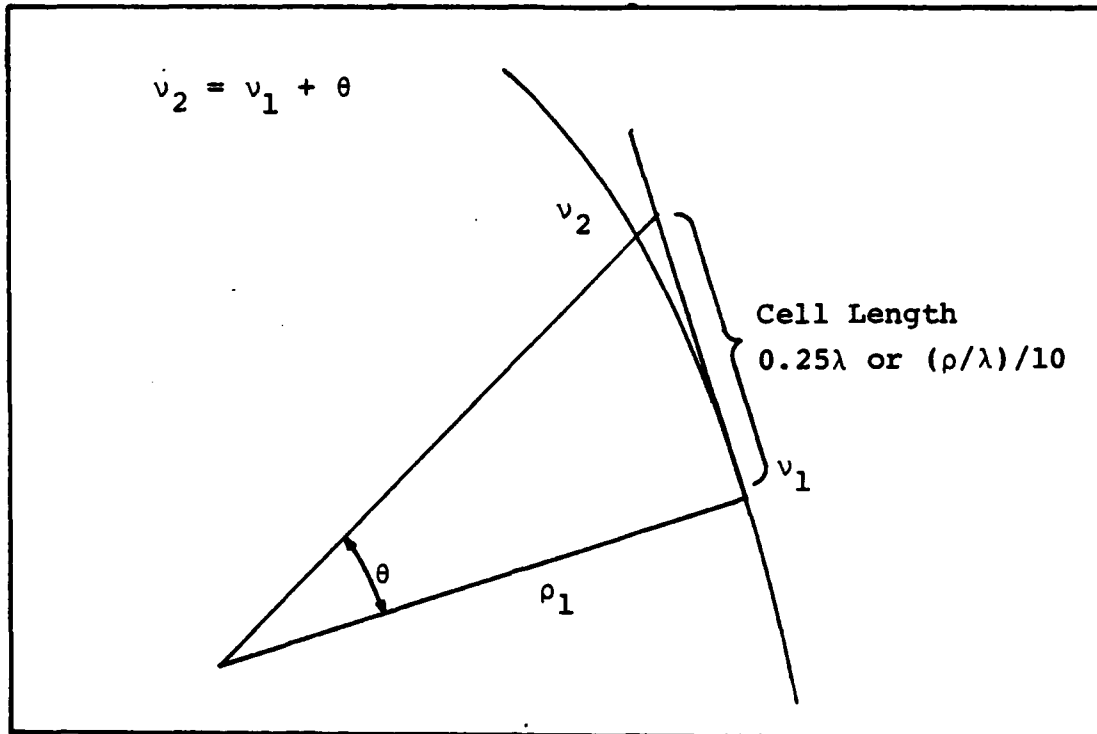


Figure 19. Cell Endpoint Determination

Matrix Generation and Algebra Solver

The second program has three main functions:

1. Determine the matrix elements of the reaction matrix, Z_{MN} .
2. Determine the Vector elements for V_{MN} .
3. Solve the linear algebra problem, $\bar{V}_{MN} = \bar{C}(Z_{MN})$.

The double integral generates a full matrix of complex elements since the integral over the nth cell (primed coordinates) is independent of the integration over the mth cell. The total E field integral generates real numbers only and contributes only to the matrix diagonal and to the major codiagonals. Due to the E field integral, a blocked IF-THEN-ELSE statement is used to test which contribution

to include. The program calculates the real and the imaginary parts separately because the IMSL integrators are real functions.

Algorithm. The sinusoidal basis function had to be divided up into two subintervals; v_{n-1} to v_n and v_n to v_{n+1} [24:535] (see also Chapter III). In the double integral, the multiplication of the sinusoid for the m th cell and the sinusoid for the n th cell results in four double integrals for each cell.

$$\int_{v_{m-1}}^{v_{m+1}} \int_{v_{n-1}}^{v_{n+1}} \left\{ \frac{\sin[k(v-v_{m-1})]}{\sin[k(v-v_{m-1})]} + \frac{\sin[k(v_{m+1}-v)]}{\sin[k(v_{m+1}-v)]} \right\} \cdot \left\{ \frac{\sin[k(v'-v_{n-1})]}{\sin[k(v'-v_{n-1})]} + \frac{\sin[k(v_{n+1}-v')]}{\sin[k(v_{n+1}-v')] } \right\} dA'dA \quad (4.11a)$$

$$\begin{aligned} & \int_{v_{m-1}}^{v_m} \int_{v_{n-1}}^{v_n} \frac{\sin[k(v-v_{m-1})] \sin[k(v'-v_{m-1})]}{\sin[k(v-v_{m-1})] \sin[k(v'-v_{m-1})]} dA'dA \\ & + \int_{v_{m-1}}^{v_m} \int_{v_n}^{v_{n+1}} \frac{\sin[k(v-v_{m-1})] \sin[k(v_{n+1}-v')]}{\sin[k(v-v_{m-1})] \sin[k(v_{n+1}-v')] } dA'dA \\ & + \int_{v_m}^{v_{m+1}} \int_{v_{n-1}}^{v_n} \frac{\sin[k(v_{m+1}-v)] \sin[k(v'-v_{n-1})]}{\sin[k(v_{m+1}-v)] \sin[k(v'-v_{n-1})]} dA'dA \\ & + \int_{v_m}^{v_{m+1}} \int_{v_n}^{v_{n+1}} \frac{\sin[k(v_{m+1}-v)] \sin[k(v_{n+1}-v')]}{\sin[k(v_{m+1}-v)] \sin[k(v_{n+1}-v')] } dA'dA \quad (4.11b) \end{aligned}$$

This also occurs in the total field expansion except the integration is only over the mth cell as shown in (4.11c)

$$\int_{v_{m-1}}^{v_m} \frac{\sin[k(v-v_{m-1})]}{\sin[kv_{m-1}-v]} \left\{ \frac{\sin[k(v-v_{n-1})]}{\sin[k(v_{n-1}-v)]} + \frac{\sin[k(v_{n+1}-v)]}{\sin[k(v_{n+1}-v_n)]} \right\} dA \quad (4.11c)$$

$$+ \int_{v_m}^{v_{m+1}} \frac{\sin[k(v_{m+1}-v)]}{\sin[k(v_{m+1}-v_m)]} \left\{ \frac{\sin[k(v-v_{n-1})]}{\sin[k(v_{n-1}-v)]} + \frac{\sin[k(v_{n+1}-v)]}{\sin[k(v_{n+1}-v_n)]} \right\} dA$$

where

$$dA' = c^2 (\cosh^2 \mu_0 - \cos^2 v') dv'$$

$$dA = c^2 (\cosh^2 \mu_0 - \cos^2 v) dv$$

Endpoints. Figure 20 is a graphical presentation of the double integration over v and v' . The $v = v'$ line is the line singularity where the integrand is singular due to the Bessel function of the second kind. Each cell has four contributions according to equation (4.11b). This can be seen in Figure 20. As an example, let $m = 4$ and $n = 2$. The coverage goes back to $m = 3$ and up to $m = 5$. The integration over v_n has the same feature. The shaded block represents the total contribution to the (4,2) cell.

Integration on the cells near the end points presents a special problem. Since the scatterer is a continuous object, the contribution of all cells must be the same. The affect of the current in an adjacent region, but beyond the symmetric boundary must be included.

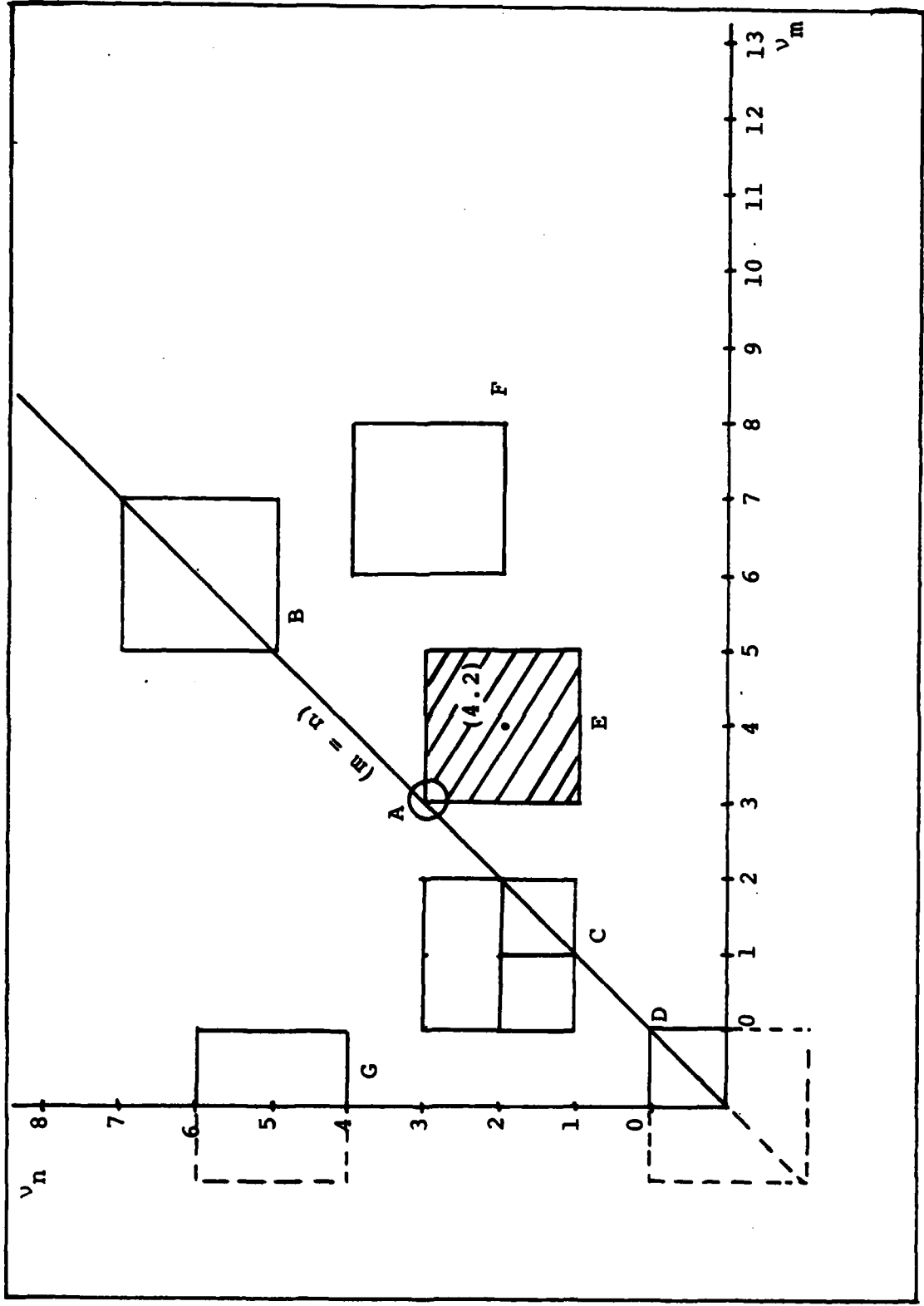


Figure 20. Integration Over Cells

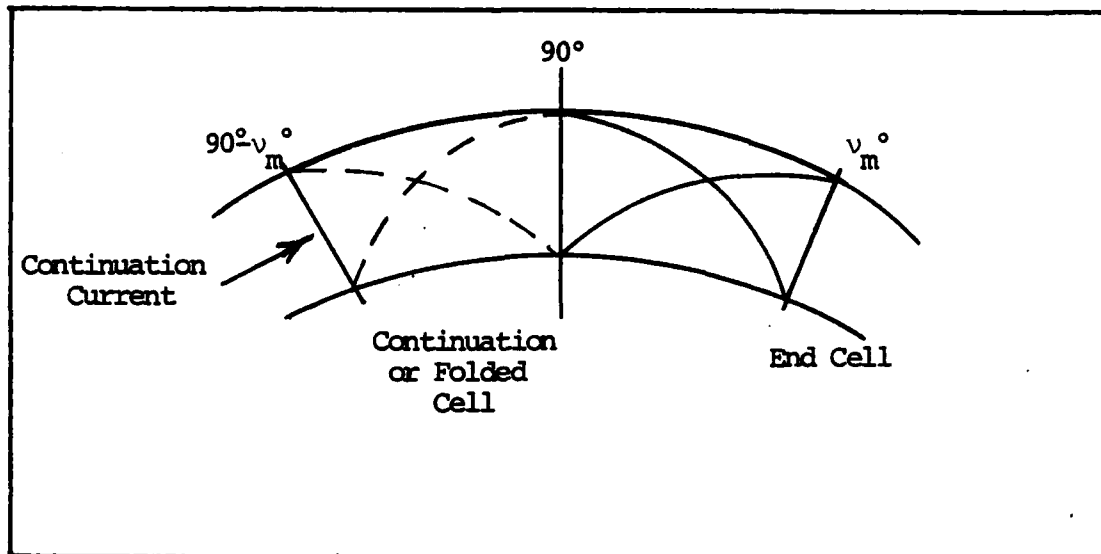


Figure 21. Current Contribution from Beyond the Line of Symmetry

For example, the (0,0) cell has three contributions below the axis in Figure 20. Originally, the program handled each case on the end points as a separate entity, multiplying the (0,0) and (N,N) cell contribution by four and the ones in between by two (point G on Figure 20). However, this resulted in a long, bulky program and it was difficult to ascertain if the contributions from cells beyond the symmetric line were equal. Thus a question came up if multiplying by a constant would produce correct results. Therefore, a "negative cell" was created by folding the cell on the $\pm 90^\circ$ line over the other side. In other words, one cell was created that was equal in length to the 0th and Nth cell, but on the other side of the $\pm 90^\circ$ lines (see Figure 21).

To assume that any cells on the other side of the line were equal in length to the adjacent cell was an

excellent assumption since the region of concern is the essentially flat region of the ellipse. In the case of a circular shell, as the scatterer becomes more circular, the length of the cells becomes more nearly equal. This greatly simplified the program from now only contribution from the total field expansion had to be checked.

Additional contributions from the other side of the ellipse had to be considered due to the assumed symmetry of the problem and restriction of ν to $\pm 90^\circ$ (see Figure 22). Since the line source is on the y axis (see Figure 6), the incident energy on the right side of the shell ($+90$ to -90°) is equal to that which is incident on the left side (180° to 270°). Therefore, only one-half of the ellipse had to be directly evaluated, thus reducing the number of cells needed by a half. It would not be correct to either neglect the other side or to simply multiply the field by two.

In evaluating the Richmond integral equation (equation (2.8)), the interaction between the field generated by the source cell and the observation cell is being calculated (see Figure 8). This must also be considered with the image cells as shown in Figure 22(a). This was done in the program by integrating over a cell 180° opposite the observation cell.

To multiply the field calculated by two to account for the image contribution would give erroneous results for the distance changes as the position on the ellipse

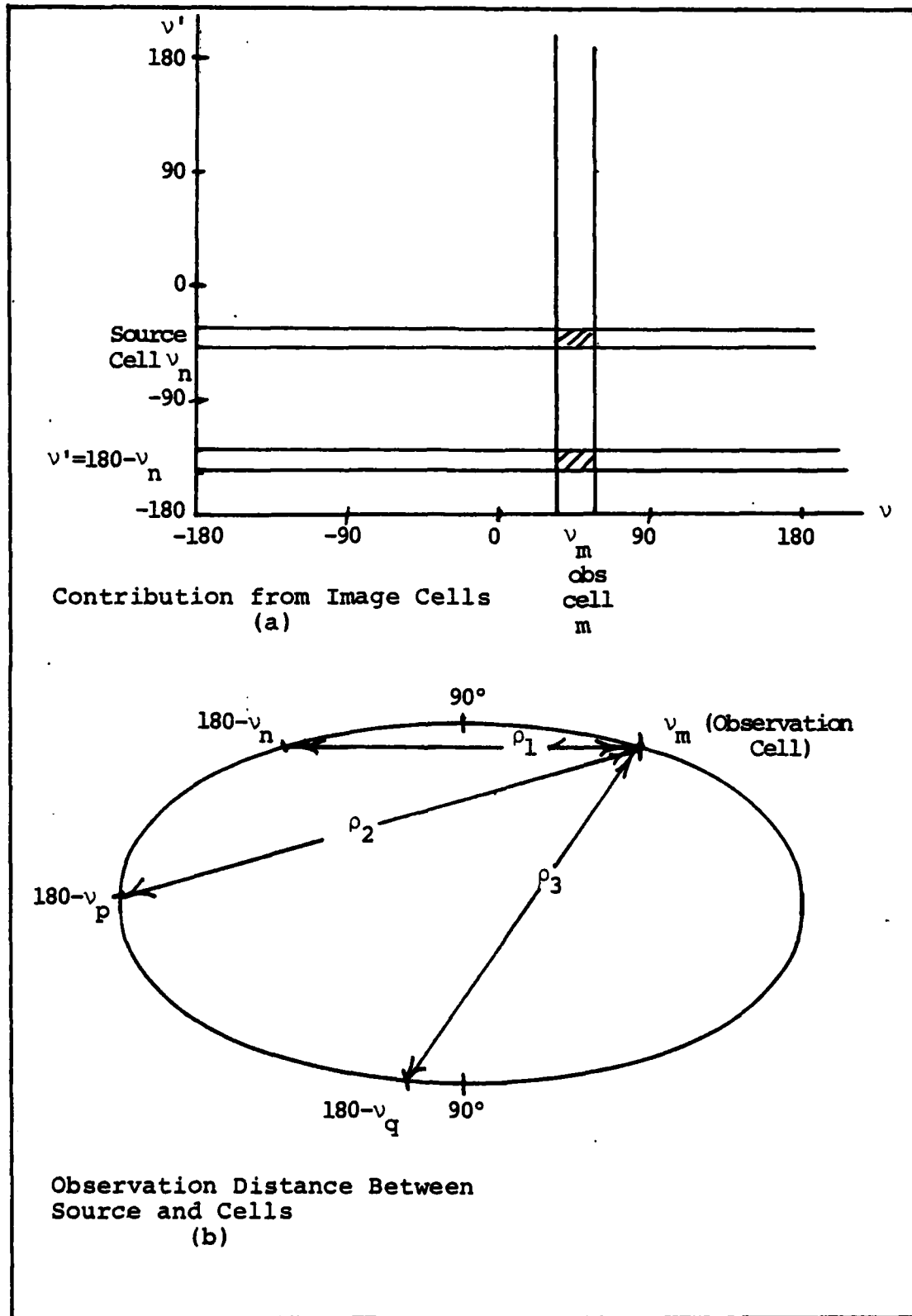


Figure 22. Image Cells

changes (see Figure 22(b)). The use of symmetry does not reduce the number of calculations. It reduces the amount of core required to solve the problem, a critical factor when large (greater than one wavelength) is considered.

Singularity. The program had to evaluate the principal value integral around the singular points. A numerical integration routine can not take the limiting value of a function and special routines must account for these regions. In this problem, there were three types of singularities encountered which could be considered as two classes. Table 5 gives the class and type of singularities encountered. Figure 23 is a graphic presentation of each class.

Table 5. Program Singularities

Type of Singularity	Class	Cross-Reference to Figure 20
<u>Overlapping cells</u>		
$n = m$	line	Region B
$m = n \pm 1$	line	Region C
<u>Corner</u>		
$v_m = v_n$	point	Point A

There were three separate methods tested in consideration of the singular cells with a goal that accurate results were returned, but with the CPU time being held to a minimum. The first routine integrated up to the line

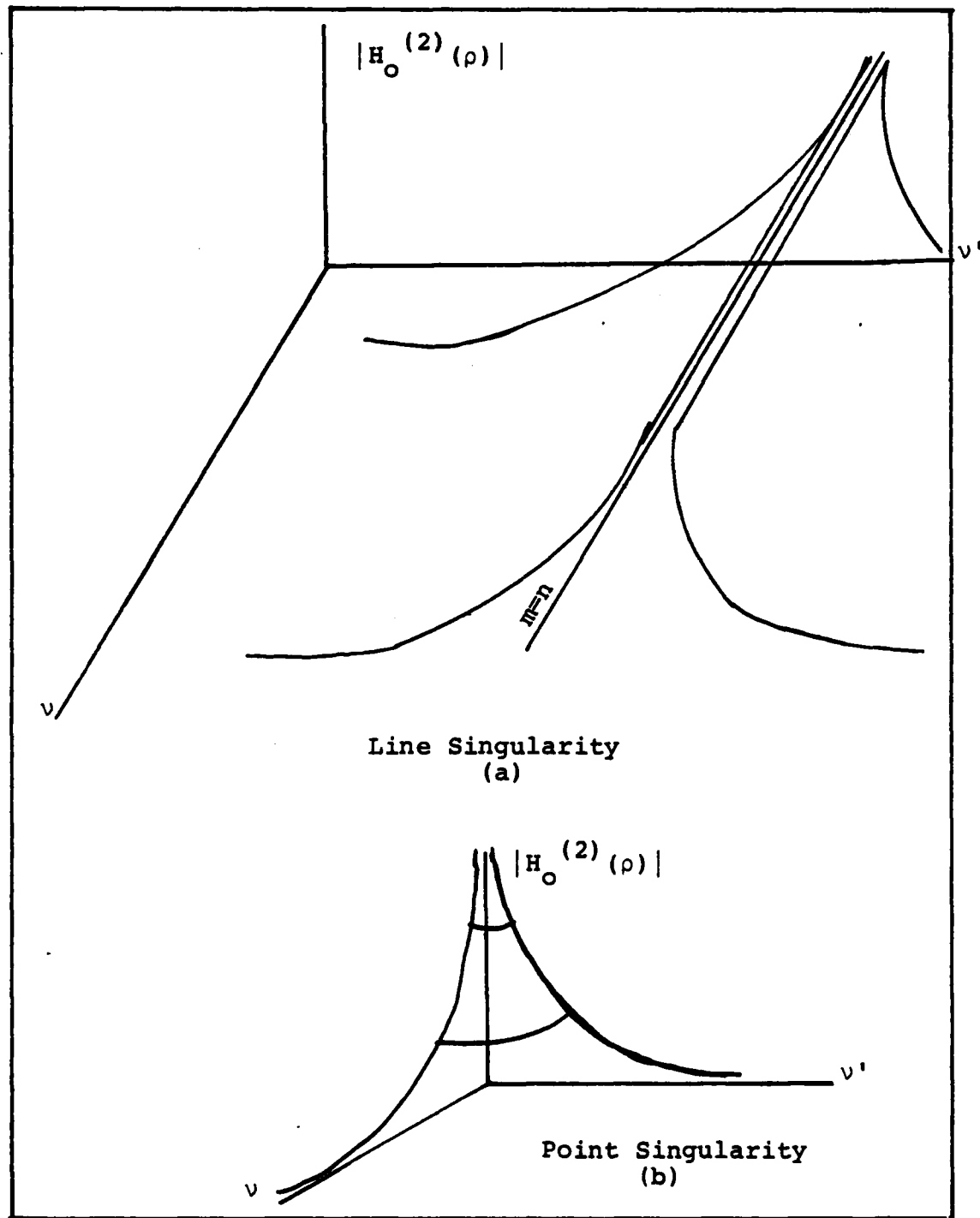


Figure 23. Singularity Classes

singularity, but left an area surrounding the singularity. James, et al. [38:339-342] suggested that the function be expanded in a Taylor Series around the singular point, integrating term by term. A test routine was written integrating $\ln |x-x'|$ over -1 to 1 using a Simpson Rule routine [38:331] and the IMSL DCADRE routine, but with the singular region ignored. Testing only 10 subdivisions, the error was -0.193 percent. Using 1000 subdivisions, the error was -2.5×10^{-3} percent.

The point singularity was handled by excluding the point. This problem occurred when the range of each integration overlapped, say going from 1 to 2 and 2 to 3. Using the $\ln |x-x'|$ function again, it was found that by integrating the inner integral from 1 to 1.999999999999 and then the outer from 2 to 3, the results were limited only by the limitation on the accuracy of the Simpson routine and the number of subdivisions used.

The disadvantage of this is now special cases have to be drawn up for the possible singularities. The corner singularities were generally found by trial and error (i.e., the program hit a divide by zero error and quit).

The first method discussed involved special programs and calls to avoid the problem. In either case, the singular point was approached, but not integrated over. However, it was decided that these special routines were not necessary. Instead, if the argument of the Hankel

function went to zero in the program, it was declared to have a small value. The minimum value that the FUNPACK routine could handle was 2^{-128} or 2.938×10^{-39} .

The range of values tried was from 10^{-4} to 10^{-25} . This routine was very easy to program; however, the run times doubled. The DCADRE integrator would continuously subdivide the interval from the last actual value to the declared value. Using a larger number did not resolve the problem since the integrator would bog down in trying to resolve the sharp cutoff that resulted.

The final routine involved "capping" the singular point with a parabolic approximation. This cut run times by one-half since now the singular region had a smooth peak, as opposed to a sharp peak or flat top.

Equation (4.12) is the function used. Let $H^*(\delta) = a_0$ and $H^{*'}(\delta) = a_1$

$$H_0^{(2)}(\rho) = C_0 + C_2 \rho^2 \quad (4.12)$$

The (δ) used was 10^{-3} . Using a_0 and a_1 with (4.12) results in

$$C_0 = a_0 - \frac{a_1 \delta}{2} \quad C_2 = \frac{a_1}{2\delta} \quad (4.13)$$

Using this function simplified the problem since the result could be used by either class of singular region. The routine significantly reduced run times also.

Test Runs. To test the program, the scatterer was made to be as circular as possible. The resultant

Z_{MN} should be a toeplitz matrix. In such a matrix, all of the elements along each diagonal are equal. The toeplitz matrix results because the array elements are calculated on a basis of geometry [14:341]. All of these elements are the result of integration of equally sized self cells. Schneider's results showed that this matrix does result [4:18]. The test program included a repeat of Schneider's results [4:27-30,47-49] for the small scatterer. This would validate the program since his results are correct and the solution is unique [40:532-534].

Unresolved Problems. The test case run did show that the toeplitz matrix does result for the circular scatter. This validates the fact that the geometry of the problem is being described correctly by the program. It does not validate that the values obtained are correct. Herein lies the problem. The resultant reaction matrix should be banded in that the elements of the main diagonal and the right and left codiagonals are significantly higher than the rest of the array. Additionally, the magnitude of the voltage vector should increase as you evaluate from the 0th cell to the Nth cell. This increase should be significant.

Neither of the described conditions was met by the resultant array or vector. The voltage vector gradually increases as you get closer to the line source, but only by a factor of 3. The main diagonals are only an order of 10 higher than the other elements of the reaction

array. The other elements then varied in sign and magnitude across a row. Their magnitude did not go to zero as expected.

Radiation Calculation

The final program was to calculate the far field electric field and display the results. The current in each cell would be obtained by going back to the expansion function and putting the calculated C_n back into the equation. However, the far field is very insensitive to small changes over a small area. Therefore, the electric field for the cells was assumed to be $V_{MN}(M)$ across the entire m th cell. The far field approximation for the vector potential is

$$A_z = \frac{e^{-jk_0 \rho}}{\sqrt{8j\pi k_0 \rho}} \iint_{\text{cell } m} J_z(\rho') e^{jk_0 \rho' \cos(\phi - \phi')} dA' \quad (4.14)$$

[10:229]

or in elliptic coordinates, if ρ is the distance from the origin to the point on the ellipse

$$A_z = \frac{\epsilon_0^2 e^{-jk\rho}}{\sqrt{8j\pi k\rho}} \int_{v_n}^{v_{n+1}} J_z(\mu_0, v') e^{jk [a^2 \cos^2 \phi + b^2 \sin^2 \phi]^{\frac{1}{2}} \cos(v-v')} dA' \quad (4.15)$$

a = semi-major axis

b = semi-minor axis

$$\begin{aligned}\phi &= \tan^{-1}((a/b) \tan v) \\ \phi' &= \tan^{-1}((a/b) \tan v') \\ dA' &= (\cosh^2 \mu_0 - \cos^2 v') dv'\end{aligned}$$

The far field observation point is $2a^2/\lambda$ [14:24]. The far field electric field is then determined from

$$E_z = j\omega\mu_0 A_z \quad [14:25] \quad (4.16)$$

or

$$\begin{aligned}E_z &= \frac{3k^2 c^4 \omega \mu_0 \tau^3 e^{-jk_0 \rho}}{\sqrt{8j\pi k_0 \rho}} \int_{v_n}^{v_{n+1}} J_z(\mu_0, v) \\ &\cdot e^{jk[a^2 \cos^2 \phi + b^2 \sin^2 \phi]^{1/2}} \cos(v-v') \\ &\cdot (\cosh^2 \mu_0 - \cos^2 v') dv' \quad (4.17)\end{aligned}$$

Since program 2 never worked, the radiation program was not developed. The contribution from each cell would be summed over the entire 360° . The plot was to be displayed on the off line calcomp plotter using the DISSPLA package.

V. Lessons Learned

The exact reason that the program failed is not known. Sources of error could have come from a myriad of sources. Countless checks have been performed on the program and no error can be found. A better method needs to be used in the integration if the method of moments has to be used to solve this problem. Blue's article showed that the number of cells could be kept small by using different basis functions [26]. A fewer number of cells would have substantially improved this procedure since fewer integrations would have been necessary.

Despite the program failure, this thesis showed that straight application of the moment method, even with the use of the more complicated basis functions, is not practical for larger scatterers. While the core problem has been solved, a real time problem has surfaced. If it takes 1300 seconds to process a 33 by 33 array, a 120 x 120 array would take way too long. The expense in that much computing would be high.

When computing with wire scatterers, the observation point is done on the inside of the metal, while the source is considered on the outside skin. With this in mind, the observation point could have been made just above μ_0 . Since the electric field, and therefore the

current, is constant throughout, the electric field would not have changed. The runs done so far show that the singular cells take 10 seconds, nonsingular take 1.5 to 0.5 seconds, and the voltage matrix takes less than 0.1 seconds. Therefore, the problem is in the singularity. The removal of the singular point would greatly speed operations. While time would not permit this condition, it is worth continued investigation.

VI. Conclusions

This study analyzed the scattering of cylindrical electromagnetic waves off of dielectric scatterers. The scatterer was an elliptic shell, designed to model the radome of the F-16. The equation developed by Richmond [10] was used and solved by the method of moments. To reduce the amount of storage needed, the basis and testing functions were the sinusoidal basis functions. The result was a complicated integral that took a great deal of time to compute over each cell.

The program never worked and there were no plots produced. The exact source of error is unknown, but the most probable are either a programming or an error in the integration over the shell thickness. The study did show that this method was impractical for large scatterers. The amount of integration required to fill the reaction matrix was far too much to be practical. The cost of such runs made justification difficult.

While the program never produced valid results, it is felt that the conclusion that the method is impractical is valid. The evaluation of the individual contributions would still require 16 integrations to be done per cell. Each integration takes considerable amount of time. The improbable values of the array and vector elements are

more likely due to the handling of the singular region rather than in a programming error. The removal of the singularity may have removed the main reason for the side lobe. Thus the array elements were only gradually varying.

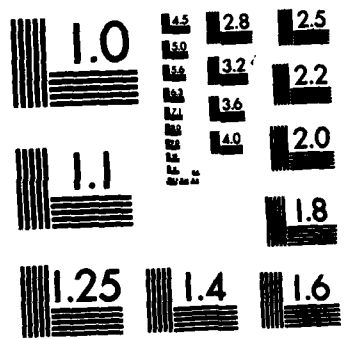
As recommendations for future study, Blue's method of different basis functions bears more study. The reduction in the number of basis functions would greatly reduce the number of integrations needed.

The method used here may be improved by breaking up the singular cells into subregions. If the singular area was square, Richmond's analytical integration [10:336] could be applied. The rest of the cell would be considered using the methods described in this report. The contributions would then be added together.

Looking at other methods, if an efficient program could be written for the generation of Mathieu functions, then a series solution would be possible. Finally, an asymptotic evaluation of the integrals would then enable a solution to the integral equation to be computed since the integration would no longer be necessary.

Bibliography

1. General Dynamics. F-16 AN/ALR-69 GD Antenna Study. Unpublished briefing, Wright-Patterson AFB OH: Directorate of Avionics Engineering, Aeronautical Systems Division (ASD/ENAMA), 1979.
2. Kent, William J., Group Leader. Private communication. Directorate of Avionics Engineering, Aeronautical Systems Division (ASD/ENAMA), January 1982.
3. _____. Personal working papers. Directorate of Avionics Engineering, Aeronautical Systems Division (ASD/ENAMA), Wright-Patterson AFB OH, 1979.
4. Schneider, Robert K. The Effect of Radome Scattering on ECM Antenna Patterns. MS thesis. Wright-Patterson AFB OH: School of Engineering, Air Force Institute of Technology, December 1981. AFIT/GE/EE/81D-52, DTIC AD-A.
5. _____. Electronic Engineer. Private communication. Directorate of Avionics Engineering, Aeronautical Systems Division (ASD/ENAMA), Wright-Patterson AFB OH, February 1982.
6. Holt, A. R., N. K. Uzunoglu, and B. G. Evans. "An Integral Equation Solution to the Scattering of Electromagnetic Radiation by Dielectric Spheroids and Ellipsoids," IEEE Transactions on Antennas and Propagation, AP-26 (5), pp. 706-712, September 1978.
7. Wang, Johnson J. H. and C. Papanicolopoulos. A Study of the Analysis and Measurements of Three-dimensional Arbitrarily-shaped Dielectric Scatters. Griffiss AFB NY: Rome Air Development Center (RADC/EEC), December 1980 (RADC-TR-80-372).
8. Chang, Shu-Kong and Kenneth K. Mei. "Application of the Unimoment Method to Electromagnetic Scattering of Dielectric Cylinders," IEEE Transactions on Antennas and Propagation, AP-24 (1), pp. 35-42, January 1976.
9. Mei, Kenneth K. "Unimoment Method of Solving Antenna and Scattering Problems," IEEE Transactions on Antennas and Propagation, AP-22 (6), pp. 760-766, November 1975.



MICROCOPY RESOLUTION TEST CHART
NATIONAL BUREAU OF STANDARDS-1963-A

10. Richmond, Jack E. "Scattering by a Dielectric Cylinder of Arbitrary Cross Section Shape," IEEE Transactions on Antennas and Propagation, AP-13 (3), pp. 334-341, May 1965.
11. Yeh, Cavour, W. H. Scattering of Waves by Penetrable Objects. Los Angeles: School of Engineering and Applied Science, University of California, January 1969 (AD-681-702).
12. Poggio, A. J. and E. K. Miller. "Integral Equation Solutions of Three-dimensional Scattering Problems," in Computer Techniques for Electromagnetics, edited by Raj Mittra. Oxford, Great Britain: Pergamon Press, Ltd., 1973.
13. Harrington, Roger F. Field Computation by Moment Methods. Lamabar FL: Robert E. Krieger Publishing Company, 1982 (reprint).
14. Stutzman, Warren L. and Gary A. Thiele. Antenna Theory and Design. New York: John Wiley and Sons, Inc., 1981.
15. Johnson, Thomas W., Assistant Professor. Private communication. School of Engineering, Air Force Institute of Technology (AFIT/ENG), May 1982.
16. Harrington, Roger F. Time-Harmonic Electro-Magnetic Fields. New York: McGraw-Hill Book Company, 1961.
17. Chen, Kun-Mu. "A Simple Physical Picture of Tensor Green's Function in [the] Source Region," Proceedings of the IEEE, 65 (8), pp. 1202-1204, August 1977.
18. Mathews, John H. Basic Complex Variables for Mathematics and Engineering. Boston: Allyn and Bacon, Inc., 1982.
19. Tychonov, A. N. and A. A. Samarski. Partial Differential Equations of Mathematical Physics, Volume 1. San Francisco: Holden Day, Inc., 1964.
20. Yaghjian, Arthur D. A Direct Approach to the Derivation of Electric Dyadic Green's Function, NBS Technical Note 1000. Boulder CO: National Bureau of Standards, January 1978.
21. _____. "Electric Dyadic Green's Function in the Source Region," Proceedings of the IEEE, 68 (2), pp. 248-263, February 1980.

22. Lee, Shung-Wu, Mysore L. Sheshadri, Vahraz Jamnejad, and Raj Mittra. "Wave Transmission Through a Spherical Dielectric Shell," IEEE Transactions on Antennas and Propagation, AP-30 (3), pp. 373-380, May 1982.
23. Sarkar, Tapan Kumar. Method of Moments: Its Content, Method, and Meaning. Rochester NY: Department of Electrical Engineering, Rochester Institute of Technology, March 1979 (TR-2).
24. Butler, Chalmers M. and Donald R. Wilton. "Analysis of Various Numerical Techniques. Applied to Thin Wire Scatterers," IEEE Transactions on Antennas and Propagation, AP-23 (4), pp. 534-540, July 1975.
25. Hagmann, M. J., O. P. Gandhi, and C. H. Durney. "Procedures for Improving Convergence of Moment Method Solutions in Electromagnetics," IEEE Transactions on Antennas and Propagation, AP-26 (5), pp. 743-748, September 1980.
26. Blue, J. L. "Integral Equations for Electro-magnetic Scattering by Wide Scatterers," The Bell Systems Technical Journal, 59 (10), pp. 1893-1908, December 1980.
27. Marcatile, E. A. J. "Bends in Optical Dielectric Guides," The Bell Systems Technical Journal, 48 (7), pp. 2103-2132, September 1979.
28. Balanis, Constantine A. Antenna Theory Analysis and Design. New York: Harper and Row, Publishers, Inc., 1982.
29. Richmond, Jack H. Computer Analysis of Three Dimensional Wire Antennas. Columbus OH: Electro-science Laboratory, The Ohio State University, 22 December 1979.
30. Wang, Johnson J. H. Analysis and Measurements of Three Dimensional Arbitrarily-shaped Dielectric Scatterers (Interim Report). Griffiss AFB NY: Rome Air: Development Center, May 1980.
31. Air Force Institute of Technology. Data Automation General Information Guide. Wright-Patterson AFB OH: School of Engineering, Air Force Institute of Technology, July 1981.

32. Control Data Corporation. FORTRAN Version 5 Reference Manual, Revision F. Sunnyvale CA: Control Data Corporation Publications and Graphics Division, 14 May 1982 (604 81300).
33. Clemm, Donald. Evaluation of Special Functions on the CDC 6000/Cyber 74 Processors. Wright-Patterson AFB OH: Air Force Flight Dynamics Laboratory, December 1977 (AFFDL-TM-77-89-FBR).
34. Karam, James, Charles W. Richard, Jr., and Constantine F. Houpis. AFIT Digital Computer Manual for Faculty and Students of the School of Engineering. Wright-Patterson AFB OH: School of Engineering, Air Force Institute of Technology, July 1980.
35. International Mathematical and Statistical Libraries, Inc. IMSL Library Reference Manual (Edition Nine). Houston: International Mathematical and Statistical Libraries, Inc., June 1982 (IMSL LIB-0009).
36. Dongarra, J. J., C. B. Moler, J. R. Bunch, and G. W. Stewart. LINPAK Users' Guide. Philadelphia: Society for Industrial and Applied Mathematics, 1979.
37. Johnson, Thomas W., Assistant Professor. Lecture notes from EE 5.24, Electromagnetic Waves I. School of Engineering, Air Force Institute of Technology, Wright-Patterson AFB OH, 1981.
38. James, Merlin L., Gerald M. Smith, and J. C. Wolford II. Applied Numerical Methods for Digital Computers with FORTRAN and CSMP (Second edition). New York: Harper and Row, Publishers, Inc., 1977.
39. Olver, F. W. J. "Bessel Functions of Integer Order" in Handbook of Mathematical Functions with Formulas, Graphs, and Mathematical Tables, edited by Milton Abramowitz and Irene A. Stegun. New York: Dover Publications, Inc., 1972.
40. Jones, Douglas S. Methods in Electromagnetic Wave Propagation. Oxford, Great Britain: Oxford University Press, 1979.
41. General Dynamics, Inc. F-16 Flight Manual. Ogden UT: Ogden Air Logistics Center, 9 October 1981 (AF T.O. 1F-16A-1).

42. Moon, Parry and Domina E. Spencer. Field Theory Handbook Including Coordinate Systems, Differential Equations and Their Solutions. Berlin: Springer-Verlag, 1961.
43. Spiegel, Murray R. Schaum's Outline Series Vector Analysis. New York: McGraw-Hill Book Company, 1959.
44. Burnside, Walter D., Melvin C. Gilreath, Ronald J. Marhefka, and Chong L. Yu. "A Study of KC-135 Aircraft Antenna Patterns," IEEE Transactions on Antennas and Propagation, AP-23 (3), pp. 309-316, May 1975.
45. Beyer, William H. Standard Mathematical Tables (Twenty-fourth edition). Cleveland: CRC Press, Inc., 1976.
46. Lockwood, E. H. A Book of Curves. Cambridge, Great Britain: University Press, 1961.
47. Thiele, Gary A. "Wire Antennas" in Computer Techniques for Electromagnetics, edited by Raj Mittra. Oxford, Great Britain: Pergamon Press, Ltd., 1973.

Appendix A

The Elliptic Coordinate System

The elliptic-hyperbolic coordinate system is one of the eleven orthogonal coordinate systems which is formed from first- and second-degree surfaces. This appendix will provide a compendium of information and relationships useful in analyzing the elliptic shell. The best overall source for coordinate system information was Moon and Spencer's Field Theory Handbook [42]. The Schaum's Outline Series handbook, Vector Analysis by Spiegel [43] and Morse and Feshback's Methods of Theoretical Physics also provide some valuable insight into the system. Moon and Spencer and Morse and Feshback have considerable discussion on the separation of variables, especially in terms of the Laplace and Helmholtz equations. Burnside [44], had a very complete list of relationships related to the elliptical geometry.

Figure A-1 shows the coordinate system relative to the xy plane. The positive z axis is up, out of the page. The defining relationships are

$$\begin{aligned}x &= c \cosh \mu \cos \nu \\y &= c \sinh \mu \sin \nu \\z &= z\end{aligned}\tag{A.1}$$

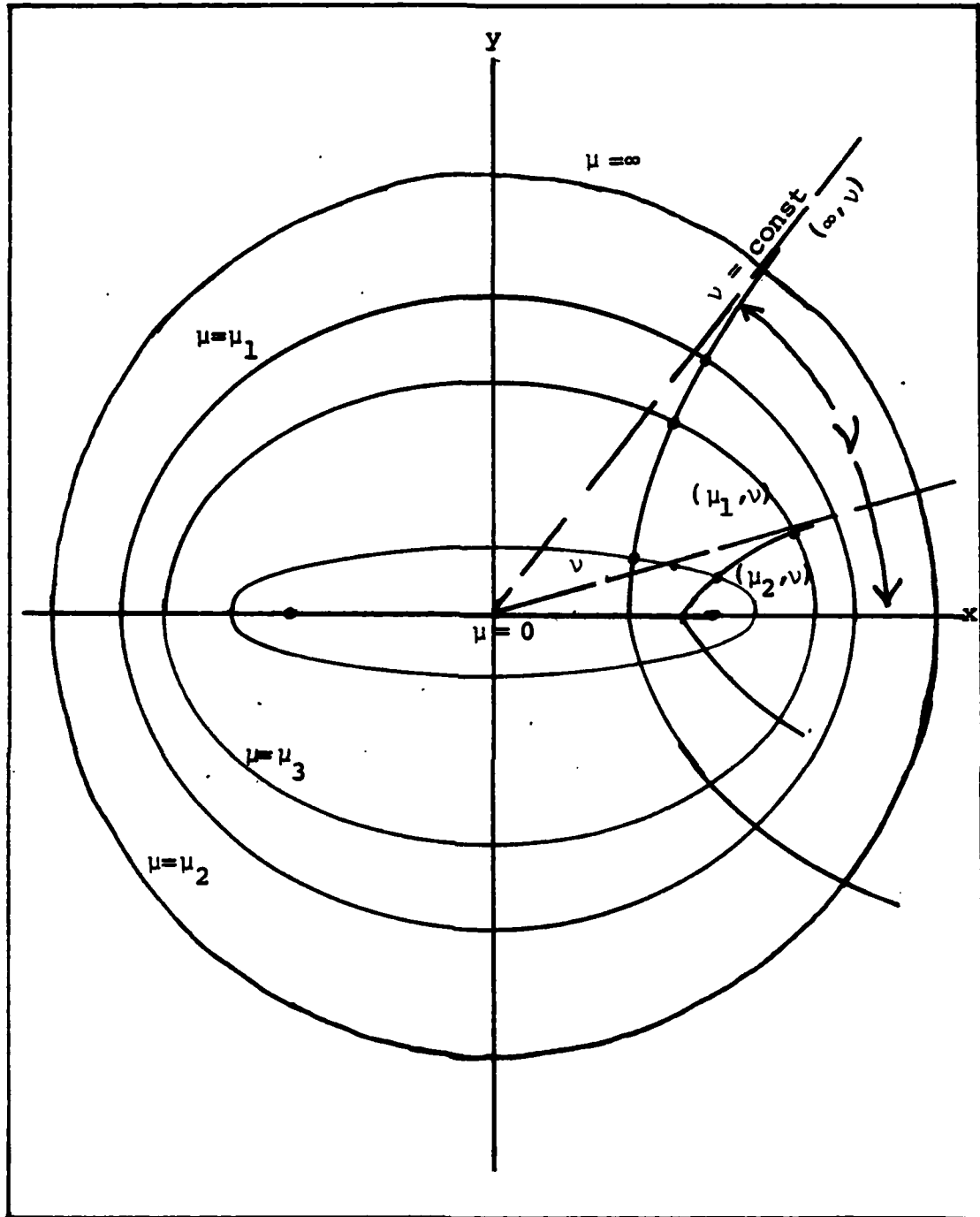


Figure A-1. Elliptic-Hyperbolic Cylinder Coordinate System

where c is the focal length; μ and ν are the coordinates of the system. Surfaces of constant, μ , are elliptical cylinders and surfaces of constant, ν , are hyperbolic cylinders.

μ is defined as

$$\mu = \tanh^{-1}(b/a) \quad (\text{A.2})$$

where a is the semi-major axis and b is the semi-minor axis. The limiting case for $\mu \rightarrow \infty$ describes a circle. The range of μ is from 0 to ∞ and is radius independent.

The angular coordinate, ν , is the angle from the x axis to the asymptote of the hyperbola that intersects the point in question (see Figure A-2). The polar angle ϕ , does not equal ν except at 0, 90, 180, and 270°.

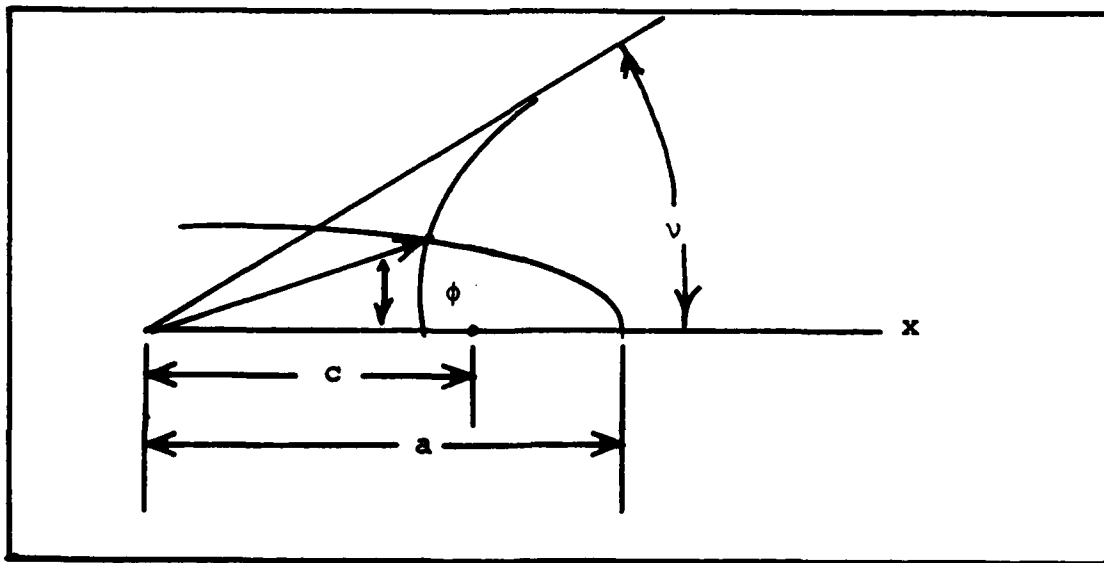


Figure A-2. Angular Coordinates

The relationship between ϕ and ν is

$$\phi = \tan^{-1}[(b/a) \tan \nu] \quad (\text{A.3})$$

This is based on the fact that $a = c \cosh \mu$ and $b = c \sinh \mu$. The range of ν is from 0 to 360° .

The unit vectors $\hat{\mu}_\mu$ and $\hat{\mu}_\nu$ are

$$\begin{aligned} \hat{\mu}_\mu &= \frac{c \sinh \mu \cos \nu \hat{\mu}_x + c \cosh \mu \sin \nu \hat{\mu}_y}{\sqrt{\sinh^2 \mu \cos^2 \nu + \cosh^2 \mu \sin^2 \nu}} \\ &= \frac{b \cos \nu \hat{\mu}_x + a \sin \nu \hat{\mu}_y}{\sqrt{\sinh^2 \mu \cos^2 \nu + \cosh^2 \mu \sin^2 \nu}} \end{aligned} \quad (\text{A.4a})$$

$$\begin{aligned} \hat{\mu}_\nu &= \frac{-c \cosh \mu \sin \nu \hat{\mu}_x + c \sinh \mu \cos \nu \hat{\mu}_y}{\sqrt{\cosh^2 \mu \sin^2 \nu + \sinh^2 \mu \cos^2 \nu}} \\ &= \frac{a \sin \nu \hat{\mu}_x + b \cos \nu \hat{\mu}_y}{\sqrt{\cosh^2 \mu \sin^2 \nu + \sinh^2 \mu \cos^2 \nu}} \end{aligned} \quad (\text{A.4b})$$

$\hat{\mu}_\nu$ is the vector tangent to the ellipse and $\hat{\mu}_\mu$ is the vector tangent to the hyperbola or the outward normal from the ellipse [44:310-311].

The following is then a list of relationships used or noted during the course of this research:

Differential area:

$$dA = c^2 (\cosh^2 \mu - \cos^2 \nu) d\mu d\nu \quad [42:18] \quad (\text{A.5a})$$

$$dA = c^2 (\sinh^2 \mu + \sin^2 \nu) d\mu d\nu \quad [43:139] \quad (\text{A.5b})$$

These equations are equivalent.

Elliptic cylinders:

$$(x/c \cosh \mu)^2 + (y/c \sinh \mu)^2 = 1 \quad [42:17] \quad (\text{A.6})$$

arc length:

$$l = \int_{\nu_1}^{\nu_2} \sqrt{a^2 \sin^2 \nu + b^2 \cos^2 \nu} \quad [44:310] \quad (\text{A.7})$$

Circumference:

$$L = 4aE(a/c) \quad [45:12]$$

$$\cong \pi [3(a+b) - \sqrt{(a+3b)(3a+b)}] \quad [46:18] \quad (\text{A.8})$$

$$\cong 2\pi \sqrt{1/2(a^2+b^2)} \quad [45:12]$$

$E(a/c)$ is the complete elliptic integral of the second kind.

Area

$$A = \pi ab \quad [46:18] \quad (\text{A.9})$$

Radius of curvature:

$$\rho = (a^2 \sin^2 \nu + b^2 \cos^2 \nu)^{3/2} / ab \quad [46:21] \quad (\text{A.10})$$

$$\nabla \cdot \bar{E} = \frac{1}{c[\cosh^2 \mu - \cos^2 \nu]^{\frac{1}{2}}} \left\{ \frac{\partial}{\partial \mu} [(\cosh^2 \mu - \cos^2 \nu)^{\frac{1}{2}} E_{\mu}] \right. \\ \left. + \frac{\partial}{\partial \nu} [(\cosh^2 \mu - \cos^2 \nu)^{\frac{1}{2}} E_{\nu}] \right\} + \frac{\partial E}{\partial z} \quad [42:18] \quad (A.11)$$

$$\nabla \phi = \frac{1}{c[\cosh^2 \mu - \cos^2 \nu]^{\frac{1}{2}}} \left[\hat{\mu}_{\mu} \frac{\partial \phi}{\partial \mu} + \hat{\mu}_{\nu} \frac{\partial \phi}{\partial \nu} \right] + \hat{\mu}_z \frac{\partial \phi}{\partial z} \quad [42:18] \quad (A.12)$$

$$\nabla \times \bar{E} = \frac{1}{(\cosh^2 \mu - \cos^2 \nu)} \cdot$$

$$\begin{vmatrix} \bar{\mu}_{\mu} (\cosh^2 \mu - \cos^2 \nu)^{\frac{1}{2}} & \bar{\mu}_{\nu} (\cosh^2 \mu - \cos^2 \nu)^{\frac{1}{2}} & \bar{\mu}_z/a \\ \frac{\partial}{\partial \mu} & \frac{\partial}{\partial \nu} & \frac{\partial}{\partial z} \\ E_{\mu} (\cosh^2 \mu - \cos^2 \nu)^{\frac{1}{2}} & E_{\nu} (\cosh^2 \mu - \cos^2 \nu)^{\frac{1}{2}} & E_z/a \end{vmatrix} \quad (A.13)$$

$$\nabla^2 \phi = \frac{1}{c^2[\cosh^2 \mu - \cos^2 \nu]} \left[\frac{\partial^2 \phi}{\partial \mu^2} + \frac{\partial^2 \phi}{\partial \nu^2} \right] + \frac{\partial^2 \phi}{\partial z^2} \quad [42:18] \quad (A.14)$$

See [42] for equations related to the separation of Laplace's equation and the Helmholtz Equation [42:18-20]. See [45] and [46] for the more novel relationships for ellipse. Lockwood also has a great deal of information on the geometrical properties of curves in general.

Appendix B
FUNPACK Release 2

The following is a copy of a listing executed from the EDIT LIB Users Library. Since the special functions were all generated using the FUNPACK library, and since there is not a commercially published manual available, this file is included as part of this thesis. More detailed information on FUNPACK is available in AFFDL-TM-77-89-FBR [33]. For detailed data on LINPACK and the IMSL see [36] and [35], respectively.

LFUN

THIS LISTING IS OUTPUT FROM PROCEDURE LFUN(LFN) EXECUTED FROM THE EDITLIB USER LIBRARY. IT DOCUMENTS CODES SELECTED FROM ARGONNE CODE CENTER NO. 610, FUNPACK RELEASE 2, TO EVALUATE CERTAIN SPECIAL FUNCTIONS. THE CODES DESCRIBED ARE IN AN EDITLIB USER LIBRARY AS CENTRAL PROCESSOR PROGRAMS COMPILED UNDER FORTRAN EXTENDED, VERSION 4.5+414, USING THE ROUNDED ARITHMETIC OPTION. THE SOURCE CODES FROM WHICH THEY ARE DERIVED ARE IN AN UPDATE OLDPL. BOTH THE USER LIBRARY AND OLDPL RESIDE ON MAGNETIC TAPE. FOR FURTHER INFORMATION ON THESE CODES OR TO ACCESS THEM FROM TAPE, CALL

DONALD S. CLEMM / AFWAL/FIBR / 513-255-5350 (Av 785-5350).

ACC ABSTRACT 610

1. NAME OR DESIGNATION OF PROGRAM - FUNPACK RELEASE 2
2. COMPUTER FOR WHICH PROGRAM IS DESIGNED AND OTHERS UPON WHICH IT IS OPERABLE - IBM360,370, CDC6000-7000, UNIVAC1108,1110
3. DESCRIPTION OF PROBLEM OR FUNCTION - FUNPACK IS A COLLECTION OF FORTRAN SUBROUTINES TO EVALUATE CERTAIN SPECIAL FUNCTIONS. THE INDIVIDUAL SUBROUTINES ARE -

IDENTIFICATION	DESCRIPTION
NATSIO	F2IO BESSEL FUNCTION I-SUB-0
NATSII	F2II BESSEL FUNCTION I-SUB-1
NATSJO	F2JO BESSEL FUNCTION J-SUB-0
NATSJI	F2JI BESSEL FUNCTION J-SUB-1
NATSKO	F2KO BESSEL FUNCTION K-SUB-0
NATSKI	F2KI BESSEL FUNCTION K-SUB-1
NATSBESY	F2BY BESSEL FUNCTION Y-SUB-NU
DAW	F1DW DAWSON'S INTEGRAL
ELIPK	F1EK COMPLETE ELLIPTIC INTEGRAL OF THE FIRST KIND
ELIPE	F1EE COMPLETE ELLIPTIC INTEGRAL OF THE SECOND KIND
EI	F1EI EXPONENTIAL INTEGRALS
NATSPSI	F2PS PSI (LOGARITHMIC DERIVATIVE OF GAMMA FUNCTION)
MONERR	F1MO ERROR MONITORING PACKAGE
4. METHOD OF SOLUTION - FUNPACK USES EVALUATION OF MINIMAX APPROXIMATIONS.
5. RESTRICTIONS ON THE COMPLEXITY OF THE PROBLEM -
6. TYPICAL RUNNING TIME -
7. UNUSUAL FEATURES OF THE PROGRAM - THESE ROUTINES HAVE BEEN CERTIFIED UNDER THE NATS PROJECT FOR THE MACHINES AND OPERATING SYSTEMS INDICATED IN ITEM 13 AND FOR THE COMPILERS INDICATED IN ITEM 12. EXTENSIVE TESTING ON THESE MACHINES HAS SHOWN NO EVIDENCE OF PERFORMANCE DIFFICULTIES. EXCEPTIONS, IF ANY, FOLLOW -

CDC VERSIONS OF THESE SUBROUTINES ARE TUNED TO PERFORM BEST USING THE ROUNDED ARITHMETIC OPTION ON CDC COMPILERS.

THE ACCURACY OF THE SUBROUTINES FOR THE ELEMENTARY FUNCTIONS (EXP, ALOG, ETC.) CAN AFFECT THE ACCURACY OF FUNPACK SUBROUTINES.

THE IBM VERSION OF THIS PACKAGE ASSUMES THE IBM-SUPPLIED TRACEBACK SUBROUTINE ERRTRA IS AVAILABLE.

THE NATS PROJECT FULLY SUPPORTS CERTIFIED ROUTINES IN THE SENSE THAT REPORTS OF POOR OR INCORRECT PERFORMANCE ON AT LEAST THE MACHINES AND OPERATING SYSTEMS LISTED WILL BE EXAMINED AND

NECESSARY CORRECTIONS MADE. THIS ASSURANCE OF SUPPORT APPLIES ONLY WHEN THE SOFTWARE IS OBTAINED DIRECTLY FROM THE ARGONNE CODE CENTER AND HAS NOT BEEN MODIFIED.

8. RELATED AND AUXILIARY PROGRAMS - FUNPACK RELEASE 2 REPLACES FUNPACK, AN EARLIER PACKAGE SUBMITTED IN JULY 1973 AND DISTRIBUTED BY THE CODE CENTER AS ACC NO. 610 PRIOR TO THIS RELEASE. SUBROUTINES IDENTIFIED AS FIXX IN ITEM 3 ABOVE ARE UNMODIFIED FROM THE PREVIOUS RELEASE, WITH THE POSSIBLE EXCEPTION OF THE TEST MATERIAL FOR THE IBM MACHINES.
9. STATUS - ABSTRACT FIRST DISTRIBUTED JULY 1973.
IBM360,370 VERSION OF FUNPACK SUBMITTED AUGUST 1973,
REPLACED BY FUNPACK RELEASE 2 SEPTEMBER 1976, SAMPLE PROBLEMS EXECUTED BY ACC SEPTEMBER 1976 ON AN IBM370/195.
CDC6000-7000 VERSION OF FUNPACK SUBMITTED AUGUST 1973,
REPLACED BY FUNPACK RELEASE 2 SEPTEMBER 1976, SAMPLE PROBLEMS EXECUTED BY ACC OCTOBER 1976.
UNIVAC1108 VERSION OF FUNPACK SUBMITTED AUGUST 1973,
REPLACED BY UNIVAC1108,1110 VERSION OF FUNPACK RELEASE 2 SEPTEMBER 1976.
10. REFERENCES - J. M. BLAIR AND C. A. EDWARDS, STABLE RATIONAL MINIMAX APPROXIMATIONS TO THE MODIFIED BESSEL FUNCTIONS $I_0(X)$ AND $I_1(X)$, AECL-4928, 1974.
J. M. BLAIR AND A. E. RUSSON, RATIONAL FUNCTION MINIMAX APPROXIMATIONS FOR THE BESSEL FUNCTIONS $K_0(X)$ AND $K_1(X)$, AECL-3461, 1969.
W. J. CODY, CHEBYSHEV APPROXIMATIONS FOR THE COMPLETE ELLIPTIC INTEGRALS K AND E , MATH. COMP. 19, 105-112 (1965).
W. J. CODY, R. M. MOTLEY, AND L. W. FULLERTON, THE COMPUTATION OF REAL FRACTIONAL ORDER BESSEL FUNCTIONS OF THE SECOND KIND, APPLIED MATHEMATICS DIVISION TECHNICAL MEMORANDUM NO. 291, ANL, 1976.
W. J. CODY, K. A. PACIOREK, AND H. C. THACHER, JR., CHEBYSHEV APPROXIMATIONS FOR DAWSON'S INTEGRAL, MATH. COMP. 24, 171-178 (1970).
W. J. CODY, A. J. STRECOK, AND H. C. THACHER, JR., CHEBYSHEV APPROXIMATIONS FOR THE Ψ FUNCTION, MATH. COMP. 27, 123-127 (1973).
W. J. CODY AND HENRY C. THACHER, JR., RATIONAL CHEBYSHEV APPROXIMATIONS FOR THE EXPONENTIAL INTEGRAL $E_1(X)$, MATH. COMP. 22, 641-649 (1968).
W. J. CODY AND HENRY C. THACHER, JR., RATIONAL CHEBYSHEV APPROXIMATIONS FOR THE EXPONENTIAL INTEGRAL $E_1(X)$, MATH. COMP. 23, 289-303 (1969).
11. MACHINE REQUIREMENTS -
12. PROGRAMMING LANGUAGES USED -
FORTRAN IV(G) IBM360/75,195,IBM370/165,195
FORTRAN IV(G 21) IBM360/65,75,91,IBM370/158
FORTRAN IV(G1) IBM360/75,195
FORTRAN IV(H) IBM360/65,67,75,195,IBM370/165
FORTRAN IV(H 20.1) IBM360/65,75,195,AMDAHL470V/6
FORTRAN IV(H 21.6) IBM360/75,91
FORTRAN IV(H 21.7) IBM360/75
FORTRAN IV(H 21.8) IBM360/65

FORTRAN IV(H EXTENDED)	IBM370/195
FORTRAN IV(H EXTENDED 2.1)	IBM360/75, 91, IBM370/168, 168-II
FORTRAN IV(WATFIV)	IBM360/67
FORTRAN IV(WATFIV 1.4)	IBM370/158
FTN	CDC6400, 6500
FTN(4.642)	CDC6600, CY173, 175
FTN(3.0)	CDC6400
RUN	CDC6400, 6500, 6600-6400, 7600
RUN(2.3)	CDC6400
FUN	CDC6400-6500, 6600, 6700
FTN V	UNIVAC1108
FTN V(S10A-0)	UNIVAC1108
FTN V(MACC 1.175)	UNIVAC1110
13. OPERATING SYSTEM OR MONITOR UNDER WHICH PROGRAM IS EXECUTED -	
OS/360	IBM360/67
OS/360(19.6)	IBM360/65
OS/360(20.1)	IBM370/165
OS/360(20.7)	IBM360/75, 195
OS/360(21.0)	IBM360/75, 91
OS/360(21.7)	IBM360/75, 370/195
OS/360(21.8)	IBM360/75
OS/MVT(21.7)	IBM370/165-II
OS/MVT(21.8)	IBM360/65, 91, IBM370/158
OS/VS2(1.6)	IBM370/168
MTS	IBM360/67, AMDAHL470V/6
STANFORD UNIVERSITY	IBM360/67
PURDUE UNIVERSITY	CDC6500, 6400-6500
BERKELEY LABORATORY	CDC6600, 7600
LIVERMORE LABORATORY	CDC6600, 7600
NCAR	CDC6600, 7600
SCOPE(3.3)	CDC6400
SCOPE(3.4)	CDC6600
UT2D	CDC6600-6400
EXEC 8	UNIVAC1108
EXEC 31.244E	UNIVAC1108
EXEC MACC 31.66	UNIVAC1110
14. OTHER PROGRAMMING OR OPERATING INFORMATION OR RESTRICTIONS -	
LOCATIONS AND MACHINES USED FOR FUNPACK TESTING WERE -	
MACHINE	TEST SITE
IBM360/65, IBM370/158	AMES LABORATORY, IOWA STATE UNIVERSITY
IBM360/75, 195, 370/195	ARGONNE NATIONAL LABORATORY
IBM360/75, 91	OAK RIDGE NATIONAL LABORATORY
IBM360/67, 91, 370/168	STANFORD UNIVERSITY
IBM360/75	STOCKHOLM DATA CENTER
IBM360/65	THE UNIVERSITY OF CHICAGO
IBM360/75	UNIVERSITY OF ILLINOIS AT URBANA-CHAMPAIGN
IBM360/67, AMDAHL470V/6	THE UNIVERSITY OF MICHIGAN
IBM360/67	THE UNIVERSITY OF NEW MEXICO
IBM370/165, 165-II	UNIVERSITY OF TORONTO
CDC6600	KIRTLAND AIR FORCE BASE/AFWL
CY173, 175	ICASE/NASA LANGLEY RESEARCH CENTER
CDC6600, 7600	LAWRENCE BERKELEY LABORATORY

CDC6600,7600
CDC6600,7600

CDC6400
CDC6400-6500
CDC6600-6400
UNIVAC1108
UNIVAC1108
UNIVAC1108,1110

LAWRENCE LIVERMORE LABORATORY
NATIONAL CENTER FOR ATMOSPHERIC
RESEARCH
NORTHWESTERN UNIVERSITY
PURDUE UNIVERSITY
THE UNIVERSITY OF TEXAS AT AUSTIN
ILLINOIS INSTITUTE OF TECHNOLOGY
JET PROPULSION LABORATORY
UNIVERSITY OF WISCONSIN

15. NAME AND ESTABLISHMENT OF AUTHOR -

W. J. CODY
CONTACT BURTON S. GARBOW
APPLIED MATHEMATICS DIVISION
ARGONNE NATIONAL LABORATORY
9700 SOUTH CASS AVENUE
ARGONNE, ILLINOIS 60439

16. MATERIAL AVAILABLE - MAGNETIC TAPE TRANSMITTAL

SOURCE DECKS (370-3902 CARDS, 7600-3983 CARDS, 1110-4115
CARDS)
DEMONSTRATION PROGRAM SOURCE DECKS (370-2083 CARDS, 7600-2151
CARDS, 1110-2211 CARDS)
DEMONSTRATION OUTPUT (370-61 PAGES, 7600-58 PAGES, 1110-44
PAGES)
MACHINE-READABLE DOCUMENTATION (370-4532 CARDS, 7600-4518
CARDS, 1110-4518 CARDS)

17. CATEGORY - P

KEYWORDS - SPECIAL FUNCTIONS, EXPONENTIAL INTEGRALS, COMPLETE
ELLIPTIC INTEGRALS, DAWSON'S INTEGRAL, BESSEL
FUNCTIONS, NEUMANN FUNCTIONS, PSI FUNCTION

Appendix C

Input and Segmentation Program

The following is a copy of the source code for program 1. Detailed description of the program is provided in Chapter IV of this report and in the comments located within the code.

```
PROGRAM READIN(INPUT,OUTPUT,DATA,TAPE5=INPUT,TAPE6=OUTPUT,
1 TAPE7=DATA)
```

```

C
C THIS SECTION WILL READ IN THE VALUES FOR THE SIZE OF THE
C ELLIPTIC SHELL, COMPUTE THE ELLIPTIC COORDINATES, OUTPUT
C THOSE VALUES, PLOT THE CYLINDER, AND SKETCH IN (WITH THE
C SEGMENTS NUMBERED) THE LOCATION OF THE SEGMENTS.
C
DIMENSION RADII(0:100),ROW(0:100), PHI(0:100)
REAL K,KNOT,LAMDA
REAL MUNOT, MUIN, MUOUT, LENSIG(0:100), NUSEG(0:100)
C
PI = 3.1415926535898
READ(5,100,END=9999)A,B,T,XS,YS,FREQ
100 FORMAT(6F10.6)
IF (A.EQ.B) THEN
    B = A * 0.999999999999999
END IF
C = SQRT(A**2 - B**2)
E = C / A
CIRCUM = 4.0 * A * ELIE1(E)
DISTSC = SQRT(XS**2 + YS**2)
KNOT = 2.0 * PI * FREQ * 1.0E09 / 2.997925E03
MUNOT = ATANH(B/A)
TAU = T/A
IF ((XS.EQ.0.).AND.(YS.GT.0.)) THEN
    THETAS = 90.0
    VS = 90.0
ELSE IF ((XS.EQ.0.).AND.(YS.LT.0.)) THEN
    THETAS = 270.0
    VS = 270.0
ELSE IF ((XS.EQ.0.).AND.(YS.EQ.0.)) THEN
    THETAS = 0.0
    VS = 0.0
ELSE
    THETAS = ATAN(YS/XS) * (180.0/PI)
    VS = ATAN(A*TAND(THETAS)/B) * (180.0/PI)
END IF
IF ((XS.EQ.0.).AND.(YS.EQ.0.0)) THEN
    CS = 0.0
ELSE IF (XS.EQ.0.0) THEN
    CS = YS/(SINH(MUNOT)*SIND(VS))
ELSE
    CS = XS/(COSH(MUNOT)*COSD(VS))
END IF
WAVELT = 2.997925E08/(FREQ*1.0E09)
AW = A/WAVELT
BW = B/WAVELT
CW = C/WAVELT
TW = T/WAVELT
K = SQRT(16.0*(PI**2)-(80.0*SQRT(3.0*(PI**2)+100.0)-800.0))/WAVELT

```

```

LAMBDA = 0.75 * (W*C)**2
FC = K * C * SINH(2.0*MUNOT) * (TAU * COSH(TAU) - SINH(TAU)) /8.0
FCONS1 = -(KNOT**2)/(8.0 * PI * FREQ * 8.854185E-3)
FCONS2 = (KNOT**3) * (SINH(2.0 * MUNOT)**2)
1      * (TAU * COSH(TAU) - SINH(TAU))
2      / (64.0 * PI * FREQ * 8.854185E-03)
MUIN = MUNOT - TAU/2.0
MUOUT = MUNOT+ TAU/2.0
WRITE(6,1030)
1030 FORMAT('1',132('*'))
WRITE(6,1040) A, T, AW, TW, B, BW, XS, YS, C, E, CIRCUM
1040 FORMAT('0',15X,'INPUT DATA: '/25X,'SEMI-MAJOR AXIS: ',F10.6,
1' METERS.',10X,'SHELL THICKNESS: ',F10.6,' METERS.'/
A 30X,'(',F10.6,' WAVELENGTHS)',15X,'(',F10.6,' WAVELENGTHS)'/
225X,'SEMI-MINOR AXIS: ',F10.6,' METERS.',10X,'(',F10.6,' WAVE-
B ',LENGTHS)'/25X,'SOURCE X',
4' COORDINATE: ',F10.6,' METERS.',10X,'SOURCE Y COORDINATE: ',
5F10.6,' METERS.'//15X,'CALCULAT'
6,'ED DATA: '/25X,'FOCAL LENGTH: ',5X,F10.6,' METERS.',10X,
7'ECCENTRICITY : ',F10.6,'.'/25X,'CIRCUMFERENCE: ',
6F10.6,' METERS.')
WRITE(6,1050) MUOUT,TAU,MUIN,MUOUT
1050 FORMAT('-',15X,'CONSTANT ELLIPTIC COORDINATES: '//,25X,
1'MUNOT: ',F10.6,'.',10X,'TAU(=T/A): ',F10.6/25X,'INNER ',
2'RADIUS: ',F10.6,10X,'OUTER RADIUS: ',F10.6,')
WRITE(6,1055) MUOUT, VS, DISTSC, THETAS, CS
1055 FORMAT('0',15X,'SOURCE LOCATION: '/15X,'(SECOND SOURCE LOCATED '
1,'180 DEGREES FROM THE ONE INPUTTED)'/25X,'ELLIPTIC COORDINATE: '
2,2X,F10.6,10X,'ELLIPTIC ANGULAR COORDINATE: ',F10.6,' DEGREES.'/
325X,'POLAR DISTANCE FROM CENTER: ',F10.6,' METERS.',10X,'POLAR ',
4'ANGLE: ',F10.6,' DEGREES.'/50X,'FOCAL LENGTH FOR SOURCE ELLIPSE'
5': ',F10.6,' METERS.'////)
WRITE(6,1065) FREQ,WAVELT,K,KNOT
1065 FORMAT(' ',15X,'ELECTROMAGNETIC PARAMETERS'/25X,'FREQUENCY: ',
1F10.6,' GIGAHERTZ.',10X,'WAVELENGTH: ',F10.6,' METERS.'/25X,
2'WAVE NUMBER(DIELECTRIC): ',F10.6,'.',10X,'WAVE NUMBER(FREE ',
3'SPACE): ',F10.6,'.'/////)
C
C
C
C
C
      CONVERT ALL METER MEASURES TO WAVELENGTH MEASURES.
CIRCUM = (CIRCUM/2.0)/WAVELT
J=0
PHI(0)=-90.0
LENSIG(0)=0.0
NUSEG(0)=-90.0
CURLEN=0.0
THETA = -90.0
50 CONTINUE
      ROW(J) = ((AW*AW*SIND(THETA)*SIND(THETA)) + (BW*BW*COSD(THETA))*

```

```

1      COSD(THETA))**1.5/(AW*BW)
      RADII(J)=SORT(AW*AW*COSD(THETA)*COSD(THETA)+
1      BW*BW*SIND(THETA)*SIND(THETA))
      J = J + 1
      IF(ROW(J-1).GE.2.5) THEN
          LENSIG(J) = .25
      ELSE
          LENSIG(J) = ROW(J-1)/10.0
      END IF
      CHI=ATAN(LENSIG(J)/RADII(J-1))*180.0/PI
      CURLEN = CURLEN + LENSIG(J)
      THETA=THETA+CHI
      PHI(J)=THETA
      IF (PHI(J).EQ.-90.0) THEN
          NUSEG(J) = PHI(J)
      ELSE IF (PHI(J).EQ.90.0) THEN
          NUSEG(J) = PHI(J)
      ELSE
          NUSEG(J) = ATAN((A/B)*TAND(PHI(J))) * 180.0/PI
      END IF
      IF (THETA.LT.90.) THEN
          GO TO 50
      ELSE
          LENSIG(J)=CIRCUM-CURLEN
          PHI(J)=90.0
          NUSEG(J)=90.0
      END IF
      WRITE(6,1060)
      DO 60 KK=0,J
          WRITE(6,1070)KK,LENSIG(KK),PHI(KK),NUSEG(KK)
60 CONTINUE
          WRITE(6,1080)
          WRITE(6,1090)
1060   FORMAT('0',5X,'SEGMENT NUMBER',6X,'SEGMENT LENGTH',8X,'END POI'
1      'NT ANGLE',11X,'END POINT ANGLE'/26X,'(WAVELENGTHS)',
26X,'(DEGREES-CYLINDRICAL)',6X,'(DEGREES-ELLIPTICAL)')//)
1070   FORMAT(' ',11X,13,13X,F10.6,12X,F10.6,12X,F10.6)
1080   FORMAT('1')
1090   FORMAT('+',25X,'END OF JOB.')
      WRITE(7) PI,MUNOT,TAU,VS,CS,KNOT,K,WAVELT,LAMDA,FC,FCONS1,FCONS2,
1      C,J,NUSEG,PHI,A,R,T,FREQ
9999 CONTINUE
      STOP
      END

```

INPUT DATA:

SEMI-MAJOR AXIS: .037474 METERS. SHELL THICKNESS: .007495 METERS.
 (.250000 WAVELENGTHS) (.050001 WAVELENGTHS)
 SEMI-MINOR AXIS: .037474 METERS. (.250000 WAVELENGTHS)
 SOURCE X COORDINATE: 0.000000 METERS. SOURCE Y COORDINATE: .074950 METERS.

CALCULATED DATA:

FOCAL LENGTH: .000000 METERS. ECCENTRICITY : .000001.
 CIRCUMFERENCE: .235456 METERS.

CONSTANT ELLIPTIC COORDINATES:

IMNOT: 14.261155. TAU(=T/A): .200005
 INNER RADIUS: 14.061150 OUTER RADIUS: 14.261155.
 SOURCE LOCATION:

ELLIPTIC COORDINATE: 14.261155 ELLIPTIC ANGULAR COORDINATE: 90.000000 DEGREES.
 POLAR DISTANCE FROM CENTER: .074950 METERS. POLAR ANGLE: 90.000000 DEGREES.
 FOCAL LENGTH FOR SOURCE ELLIPSE': .000000 METERS.

ELECTROMAGNETIC PARAMETERS

FREQUENCY: 2.000000 GIGAHERTZ. WAVELENGTH: .149896 METERS.
 WAVE NUMBER(DIELECTRIC): 45.807338. WAVE NUMBER(FREE SPACE): 41.916895.

SEGMENT NUMBER	SEGMENT LENGTH (WAVELENGTHS)	END POINT ANGLE (DEGREES-CYLINDRICAL)	END POINT ANGLE (DEGREES-ELLIPTICAL)
0	0.000000	-90.000000	-90.000000
1	.025000	-84.289407	-84.289407
2	.025000	-78.578814	-78.578814
3	.025000	-72.868221	-72.868221
4	.025000	-67.157627	-67.157627
5	.025000	-61.447034	-61.447034
6	.025000	-55.736441	-55.736441
7	.025000	-50.025848	-50.025848
8	.025000	-44.315255	-44.315255
9	.025000	-38.604662	-38.604662
10	.025000	-32.894069	-32.894069
11	.025000	-27.183475	-27.183475
12	.025000	-21.472882	-21.472882
13	.025000	-15.762289	-15.762289
14	.025000	-10.051696	-10.051696
15	.025000	-4.341103	-4.341103
16	.025000	1.369490	1.369490
17	.025000	7.080083	7.080083
18	.025000	12.790676	12.790676
19	.025000	18.501270	18.501270
20	.025000	24.211863	24.211863
21	.025000	29.922456	29.922456
22	.025000	35.633049	35.633049
23	.025000	41.343642	41.343642
24	.025000	47.054235	47.054235
25	.025000	52.764828	52.764828
26	.025000	58.475422	58.475422
27	.025000	64.186015	64.186015
28	.025000	69.896608	69.896608
29	.025000	75.607201	75.607201
30	.025000	81.317794	81.317794
31	.025000	87.028387	87.028387
32	-.014602	90.000000	90.000000

Appendix D

Matrix Program and Linear Algebra Solver

The following is a copy of the source code for program 2 set up for the small circular case. Descriptions of the code are provided in Chapter IV of this report.

```

PROGRAM ARRAY(DATA,OUTPUT,RESULT,TAPE7=DATA,TAPE6=OUTPUT,
1  TAPE8=RESULT)

C
C   THIS SUBROUTINES CALCULATES THE FIELD ARRAY, ZMN, AND THE
C   SOURCE VECTOR, VMN. THIS IS DONE BY FIRST CALCULATING THE
C   ZMN TERMS WITH M BEING HELD CONSTANT. BEFORE LOOPING THE M
C   DO LOOP, THE COORESPONDING VOLTAGE VECTOR VALUE IS CALCULATED
C   BY CALLING THE SUBROUTINE KNOWN AS "VOLTS".
C
COMMON/CELLS/NU5,NU6,NU1,NU2,NU3,NU4,M,N,NOSEG,NUSEG
COMMON/ELLIPS/MU,C,TAU,K
COMMON/CONST/IFLAG,FC,FCONS1,FCONS2,PI,LAMDA
COMMON/SOURCE/CS,KNOT,VS
COMMON/SINGLE/AZERO,AONE
REAL K,KNOT,LAMDA,MU,NUSEGD,NUSEG(0:32),NU1,NU2,NU3,NU4,NU5,NU6
COMPLEX ZMN(0:32,0:32),VMN(0:32)
DIMENSION IPVT(32),Z(32)

C
CALL UERSET(1,IX)
READ(7) PI,MU,TAU,VS,CS,KNOT,K,MAVELT,LAMDA,FC,FCONS1,FCONS2,
1  C,NOSEG,NUSEG
PRINT *,',',PI,',',MU,',',TAU,',',VS,',',CS,',',KNOT
PRINT *,',',K,',',MAVELT,',',LAMDA,',',FC,',',FCONS1,', '
PRINT*,',',C,',',NOSEG
RADCVT = PI/180.0
DO 111 KKK=0,NOSEG
    NUSEGD = NUSEG(KKK)
    NUSEG(KKK) = NUSEG(KKK) * RADCVT
    PRINT*,',',NUSEG(KKK),',',NUSEGD
111 CONTINUE
WRITE(6,30)
30 FORMAT('1',7X,'M',8X,'N',12X,'REAL',14X,'IMAGINARY',12X,
1  'MAGNITUDE',14X,'PHASE',14X,'TIME')

C
C   CALCULATE CONSTANTS FOR USE IN THE MAIN SUBROUTINE AND RELATED
C   FUNCTIONS.
C
FCONS2 = ((C**2)/2.0) * (COSH(2.0*MU)*SINH(TAU) + TAU)
AZERO = YNU(1.0E-03,0)
AONE = -Y1(1.0E-03)
DO 20 M=0,NOSEG
    DO 10 N = 0,NOSEG
        CALL CLZMNR(ZMNR,ZMNI)

C
C   THE RETURNED VALUES FROM CLZMNR ARE REVERSED DUE TO THE PRE-
C   SENCE OF THE "J" IN THE EXPRESSION OF THE KERNAL. THIS IS
C   LAMDA FOR THE FREDHOLM INTEGRAL EQUATION OF THE SECOND KIND.
C
ZMN(M,N) = CMPLX(ZMNI,ZMNR)
RMAG = SQRT(ZMNI**2 + ZMNR**2)
PHASE = ATAN(ZMNR/ZMNI) * 180.0/PI

```

```

IF (M.EQ.N) THEN
  WRITE(6,40) M,N,ZMNI,ZMNR,RMAC,PHASE
ELSE
  WRITE(6,50)M,N,ZMNI,ZMNR,RMAC,PHASE
END IF
40 FORMAT('0',6('*'),I3,6X,I3,4(6X,E15.8))
50 FORMAT(' ',6X,I3,6X,I3,4(6X,E15.8))
10  CONTINUE
    CALL VOLTS(VMN)
20 CONTINUE

```

C

```

CALL CGECO(ZMN,NOSEG,NOSEG,IPVT,RCOND,Z)
PRINT *,'RCOND = ',RCOND
CALL CGESL(ZMN,NOSEG,NOSEG,IPVT,VMN,0)
WRITE (8) VMN
STOP
END

```

```

SUBROUTINE CLZMNR(ZMNR,ZMNI)

```

C
C
C
C
C
C

```

THIS SUBROUTINE DOES THE CALCULATION OF THE REAL AND THE IMAG-
INARY PARTS OF ZMN. SINCE THE IMSL INTEGRATOR DOES ONLY REAL
ARITHMETIC, THE PARTS HAD TO BE SEPERATED. HENCE THERE IS NO
HANKEL FUNCTION SUBROUTINE AS MIGHT BE EXPECTED.

```

```

COMMON/ELLIPS/MU,C,TAU,K
COMMON/CELLS/MU5,NU6,NU1,NU2,NU3,NU4,M,N,NOSEG,NUSEG
COMMON/CONST/IFLAG,FC,FCONS1,F1,PI,LAMDA
EXTERNAL FA1, FA3, FA5, FA7, FA11, FA31, FA51, FA71
EXTERNAL FSIA1,FSIA2,FSIA3,FSIA4,FSIB1,FSIB2,FSIB3,FSIB4
REAL LAMDA,K,MU,NUSEG(0:32),NU1,NU2,NU3,NU4,NU5,NU6

```

C
C
C
C
C
C

```

IFLAG = 0 - REAL FUNCTION
IFLAG = OTHER - IMAGINARY FUNCTION

```

```

PI2 = PI/2.0
F1 = ((C**2)/2.0) * (COSH(2.0*MU)*SINH(TAU) + TAU)
IF (M.GT.0) THEN
  NU1=NUSEG(M-1)
ELSE
  NU1 = -PI2 - (PI2+NUSEG(1))
END IF
  NU2=NUSEG(M)
IF (M.EQ.NOSEG) THEN
  NU3 = PI2 + (PI2-NUSEG(NOSEG-1))

```

```

ELSE
NU3=NUSEG(N+1)
END IF
IF (N.GT.0) THEN
NU4=NUSEG(N-1)
ELSE
NU4 = -PI2 - (PI2+NUSEG(1))
END IF
NU5=NUSEG(N)
IF (N.LT.NOSEG) THEN
NU6=NUSEG(N+1)
ELSE
NU6 = PI2 + (PI2-NUSEG(NOSEG-1))
END IF

```

C

```

. ITEST = M - N
IF (ITEST.EQ.0) THEN
IFLAG = 0
ZMNR =(SINSON(FA1,NU2,NU3,NU5,NU6,0.01,ERR,IER) + SINSON(FA5,
1NU1,NU2,NU4,NU5,0.01,ERR,IER)
A + SINSON(FA3,NU2,NU3,NU4,NU5,0.01,ERR,IER)
A + SINSON(FA7,NU1,NU2,NU5,NU6,0.01,ERR,IER)
1 + SINSON(FA11,NU2,NU3,PI-NU5,PI-
2 NU6,0.01,ERR,IER) + SINSON(FA31,NU2,
3 NU3,PI-NU4,PI-NU5,0.01,ERR,IER
4) + SINSON(FA51,NU1,NU2,PI-NU4,PI-
5 NU5,0.01,ERR,IER) + SINSON(FA71,NU1,
6 NU2,PI-NU5,PI-NU6,0.01,ERR,
7 IER)) * LAMDA
IFLAG=1
ZMNI = SINSON(FA1,NU2,NU3,NU5,NU6,0.01,ERR,IER)
1 + SINSON(FA5,NU1,NU2,NU4,NU5,0.01,ERR,IER)
A + SINSON(FA3,NU2,NU3,NU4,NU5,0.01,ERR,IER)
A + SINSON(FA7,NU1,NU2,NU5,NU6,0.01,ERR,IER)
1 + SINSON(FA11,NU2,NU3,PI-NU5,
2 PI-NU6,0.1,ERR,IER) + SINSON(FA31,
3 NU2,NU3,PI-NU4,PI-NU5,0.1,
4 ERR,IER) + SINSON(FA51,NU1,NU2,PI
5 -NU4,PI-NU5,0.1,ERR,IER)
6 + SINSON(FA71,NU1,NU2,PI-NU5,
7 PI-NU6,0.1,ERR,IER)
ZMNI = ZMNI * (-LAMDA)
1 + F1 * DCADRE(FSIA1,NU1,NU2,0.0,1.E-1,ERR,IER)
2 - TAU*C*C*DCADRE(FSIR1,NU1,NU2,0.0,1.E-1,ERR,IER)
3 + F1 * DCADRE(FSIA4,NU2,NU3,0.0,1.E-1,ERR,IER)
4 - TAU*C*C*DCADRE(FSIR4,NU2,NU3,0.0,1.E-1,ERR,IER)

```

C

```

ELSE IF (ITEST.EQ.1) THEN
IFLAG = 0
ZMNR = (SINSON(FA7,NU1,NU2,NU5,NU6,0.01,ERR,IER) + SINSON(FA1,
1 NU2,NU3,

```

```

1      NUS,NU6,0.01,ERR,IER)
2      + SIMSON(FA1I,NU2,NU3,PI-NU5,
3      PI-NU6,0.01,ERR,IER) + SIMSON(FA3I,
4      NU2,NU3,PI-NU4,PI-NU5,
5      0.01,ERR,IER) + SIMSON(FA3,NU2,NU3,
6      NU4,NU5,0.01,ERR,IER) + SIMSON(FA5,
7      NU1,NU2,NU4,NU5,0.01,ERR,
8      IER) + SIMSON(FA5I,NU1,NU2,PI-NU4,PI-NU5,
9      0.01,ERR,IER) + SIMSON(FA7I,NU1,NU2,
A      PI-NU5,PI-NU6,0.01,ERR,IER)) * LAMDA
      IFLAG=1
      ZMNI = SIMSON(FA7,NU1,NU2,NU5,NU6,0.01,IER,ERR) +
1      SIMSON(FA1,NU2,NU3,NU5,
1      NU6,0.1,ERR,IER) + SIMSON(FA1I,
2      NU2,NU3,PI-NU5,PI-NU6,
3      0.1,ERR,IER) + SIMSON(FA3,NU2,NU3,
4      NU4,NU5,0.1,ERR,IER) + SIMSON(FA3I,
5      NU2,NU3,PI-NU4,PI-NU5,0.1,ERR,
6      IER) + SIMSON(FA5,NU1,NU2,NU4,NU5,0.1,ERR,
7      IER) + SIMSON(FA5I,NU1,NU2,PI-NU4,PI-NU5,0.1,
8      ERR,IER) + SIMSON(FA7I,NU1,NU2,PI-NU5,
9      PI-NU6,0.1,ERR,IER)
      ZMNI = ZMNI * (-LAMDA)
1      + F1*DCADRE(FSIA2,NU1,NU2,0.0,1.E-1,ERR,IER)
2      - TAU*C*C*DCADRE(FSIB2,NU1,NU2,0.0,1.E-1,ERR,IER)
C
      ELSE IF(ITEST.EQ.-1) THEN
          IFLAG = 0
          ZMNR = (SIMSON(FA3,NU2,NU3,NU4,NU5,0.01,ERR,IER) +
1          SIMSON(FA1,NU2,NU3,NU5,NU6,0.01,ERR
1          ,IER) + SIMSON(FA1I,NU2,NU3,PI-NU5,PI-NU6,0.01,
2          ERR,IER) + SIMSON(FA3I,NU2,NU3,PI-NU4,PI-
3          NU5,0.01,ERR,IER) + SIMSON(FA5,NU1,NU2,NU4,NU5,
4          0.01,ERR,IER) + SIMSON(FA5I,NU1,NU2,
5          PI-NU4,PI-NU5,0.01,ERR,IER) + SIMSON(FA7,
6          NU1,NU2,NU5,NU6,0.01,ERR,IER) + SIMSON(FA7I,NU1,
7          NU2,PI-NU5,PI-NU6,0.01,ERR,IER)) * LAMDA
          IFLAG = 1
          ZMNI = SIMSON(FA3,NU2,NU3,NU4,NU5,0.01,ERR,IER)
1          + SIMSON(FA1,NU2,NU3,NU5,NU6,0.01,ERR
1          ,IER) + SIMSON(FA1I,NU2,NU3,PI-NU5,PI-NU6,0.1,
2          ERR,IER) + SIMSON(FA3I,NU2,NU3,PI-NU4,PI-
3          NU5,0.1,ERR,IER) + SIMSON(FA5,NU1,NU2,NU4,NU5,
4          0.1,ERR,IER) + SIMSON(FA5I,NU1,NU2,PI-NU4,
5          PI-NU5,0.1,ERR,IER) + SIMSON(FA7,NU1,NU2,NU5,
6          NU6,0.1,ERR,IER) + SIMSON(FA7I,NU1,NU2,PI-NU5,
7          PI-NU6,0.1,ERR,IER)
          ZMNI = ZMNI * (-LAMDA)
1          + F1*DCADRE(FSIA3,NU2,NU3,0.0,1.E-1,ERR,IER)
2          - TAU*C*C*DCADRE(FSIB3,NU2,NU3,0.0,1.E-1,ERR,IER)
C

```

```

ELSE
IFLAG = 0
ZMNR = (SIMSON(FA1, NU2, NU3, NU5, NU6, 0.01,
1   ERR, IER) + SIMSON(FA3, NU2, NU3,
2   NU4, NU5, 0.01, ERR, IER) + SIMSON(FA7,
3   NU1, NU2, NU5, NU5, 0.01, ERR,
4   IER) + SIMSON(FA5, NU1, NU2, NU4, NU5
5   , 0.01, ERR, IER) + SIMSON(FA11, NU2, NU3,
6   PI-NU5, PI-NU6, 0.01, ERR, IER) +
7   SIMSON(FA31, NU2, NU3, PI-NU4, PI-
8   NU5, 0.01, ERR, IER) + SIMSON(FA71, NU1,
9   NU2, PI-NU5, PI-NU6, 0.01, ERR,
A   IER) + SIMSON(FA51, NU1, NU2, PI-
B   NU4, PI-NU5, 0.01, ERR, IER)) * LAMDA
IFLAG = 1
ZMNI = (SIMSON(FA1, NU2, NU3, NU5, NU6, 0.01,
1   ERR, IER) + SIMSON(FA3, NU2, NU3, NU4
2   , NU5, 0.01, ERR, IER) + SIMSON(FA7, NU1,
3   NU2, NU5, NU6, 0.01, ERR, IER) +
4   SIMSON(FA5, NU1, NU2, NU4, NU5, 0.01,
5   ERR, IER) + SIMSON(FA11, NU2, NU3,
6   PI-NU5, PI-NU6, 0.01, ERR, IER) +
7   SIMSON(FA31, NU2, NU3, PI-NU4, PI-
8   NU5, 0.01, ERR, IER) + SIMSON(FA71, NU1,
9   NU2, PI-NU5, PI-NU6, 0.01, ERR,
A   IER) + SIMSON(FA51, NU1, NU2, PI-NU4
B   , PI-NU5, 0.01, ERR, IER)) * (-LAMDA)
END IF
RETURN
END

```

```

REAL FUNCTION DEL(V, VP)
COMMON/ELLIPS/MU, C, TAU, K

```

C
C
C
C

```

CALCULATES THE DISTANCE BETWEEN TWO POINTS OF CONSTANT MU
ON THE ELLIPTIC SHELL

```

```

REAL MU, K
DEL = SORT((COSH(MU)**2)*((COS(V)-COS(VP))**2) +
1 (SINH(MU)**2)*((SIN(V)-SIN(VP))**2))
RETURN
END

```

```
REAL FUNCTION FKERNL(V,VP)
```

```
C
C   THIS FUNCTION DETERMINES WHICH (REAL OR IMACINARY) SECTIONS IS
C   BEING CALCULATED BY THE DEFINITION OF IFLAG SET BY THE CALLING
C   PROGRAM.  SEE APPENDIX C.
C
```

```
COMMON/CELLS/NU5,NU6,NU1,NU2,NU3,NU4,M,N,NOSEG,NUSEG
COMMON/ELLIPS/MU,C,TAU,K
COMMON/CONST/IFLAG,FC,FCONS1,F1,PI,LAMDA
COMMON/SINGLE/AZERO,AONE
REAL K,MU,NUSEC(0:32),NU1,NU2,NU3,NU4,NU5,NU6
```

```
C
C   ARG = K * C * DEL(V,VP)
C   IF (IFLAG.EQ.0) THEN
C       FKERNL = (-1.0) * BESJO(ARG) * FKERL1(V,VP) * (C**2)
C   ELSE
C       IF (ARG.LT.1.0E-03) THEN
C           SEEO = AZERO - (AONE * 5.0E-04)
C           SEETWO = AONE/2.0E-03
C           FKERNL = -(SEEO + SEETWO*(ARG**2)) * FKERL1(V,VP) * (C**2)
C       ELSE
C           FKERNL = -YNU(ARG,0) * FKERL1(V,VP) * (C**2)
C       END IF
C   END IF
C
C   RETURN
C   END
```

```
REAL FUNCTION FKERL1(V,VP)
```

```
C
C
C   COMMON/ELLIPS/MU,C,TAU,K
C   COMMON/CONST/IFLAG,FC,FCONS1,F1,PI,LAMDA
C   REAL K,MU
C
C   FUNCTION CALCULATES THOSE EXPRESSIONS ASSOCIATED WITH THE ZERO
C   ORDER HANKEL FUNCTIONS.
C
C   FKERL1=(TAU**2)*(COSH(MU)**2-COS(V)**2)*(COSH(MU)**2-COS(VP)**2)
C
C   RETURN
C   END
```


REAL FUNCTION BASE1(V,K,VMINUS,VM)

C
C
C
C

CALCULATES THE BASIS FUNCTION FOR THE VSUBMINUSONE TO THE
VSUBM TERM.

COMMON/ELLIPS/MU,C
REAL K, MU

C

DIFVVM = DEL(V,VMINUS)
DIFVMV = DEL(VM,VMINUS)
BASE1 = SIN(K*C*DIFVVM) / SIN(K*C*DIFVMV)

C

RETURN
END

REAL FUNCTION BASE2(V,K,VPLUS,VM)

C
C
C
C

FUNCTION FOR THE FALLING PORTION OF THE SINOSIDAL PORTION
OF THE BASIS CURVE - INTEGRATE FROM VSUBM TO VSUBMPLUSONE.

COMMON/ELLIPS/MU,C,TAU
REAL K,MU

C

DIFVVP = DEL(VPLUS,V)
DIFVPV = DEL(VPLUS,VM)
BASE2 = SIN(K * C * DIFVVP) / SIN(K * C * DIFVPV)

C

RETURN
END*

REAL FUNCTION FA3(VP)

```

C
COMMON/CELLS/NU5,NU6,NU1,NU2,NU3,NU4,M,N,NOSEG,MUSEC
COMMON/ELLIPS/MU,C,TAU,K
COMMON/VARY/V
REAL K,NU,MUSEC(0:32),NU1,NU2,NU3,NU4,NU5,NU6
C
FA3 = BASE1(VP,K,NU4,NU5) * BASE2(V,K,NU3,
1  NU2) * FFERNL(V,VP)
C
RETURN
END

```

REAL FUNCTION ROWSCE(V)

```

C
COMMON/ELLIPS/MU,C,TAU,K
COMMON/SOURCE/CS,KNOT,VS
REAL K,MU,KNOT
C
ROWSCE = SQRT((COSH(MU)**2) * ((C * COS(V) - CS * COS(VS))**2)
1  + (SINH(MU)**2) * ((C * SIN(V) - CS * SIN(VS))**2))
C
RETURN
END

```

SUBROUTINE VOLTS (VMN)

```

COMMON/CELLS/NU5,NU6,NU1,NU2,NU3,NU4,M,N,NOSEG,MUSEC
COMMON/CONST/IFLAG,FC,FCONS1,F1,PI,LAMDA
REAL KNOT,MUSEC(0:32),NU1,NU2,NU3,NU4,NU5,NU6
COMPLEX VMN(0:32)
EXTERNAL FS4,FS5
C
IFLAG = 0
VMNR = DCADRE(FS4,NU1,NU2,0.0,1.0E-3,ERR,IER)
1  ) +DCADRE(FS5,NU2,NU3,0.0,1.0E-3,ERR,IER)
IFLAG = 1
VMNI = DCADRE(FS5,NU2,NU3,0.0,1.0E-3,ERR,IER)
1  ) +DCADRE(FS4,NU1,NU2,0.0,1.0E-3,ERR,IER)
VMN(1) = CMPLX(VMNR,VMNI)
RMAG = SQRT(VMNR**2 + VMNI**2)
PHASE = ATAN(VMNI/VMNR) * (180.0/PI)
WRITE(6,10) M,VMNR,VMNI,RMAG,PHASE
10 FORMAT('0',6X,13,9X,4(6X,E15.8))

```

Reproduced from
best available copy.

```

RETURN
END

```

```

REAL FUNCTION FA7(VP)

```

```

C
COMMON/CELLS/NU5,NU6,NU1,NU2,NU3,NU4,N,K,NOSEG,NUSEG
COMMON/ELLIPS/MU,C,TAU,K
COMMON/VARY/V
REAL K,MU,NUSEG(0:32),NU1,NU2,NU3,NU4,NU5,NU6
C
FA7 = BASE1(V,K,NU1,NU2)
1 * BASE2(VP,K,NU6,NU5) * FIERNL(V,VP)
C
RETURN
END

```

```

REAL FUNCTION FS2(V)

```

```

C
COMMON/ELLIPS/MU,C,TAU,K
COMMON/SOURCE/CS,KNOT,VS
COMMON/CONST/IFLAG,FC,FCONS1,F1,PI,LANDA
REAL K,KNOT,MU
C
IF (IFLAG.EQ.0) THEN
  FS2 = FCONS1 * (C**2) * TAU * BESJO(KNOT*ROWSCE(V))
1 * (COSH(MU)**2 - COS(V)**2)
ELSE
  FS2 = FCONS1 * YNU((KNOT*ROWSCE(V)),0) * (C**2) * TAU
1 * (COSH(MU)**2 - COS(V)**2)
END IF
C
RETURN
END

```

REAL FUNCTION FS4(V)

C

COMMON/CELLS/NU5,NU6,NU1,NU2,NU3,NU4,M,N,NOSEG,NUSEG

COMMON/SOURCE/CS,KNOT

REAL KNOT,NUSEG(0:32),NU1,NU2,NU3,NU4,NU5,NU6

C

FS4 = BASE2(V,KNOT,NU3,NU2) * FS2(V)

C

RETURN
END

REAL FUNCTION FS5(V)

C

COMMON/CELLS/NU5,NU6,NU1,NU2,NU3,NU4,M,N,NOSEG,NUSEG

COMMON/SOURCE/CS,KNOT

REAL KNOT,NUSEG(0:32),NU1,NU2,NU3,NU4,NU5,NU6

C

FS5 = BASE1(V,KNOT,NU1,NU2) * FS2(V)

C

RETURN
END

REAL FUNCTION FA1(VP)

C

COMMON/CELLS/NU5,NU6,NU1,NU2,NU3,NU4,M,N,NOSEG,NUSEG

COMMON/ELLIPS/:TU,C,TAU,K

COMMON/VARY/V

REAL K,MU,NUSEG(0:32),NU1,NU2,NU3,NU4,NU5,NU6

C

FA1 = FKERNL(V,VP) * BASE2(V,K,NU3,NU2)

1 * BASE2(VP,K,NU6,NU5)

C

RETURN
END

```

REAL FUNCTION FA5(VP)
C
COMMON/CELLS/NU5,NU6,NU1,NU2,NU3,NU4,M,N,NOSEG,NUSEG
COMMON/ELLIPS/MU,C,TAU,K
COMMON/VARY/V
REAL K,MU,NUSEG(0:32),NU1,NU2,NU3,NU4,NU5,NU6
C
FA5 = BASE1(V,K,NU1,NU2) * FKERNL(V,VP)
1 * BASE1(VP,K,NU4,NU5)
C
RETURN
END

REAL FUNCTION SIMSON(FUNSON,A,B,C,D,E,ERROR,IER)
C
EXTERNAL FUNSON
COMMON/VARY/V1
REAL H,INT,FUNSON
C
THIS FUNCTION IS BASED ON ROUTINE GIVEN IN:
C
'APPLIED NUMERICAL METHODS FOR DIGITAL COMPUTATION
C WITH FORTRAN AND CSMP', 'SECOND EDITION', BY M. L. JAMES,
C G.M. SMITH, AND J.C. WOLFORD, NEW YORK: THOMAS Y. CROWELL.
C PAGES 328,331,(1977).
C
H=(B-A)/10.
SUM=0.0
V1=A+H
DO 10 I = 2,10
IF (MOD(I,2)) 20,20,30
20 CONTINUE
SUM1=SUM+4.*DCADRE(FUNSON,C,D,0.0,1.E-1,ERROR,IER)
GO TO 10
30 CONTINUE
SUM = SUM+2.*DCADRE(FUNSON,C,D,0.0,1.E-1,ERROR,IER)
10 V1 = V1 + H
V1 = A
INT = (H/3.0)*(DCADRE(FUNSON,C,D,0.0,1.E-1,ERROR,IER)
1 + SUM)
V1 = B
INT = INT + (H/3.0) * DCADRE(FUNSON,C,D,0.0,1.E-1,ERROR,IER)
DELT = DEL(A,B)
DELT2 = DEL(C,D)
C
SIMSON = INT
RETURN

```

END

REAL FUNCTION FA1I(VP)

C

COMMON/CELLS/NU5,NU6,NU1,NU2,NU3,NU4,H,N,NOSEC,NUSEG
 COMMON/ELLIPS/MU,C,TAU,K
 COMMON/VARY/V
 REAL K,MU,NUSEG(0:32),NU1,NU2,NU3,NU4,NU5,NU6

C

FA1I = FKERNL(V,VP) * BASE2(V,K,NU3,NU2)
 1 * BASE1(VP,K,NU6,NU5)

C

RETURN
 END

REAL FUNCTION FA3I(VP)

C

COMMON/CELLS/NU5,NU6,NU1,NU2,NU3,NU4,H,N,NOSEC,NUSEG
 COMMON/ELLIPS/MU,C,TAU,K
 COMMON/VARY/V
 REAL K,MU,NUSEG(0:32),NU1,NU2,NU3,NU4,NU5,NU6

C

FA3I = FKERNL(V,VP) * BASE2(V,K,NU3,NU2)
 1 * BASE2(VP,K,NU4,NU5)

C

RETURN
 END

REAL FUNCTION FA5I(VP)

C
COMMON/CELLS/NU5,NU6,NU1,NU2,NU3,NU4,M,N,NOSEG,NUSEG
COMMON/ELLIPS/MU,C,TAU,K
COMMON/VARY/V
REAL K,MU,NUSEG(0:32),NU1,NU2,NU3,NU4,NU5,NU6
C
FA5I = FKERNL(V,VP) * BASE1(V,K,NU1,NU2)
1 * BASE2(VP,K,NU4,NU5)
C
RETURN
END

REAL FUNCTION FA7I(VP)

C
COMMON/CELLS/NU5,NU6,NU1,NU2,NU3,NU4,M,N,NOSEG,NUSEG
COMMON/ELLIPS/MU,C,TAU,K
COMMON/VARY/V
REAL K,MU,NUSEG(0:32),NU1,NU2,NU3,NU4,NU5,NU6
C
FA7I = FKERNL(V,VP) * BASE1(V,K,NU1,NU2)
1 * BASE1(VP,K,NU6,NU5)
C
RETURN
END

REAL FUNCTION FSIA1(V)

C
COMMON/CELLS/NU5,NU6,NU1,NU2,NU3,NU4,M,N,NOSEG,NUSEG
COMMON/ELLIPS/MU,C,TAU,K
REAL K,MU,NUSEG(0:32),NU1,NU2,NU3,NU4,NU5,NU6
C
FSIA1 = BASE1(V,K,NU1,NU2)
1 * BASE1(V,K,NU4,NU5)
C
RETURN
END

REAL FUNCTION FSIB1(V)

C
COMMON/CELLS/NU5, NU6, NU1, NU2, NU3, NU4, M, N, NOSEC, NUSEG
COMMON/ELLIPS/NU, C, TAU, K
REAL K, NU, NUSEG(0:32), NU1, NU2, NU3, NU4, NU5, NU6
C
FSIB1 = FSIA1(V) * (COS(V)**2)
C
RETURN
END

REAL FUNCTION FSIA2(V)

C
COMMON/CELLS/NU5, NU6, NU1, NU2, NU3, NU4, M, N, NOSEC, NUSEG
COMMON/ELLIPS/NU, C, TAU, K
REAL K, NU, NUSEG(0:32), NU1, NU2, NU3, NU4, NU5, NU6
C
FSIA2 = BASE1(V, K, NU1, NU2)
1 * BASE2(V, K, NU6, NU5)
C
RETURN
END

REAL FUNCTION FSIB2(V)

C
COMMON/CELLS/NU5, NU6, NU1, NU2, NU3, NU4, M, N, NOSEC, NUSEG
COMMON/ELLIPS/NU, C, TAU, K
REAL NU, K, NUSEG(0:32), NU1, NU2, NU3, NU4, NU5, NU6
C
FSIB2 = FSIA2(V) * (COS(V)**2)
C
RETURN
END

REAL FUNCTION FSIA3(V)

C

COMMON/CELLS/NU5,NU6,NU1,NU2,NU3,NU4,M,N,NOSEG,MUSEG

COMMON/ELLIPS/MU,C,TAU,K

REAL MU,K,MUSEG(0:32),NU1,NU2,NU3,NU4,NU5,NU6

C

FSIA3 = BASE2(V,K,NU3,NU2)

1 * BASE1(V,K,NU4,NU5)

C

RETURN

END

REAL FUNCTION FSIB3(V)

C

COMMON/CELLS/NU5,NU6,NU1,NU2,NU3,NU4,M,N,NOSEG,MUSEG

COMMON/ELLIPS/MU,C,TAU,K

REAL MU,K,MUSEG(0:32),NU1,NU2,NU3,NU4,NU5,NU6

C

FSIB3 = FSIA3(V) * COS(V)**2

C

RETURN

END

REAL FUNCTION FSIA4(V)

C

COMMON/CELLS/NU5,NU6,NU1,NU2,NU3,NU4,M,N,NOSEG,MUSEG

COMMON/ELLIPS/MU,C,TAU,K

REAL MU,K,MUSEG(0:32),NU1,NU2,NU3,NU4,NU5,NU6

C

FSIA4 = BASE2(V,K,NU3,NU2)

1 * BASE2(V,K,NU6,NU5)

C

RETURN

END

```
REAL FUNCTION FSIP4(V)
C
COMMON/CELLS/NU5,NU6,NU1,NU2,NU3,NU4,M,N,NOSEG,NUSEG
COMMON/ELLIPS/MU,C,TAU,K
REAL MU,K,NUSEG(0:32),NU1,NU2,NU3,NU4,NU5,NU6
C
FSIB4 = FSIA4(V) * COS(V)**2
C
RETURN
END
```

REAL FUNCTION Y1(ARG)

C
C
C
C
C
C
C
C

SUBROUTINE FROM 'SYSTEM/360 SCIENTIFIC SUBROUTINE PACKAGE
(360A-CM-03X) VERSION II, PROGRAMMERS MANUAL', H20-0205-2,
INTERNATIONAL BUSINESS MACHINES (IBM) CORPORATION, WHITE
PLAINS, NEW YORK. PAGES 157 & 158, 1967.
SEE ALSO PAGE 275 FOR ACCURACY INFORMATION.

COMMON/CONST/IFLAG,FC,FCONS1,F1,PI

IF (ARG.GE.4.) THEN

T1 = 4.0 / ARG

T2 = 16.0 / ARG**2

1 P1 = (((4.2414E-06*T2-2.00920E-05)*T2+5.80759E-05)*T2
- 2.232030E-04)*T2+2.9218256E-03)*T2+0.3989422819

1 Q1 = ((((-3.6594E-06*T2+1.62200E-05)*T2-3.98708E-05)*T2
+ 1.064741E-04)*T2-6.390490E-04)*T2+3.7400836E-02

C NOTE: ERRORS WERE NOTED IN THE IBM WRITE UP ON PAGE 58. CODE
C USED IS CORRECT. SEE HITCHCOCK, A. J. M. "POLYNOMIAL APPROX-
C IMATIONS TO BESSEL FUNCTIONS OF ORDER ZERO AND ONE AND TO
C RELATED FUNCTIONS". 'MATHEMATICAL TABLES AND OTHER AIDS TO
C COMPUTATION', 'VOLUME 11'(58), PAGES 86-88, APRIL, 1957.
C

AA=2.0/SORT(ARG)

BB=AA*T1

D = ARG - PI/4.0

Y1=-AA*P1*COS(D)+BB*Q1*SIN(D)

ELSE

XX=ARG/2.0

X2=XX*XX

T =ALOG(XX)+0.5772156649015

C
C
C
C

EULER'S CONSTANT FROM 'HANDBOOK OF TABLES FOR MATHEMATICS',
'THIRD EDITION', PAGE 5, 1967.

SUM = 0.0

APPENDIX D. MATRIX CALCULATOR AND LINEAR ALGEBRA EQUATION SOLVER PAGE D- 17

TERM = XX * (T - 0.5)

YONE = TERM

DO 80 L = 2,16

SUM = SUM + 1.0 / FLOAT(L-1)

FL = FLOAT(L)

FL1 = FL - 1.00

TS = T - SUM

TERM = (TERM*(-X2)/(FL1*FL))*((TS-0.5/FL)/(TS+0.5/FL1))

YONE = YONE + TERM

80 CONTINUE

PI2 = 2.0 / PI

Y1 = (-PI2/ARG) + PI2 * YONE

END IF

RETURN

END

Vita

Edward Arthur Urbanik was born on 31 July 1955 in Burbank, California. He graduated from Henderson Senior High, West Chester, Pennsylvania in May 1973. He attended The Pennsylvania State University in the School of Engineering from which he earned a Bachelor of Science in Electrical Engineering on 25 May 1977. Captain Urbanik received a USAF commission on the same date through the ROTC program. He was subsequently assigned to the Air Force Electronic Warfare Center (AFEWC), Kelly AFB, TX. He entered the School of Engineering, Air Force Institute of Technology, in June 1981.

UNCLASSIFIED

SECURITY CLASSIFICATION OF THIS PAGE (When Data Entered)

REPORT DOCUMENTATION PAGE		READ INSTRUCTIONS BEFORE COMPLETING FORM
1. REPORT NUMBER AFIT/GE/EE/82D-67	2. GOVT ACCESSION NO. A124 682	3. RECIPIENT'S CATALOG NUMBER
4. TITLE (and Subtitle) SCATTERING OF CYLINDRICAL ELECTRIC FIELD WAVES FROM AN ELLIPTICAL DIELECTRIC CYLINDRICAL SHELL		5. TYPE OF REPORT & PERIOD COVERED MS THESIS
7. AUTHOR(s) Edward A. Urbanik, Captain, USAF		6. PERFORMING ORG. REPORT NUMBER
9. PERFORMING ORGANIZATION NAME AND ADDRESS Air Force Institute of Technology (AFIT/EN) Wright-Patterson AFB, OH 45433		8. CONTRACT OR GRANT NUMBER(s)
11. CONTROLLING OFFICE NAME AND ADDRESS Aeronautical Systems Division (ASD/ENAMA) Wright-Patterson AFB, OH 45433		10. PROGRAM ELEMENT, PROJECT, TASK AREA & WORK UNIT NUMBERS
14. MONITORING AGENCY NAME & ADDRESS (if different from Controlling Office)		12. REPORT DATE 17 December 1982
		13. NUMBER OF PAGES 126
		15. SECURITY CLASS. (of this report) UNCLASSIFIED
		15a. DECLASSIFICATION/DOWNGRADING SCHEDULE
16. DISTRIBUTION STATEMENT (of this Report) Approved for public release; distribution unlimited		
17. DISTRIBUTION STATEMENT (of the abstract entered in Block 20, if different from Report)		
18. SUPPLEMENTARY NOTES Approved for public release: IAW AFR 190-17. <i>John E. Wclaver</i> JOHN E. WCLAVER Dean for Research and Professional Development Air Force Institute of Technology (AIG) Wright-Patterson AFB OH 45433 4 JAN 1983		
19. KEY WORDS (Continue on reverse side if necessary and identify by block number) Basis functions Integral equations Testing functions Cylindrical field waves Method of moments Dielectric scatterers Principal value integral Electromagnetic scattering Singular functions Singularities(numeric methods)		
20. ABSTRACT (Continue on reverse side if necessary and identify by block number) This thesis examines the scattering of cylindrical waves by large dielectric scatterers of elliptic cross section. The solution method was the method of moments using a Galerkin approach. Sinusoidal basis and testing functions were used resulting in a higher convergence rate. The higher rate of convergence made it possible for the program to run on the Aeronautical Systems Division's CYBER computers without any special storage methods.		

UNCLASSIFIED

SECURITY CLASSIFICATION OF THIS PAGE(When Data Entered)

The program thus developed required very large run times. This makes the program impractical for scatterers of size greater than one wavelength. This report includes discussion on moments methods, solution of integral equations, and the relationship between the electric field and the source region or self cell singularity. Since the program produced unacceptable run times, no results are contained herein. The importance of this work is the evaluation of the practicality of moment methods using standard techniques. The long run times for a mid-sized scatterer demonstrate the impracticality of moments methods for dielectrics using standard techniques.

UNCLASSIFIED

SECURITY CLASSIFICATION OF THIS PAGE(When Data Entered)

END